HEL-12-9

RELATIVE EFFECT OF WAVES GENERATED BY LARGE SHIPS AND SMALL BOATS IN RESTRICTED WATERWAYS

by

M. M. DAS

HYDRAULIC ENGINEERING LABORATORY
COLLEGE OF ENGINEERING

UNIVERSITY OF CALIFORNIA
BERKELEY
NOVEMBER 1969

RELATIVE EFFECT OF WAVES GENERATED BY LARGE SHIPS AND SMALL BOATS IN RESTRICTED WATERWAYS

Report No. HEL-12-9

This is the final report on a project supported by Contract DACW 72-68-C-0034 with the Coastal Engineering Research Center, Corps of Engineers, U.S. Army.

by

M.M. Das

Faculty Investigator

J.W. Johnson

Hydraulic Engineering Laboratory
University of California, Berkeley
November 1969

ABSTRACT

The peak wave energy in a system of waves resulting from the passage of a ship is of importance in such problems as bank erosion, the motion of moored vessels, forces on fixed and floating docks, etc. With respect to the bank erosion problem, the question often asked is whether the single passage of a large ship during a day, for example, is more damaging than numerous passages of small pleasure craft during the day. With this in mind this study was conducted to determine the relative importance of the peak energy resulting from the passage of a cargo ship and a pleasure cruiser. The characteristics of the waves generated by these vessels moving at various speeds in deep and shallow water were determined from model studies. A numerical example is given in which prototype values of peak wave energy were predicted from the model data, and then ratios of the peak energies computed. The importance of ship speed is evident in these comparisons.

TABLE OF CONTENTS

LIST OF FIGURES

Page

Page

Page

Page

LIST OF TABLES

I. INTRODUCTION

1.1. General

The generation of waves due to the motion of ships and the determination of the wave-making resistance of ships have been the subjects of theoretical and experimental studies for many years.

The earliest work in the field of ship resistance were those of Rankine (46) and Froude (8). The theory of ship waves was first presented by Lord Kelvin (35). Havelock (11,12) and Ursell (61) later extended the work of Lord Kelvin. After the work of Froude, a considerable amount of work was done to predict a wave resistance of a ship from measurement of the wave pattern behind the ship in steady motion. Havelock (13,16,18), Lunde (38), Birkhoff, et al. (2), and more recently, Inui (26), Eggers (5), Gadd and Hoggben (9), Neumann (43), Sharma (50,51), Shor (54), and others have suggested methods and their application to determine wave making resistance of ships from measurements of the wave profiles generated by the ship's motion. Egger's method of computation of wave resistance is based on a free wave spectrum and has been developed for both finite and infinite water depths.

Very little work, however, has been done in obtaining quantitative information on the characteristics of ship waves at a given distance from the sailing line in terms of hull forms, displacement, speed, and water depth in unrestricted and in restricted navigable channels. Hovgaard (23) was apparently the first one to make a comprehensive set of measurements of actual ship waves generated by different types of ships. For restricted waterways, some investigations have been made to determine the form and the protection of canal banks (Carlson,

3, and Hulman, 24). Many other investigations have been made, but no reporting was made of the wave heights occurring in the tests. The works of Johnson (27,28), Sorensen (55,56,57), Hay (20), and Bidde (1) were therefore made to determine quantitative information on the waves generated by moving different ship models in a model basin. Sorensen (55), by using both parallel-wire resistance type wave gauge and stereophogrammetric technique, succeeded in obtaining quantitative information on the wave surface and compared the theoretical predictions of Lord Kelvin (35) and Havelock (11) with the actual ship waves.

1.2. Purpose

A ship moving in a canal or in a harbor causes the following phenomena to occur that are important from the point of view of the proper design of harbor and channel revetment, the effect of ship waves on moored vessels and floating docks, etc.:

(a) The height of the waves reduces along cusp-locus line as the distance from the sailing line increases.

(b) A water movement (known as backflow) which is opposite to the movement of the ship is created.

(c) There is a lowering of water level, generally known as squat, near the ship, which is dependent on the backflow velocity and the speed of the ship. The backflow velocity in turn is dependent on the wet cross-section of the channel, the immersed midship section of the ship, and decreased wet cross-section of the canal due to squat and the speed of the ship.

For the control of side slope erosion, one should have information on the peak wave energy, or maximum wave height as a function of distance from the sailing line, the angle of incidence of the waves with respect to the banks, the backflow velocity, and the amount of squat expected with different types of ships.

This report presents the results of studies with models of a Mariner cargo ship and a pleasure Cruiser model under deep water (d = 24 1/8") and shallow water (d = 4 1/8") conditions.

The procedure in all tests was to tow the models at various speeds and obtain wave records at several positions from the sailing line.

II. REVIEW OF LITERATURE

A survey of literature on the theoretical and experimental studies of the waves generated by the motion of ships or a local pressure disturbance was made. Sorensen (55) has included a survey and discussion on this subject. The literature reviewed is cited in the list of references. Those references pertinent to this study are cited in the text.

Some important literature on the theory and the methods for the determination of a ship's wave-making resistance from measurements of wave heights was also reviewed as cited in the reference; however, since these works do not relate to the problem under study, this discussion has been omitted in this report.

III. EXPERIMENTAL SET-UP

3.1. General

The results of the experiments reported herein were obtained in the model basin of the Hydraulic Engineering Laboratory, University of California, which is located at the Richmond Field Station. Two ship models, a Cruiser (Figs. 2 and 3) (scale 1:16) and a Mariner (Fig. 1) (scale 1:96) were tested in two water depths.

3.2. Model Basin

Figure 4 is a general view of the model basin and the model towing arrangement. The overall dimensions of the model basin are 149.5 ft. (length) by 63.6 ft. (width) by 2.5 ft. (depth). The same ship model towing arrangement as used by Sorensen (55), Hay (20), and Bidde (1) was used in the experiments.

3.3. Ship Model Towing System

The ship model towing system consisting of the two pulleys, a 1/16 in. diameter nylon towing line, drive weights, and a counter-weight required to return the ship to the starting position after each run has been described previously by Sorensen (55).

Different ship model speeds were obtained by varying the weights used in the drive system. The speed of the model was determined by measuring the time required for a given number of revolutions of the larger pulley which has a circumference of 4.7 feet. Since during the first few revolutions of the pulley the model accelerates to reach a uniform speed, the time for speed measurement was measured only after the pulley completed its third revolution.

The speed of the ship was not constant for a given weight in the driving system, which may be due to a variation of frictional effects in the system. Therefore, each individual run was treated as separate. In order to check that the ship speed remained uniform over the test run after the initial period of acceleration, a microswitch was mounted near the shaft of the pulley and tripped each revolution. The time period for each revolution of the pulley was recorded on a Sanborn recorder using the remote marker. As an example, Fig. 5 shows a plot of time in secs. per revolution against the revolutions for Record 33, Run 12, using Mariner model in shallow water (d = 4 1/8").

3.4. Wave Gauges

Four parallel-wire resistance type wave gauges (Wiegel, 63) were attached to point gauges and were mounted from the deck of the carriage system located in the model basin. These gauges were connected to a four-channel Sanborn amplifier-recorder to obtain the time history of the water-surface elevations (Fig. 6). These gauges were located at 2.95 ft., 8.83 ft., 14.7 ft., and 20.6 ft. along a line normal to the sailing line of the ship.

The calibrations of the wave gauges showed that these gauges were not linear. Further, the pen deflections or the voltage outputs for equal amounts of raising and lowering of the probe from the still-water position were not constant. Therefore, the gauges were calibrated for different depths by both raising and lowering the probe from the still-water level. The calibrations were also made at different attenuations of the Sanborn recorder in order to be able to record all ranges of wave heights in various runs.

With a view to making a Fourier analysis of the wave data, a simultaneous recording of the wave heights was also made on an eight channel analog-digital converter (Hydra) to be described later (Fig. 6). A few of the calibration curves were plotted from the calibration records obtained with Hydra. These showed the non-linearity of the calibrations. For purposes of computation of wave heights from the Hydra records, the average value at each step of calibration was used and linear interpolation was made between two successive steps.

3.5. Wave Height Recording System

Time histories of water surface elevations at four points along a line normal to the sailing line were recorded simultaneously on a four-channel recorder as mentioned earlier and on magnetic tape by using Hydra (Fig. 6). The digital data tape recorder "Hydra" was built by the College of Engineering, University of California, Berkeley. The essential features of this equipment are:

physical dimension - size: 22" (wide) x 25" (depth) x 62" (height)
weight: 430 lbs. (approx.)

power requirement - 600 watts, 115 v ac, 60 cycles

channel capacity - eight, of which one or two may be digital and the remainder analog, or all analog

sampling rates - tape speed (inches per sec.): 75 16 4 1
sampling rate per sec. in 8 channels:
7500 1875 468.75 117
samples per sec. per channel:
937 234 59 15

Lower sampling rates may be accomplished by single-scanning

all channels as frequently as needed (external triggering).

sensitivity - analog: ± 10 millivolts, full scale

digital: 10 binary bits plus sign

In this study a tape speed of four inches per sec, that is, 468.75 samples (or data points) per sec, was used to record the analog signal from the Sanborn recorder. All the eight channels were used for recording the analog signal from four wave gauges. Two channels were patched together meaning thereby that the wave data from each gauge were recorded on two channels.

The time interval between any two samples in each channel is

$$\frac{8}{468.75} = 0.01707 \text{ sec.}$$

3.6. Ship Models

The following two ship models were used in these experiments:

TABLE 1. MODEL CHARACTERISTICS

	Scale	Overall length (inches)	Beam (inches)	Draft (inches)	Total displaced for test (lbs.)
Mariner class cargo ship	1:96	70 - 3/4	9 - 1/4	3	37.32
Cruiser	1:16	48 - 3/4	-	2	24.913

The Mariner class cargo ship was also used by Hay (20) in his studies.

IV. EXPERIMENTAL PROCEDURE

Several test runs were conducted with the Mariner and the Cruiser models in both shallow and deep water. Simultaneous recordings of the time histories of water-surface elevations, as well as the calibration of the wave gauges, were made on a Sanborn recorder and the Hydra on magnetic tape.

Each test run was carried out in the following manner. The desired weight in the pulley system was added. The model was taken to the starting point so that the revolution counter registered zero.

The still-water signal input to Hydra from each wave gauge was checked individually by manual operation of the Test-Operate switch on Hydra, and displaying the signal on an oscilloscope, connected between the low level amplifier and the A/D converter. By adjusting the Resistance/Bal control on the associated carrier preamplifier, the wave gauge signal was set at zero volts as received by the A/D converter, thus correcting for any drift in the Sanborn recorder before each run.

Sufficient time was allowed to obtain still-water conditions in the basin. Then, the towing system was released to tow the model. After the pulley completed the first three revolutions, the timing of the counter was made with a stop watch. The average speed of the model was obtained by timing over fifteen to twenty revolutions. The Hydra and the Sanborn recorder were switched-on to obtain records as soon as the surface deformation in front of the model arrived in the close proximity of the wave gauge nearest to the sailing line. The recording was stopped after the waves passed the farthest gauge and before the

reflected waves from the end and side walls of the basin propagated to the probes. For the next run, the model was taken back to the starting point. Sufficient time again was allowed for the surface disturbances to die down before the next run was commenced.

Two sets of test runs were made with both models on two occasions. The first set of test series comprised only a few runs and provided only limited data. Therefore, it was decided to take a second set of test series at various Froude numbers. Tests with the Mariner model were done both in shallow water (d = 4 1/8") and deep water (24 7/8") at different Froude numbers. Tests with the Cruiser model could be completed only in shallow water (d = 4 1/8"), but tests with this model in deep water could not be repeated, as the model was no longer available. It is therefore important from the point of view of the study of the relative effect of waves generated by large ships and small boats that tests with small boats be carried out in deep water to compare the results with those of large ships in shallow water.

The details of the two sets of test series, i.e., the water depth, ship speed, Froude numbers, etc., are given in Tables 2, 3a, 3b, 4, and 5. The data and computational results are presented in the form of graphs.

V. ANALYSIS AND DISCUSSION OF RESULTS

5.1. Energy Density

For a linear sinusoidal progressive wave, the total energy per unit wave length is proportional to the product of the wave length and the square of the wave height.

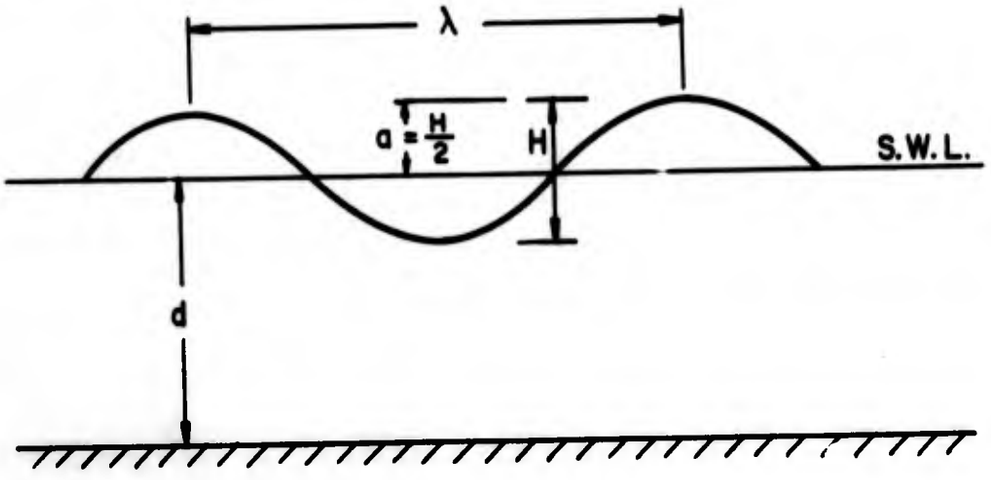

Thus total energy per unit wave length is given by

$$E_T = E_K + E_p = \frac{\gamma H^2 \lambda}{16} + \frac{\lambda H^2 \lambda}{16} = \gamma \frac{H^2 \lambda}{8} \qquad (1)$$

where γ is the unit weight of water. However, the energy density or the total energy per unit of surface area is given by

$$e_T = \frac{E_T}{\lambda} = \frac{\gamma H^2}{8} \qquad (2)$$

Therefore, the energy per unit of surface area is proportional to the square of the wave height.

Ship waves. Suppose the time history of water-surface elevations is measured by using a parallel-wire resistance gauge fixed at a point y from the sailing line. This time history, which may appear

as shown below, provides information along a fixed line extending over the complete wave pattern, if the record is taken over a sufficiently long period of time.

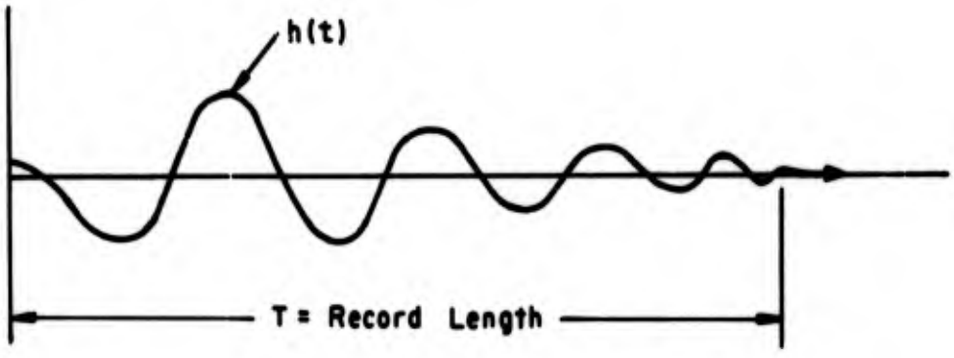

This longitudinal profile through the wave pattern distant y from the sailing line can be decomposed by Fourier analysis into regular sine and cosine components. Each component will have an apparent period T_n and amplitude C_n where $T_n = \frac{T}{n}$; n = 1,2,3... and

$$C_n = \frac{1}{T} \int_0^T h(t) \exp\left(\frac{-i\ 2\pi nt}{T}\right) dt \qquad (3)$$

The inverse transform of this equation gives

$$h(t) = \sum_{-\infty}^{\infty} C_n \exp\left(\frac{i\ 2\pi nt}{T}\right) \qquad (4)$$

The mean-square value of the surface deformations is given by

$$\overline{h^2} = \frac{1}{T} \int_0^T h(t)^2 dt = \sum_{-\infty}^{\infty} |C_n|^2 \qquad (5)$$

for the periodic wave forms.

Thus, the energy density or the total energy per unit of surface area in the wave profile obtained by the longitudinal cut is given by Gadd and Hogben (9) and Lamb (32):

$$E_n = \frac{1}{2} \gamma C_n^2 \qquad (6)$$

This indicates the contribution at each frequency f given by $\frac{n}{T}$ to the energy density or energy per unit of surface area.

5.1.1. Processing of Data

The results of the test series in set 1 were used to determine energy density or energy per unit surface area in the wave train by using a Fourier analysis. The following table gives the particulars of the test runs for which the wave data taken on magnetic tape were used for the above analysis:

TABLE 2. TEST CHARACTERISTICS (FIRST SET)

Date of Experiment	Record No.	Model	Scale	Length L (ft.)	Water depth, d (inches)	Speed of ship, V (ft./sec.)	$Fr_d = \frac{V}{\sqrt{gd}}$
July 3, 1969	13	Cruiser	1:16	4.06	4.125	2.6	0.78
"	15	Cruiser	1:16	4.06	4.125	2.7	0.81
July 16, 1969	26	Mariner	1:96	5.90	4.125	2.7	0.81
"	27	Mariner	1:96	5.90	4.125	2.66	0.78
July 18, 1969	28	Mariner	1:96	5.90	25.0	2.97	0.36
"	30	Mariner	1:96	5.90	25.0	3.80	0.46
"	35	Cruiser	1:16	4.06	25.0	4.05	0.49
"	36	Cruiser	1:16	4.06	25.0	3.95	0.48

These data include two test runs with each model both in shallow water (4.125 in.) and in deep water (25.0 in.).

The processing and analysis of the data taken with Hydra at a tape speed of 4 inches per sec., or 468.75 samples per sec. in 8 channels, were done as follows.

The tape containing 3 sec. records of calibration of the wave gauges at various heights, above and below still-water level at different sensitivities of the Sanborn recorder and the wave height records for the model runs was first processed in a 360 computer to blok the records. This is done by using the Long Blok program available in the Computer Center. This program bloks long records taken with Hydra into Scope internal tape format. The records taken with Hydra at odd parity and at a density of 200 bits per inch are usually much longer than 5120 bytes, except for the calibration records of 3 sec. length. This program bloks each of these long records into physical records of 5120 bytes and a record consisting of the remainder of bytes not divisible by 5120. The data are bloked onto another tape (output tape) and this bloked tape is used for subsequent computations and analysis by using CDC 6400. Since there is no provision in Hydra for an "end of file," it is necessary to indicate an estimate of number of records in each tape while it is bloked.

First, the records of calibration of the wave gauges were processed. Each calibration record was 3 sec. long at 59 samples per sec. per channel, thus consisting of approximately 177 samples corresponding to each depth of calibration. Since the value is not constant due to noise in the recording system or due to very small water surface

deformations, an average value was computed for each point, and this mean value was used for obtaining the time history of water-surface elevations from the wave records. As the calibration was a static one at discrete steps, linear interpolation was made between two successive calibration points to compute the water-surface elevations in the intermediate values. These calibration data converted the Hydra records given in terms of numbers between 0 and 2047 (-10 mv and +10 mv) to actual wave heights or the ordinates of water surface above or below the still-water level in feet still-water level being regarded as zero.

In order to compute and compare the energy densities at different gauge stations by using the Fourier analysis method, the position of the maximum wave crest was located by scanning through each record. A suitable length of record was selected to include the first bow wave preceding the maximum crest and to include sufficient data points after the maximum to include waves of appreciable amplitudes. Equal lengths of records or equal number of sample points were used for the different time histories in each record. It developed that 528 samples had to be used for each analysis for each gauge station. This was equal to a record length of $\frac{528 \times 8}{468.75} = 9$ secs.

Values of Cn^2 have been plotted as a function of n in Figs. 7 and 8 for the Mariner model, Figs. 9 and 10 for the Cruiser model in deep water, and Figs. 11 and 12 for the Mariner model and Figs. 13 and 14 for the Cruiser model in shallow water.

The time histories of water surface in shallow water ($d = 4\ 1/8''$) showed a long surge ahead of the first bow wave, and this was followed

by a deep and wide trough at the gauge located 2.95 feet from the sailing line (nearest gauge). The plots of energy density function therefore indicate a large contribution at low frequency, besides the second peak at the frequency or period (i.e., $\frac{T}{n}$) of the main wave system. The contribution at low frequency is absent at other gauge positions due to the non-existence of the deep and wide trough at those locations.

The analysis of wave records in deep water (d = 25.0") showed little contribution to energy density in the low frequency range. However, there are two energy peaks, as can be seen slightly in Figs. 7 and 8, for the Mariner model and more pronounced in Figs. 9 and 10 for the Cruiser model in deep water.

The total energy density or total energy per unit surface area is given by Eq. (6). This was computed for each wave record and for each test run. This quantity is also equivalent to the mean square height $\overline{h^2}$. The energy densities for each station located on a line normal to the sailing line were non-dimensionalized by considering the value of E_n at the nearest gauge (i.e., 2.95 feet from sailing line) as unity and expressing the values of E_n at other stations as ratios of that at the nearest gauge. Dimensionless total energy per unit surface area is plotted as a function of distance from the sailing line. The results of the eight test runs are shown in Fig. 15. Except for the two test runs with the Cruiser model in shallow water, the results of the gauge no. 4 located at 20.6 feet from the sailing line could not be obtained as the Sanborn amplifier malfunctioned. Figure 15 indicates the relative energy as a function of the distance

from the sailing line.

5.2. Peak Wave Energy

The Fourier analysis method shows how the energy per unit of surface area or the mean square wave height in a finite length of the wave train varies with distance longitudinally from the point of generation of the waves.

From the point of view of the design of the navigable canal banks, forces on docks,or moored vessels, the peak wave energy associated with the maximum wave height in the wave train should be of considerable interest.

The wave patterns and the magnitude of the waves generated are functions of hull form, water depth, draft, and speed of the ship. Therefore, further tests whose results are presented in subsequent sections were conducted in both shallow and deep water with the Mariner and Cruiser models, moving at various speeds. The maximum wave height, Hm , was used to characterize the variation of peak energy in the different tests.

5.2.1. Deep-Water Test Results

Results of the tests made with the Mariner model in deep water with a water depth of 24 7/8 inches are presented in Table 3a. These results are from the second set of experiments.

The maximum wave height Hm and its half-period T/2 were obtained from the wave records at the four positions. Ship speed and depth Froude numbers were calculated.

In a sinusoidal wave the total energy per unit surface area is proportional to the square of the wave height. The square of the

maximum wave height, Hm^2 is thus a measure of the peak energy in the in the wave train produced by a moving ship. The values of Hm^2 as a function of distance from the sailing line with Froude number as a parameter were plotted in Fig. 16. This plot provides information on the magnitude of the peak energy at various distances from the sailing line.

The non-dimensionalized values of $(Hm/d)^2$ have been plotted in log-log graphs, Figs. 17 to 24, as a function of y/L for various Froude numbers. An inspection of the graphs does not indicate the existence of any suitable relationship between the parameters due to the large scatter in the values. Another dimensionless parameter, Hm^2/T^2V^2, where T is twice the half-period of the highest wave, Hm, and V is the speed of the model, was chosen. This term is plotted as a function of y/L for various Froude numbers in Fig. 25. The dimensionless energy shows a systematic variation with distance and Froude numbers, except for the Froude numbers of 0.4 and 0.50. This may be due to experimental scatter.

5.2.2. Variation of Cusp Elevations

Havelock (11), Ursell (62), and others have shown that for a point pressure disturbance moving in deep water, the diverging wave crests at the cusp locus line decrease at a rate inversely proportional to the cube root of the distance from the point of wave generation. This suggests that a plot of the cusp elevations as a function of distance from the sailing line will be a straight line with a negative slope of 1/3 on log-log paper.

Figure 26 is a plot of $\frac{Hm}{d}$ as a function of distance from the

sailing line, y/L, on a log-log graph. The slopes vary from -0.59 for a Froude number of 0.35 to -0.21 for a Froude number of 0.50. The log-log plots of $\frac{Hm}{d}$ as a function of Froude number with dimensionless distance y/L as a parameter (Fig. 27) are nearly parallel straight lines suggesting a relationship of the form, $\frac{Hm}{d} = C\ (Fr_d)^m$, where m is a positive exponent and is equal to 2.8 for the graph at $y/L = 0.5$. The value of the coefficient, C, will be different for each line. The dimensionless wave heights, $\frac{Hm}{d}$, at two non-dimensional distances, y/L of 0.5 and 1.5, are plotted as a function of Froude number in Figs. 28 and 29. The trend was similar. The data for the other two gauges at $y/L = 2.5$ and 3.5 and have not been plotted herein. An inspection of the plots would show how rapidly the wave height increases with Froude number or the speed of the ship. For a two-fold increase in Froude number from 0.3 to 0.6 (i.e., also two-fold increase in ship speed, depth being constant), there is almost ten-fold increase in wave height. This increase in wave height with ship speed occurs up to a critical point. Beyond this critical speed, the wave height decreases with increase in speed as shown by Johnson (27). This critical point has not been reached in these experiments in deep water as the values of Froude numbers range from only 0.27 to 0.64.

Unfortunately, when the second set of test runs were made, the Cruiser model was not available for testing under deep-water conditions. Only the results of three runs of the first set are available under these conditions. These three runs were at Froude numbers of 0.41, 0.47, and 0.49. These results are also plotted in Figs. 20 and 21. It can be seen from Fig. 20 that the wave making potential of the

Cruiser model appears to be higher than that of the Mariner model at a distance of 2.95 ft. from the sailing line (i.e., y/L = 0.5 for the Mariner and y/L = 0.725 for the Cruiser model). Sufficient data covering a wide range of Froude numbers are necessary to arrive at any conclusion. However, this aspect is not noticeable at the second position of the wave gauge located at 8.83 ft. from the sailing line (Fig. 20).

The "half-periods," T/2, corresponding to the maximum wave height Hm, were determined from the wave records. These data for the Mariner and the Cruiser models are shown plotted as a function of Froude number in Fig. 30. The half-period was found to be almost independent of distance y/L with few exceptions (see Table 3a and 3b). Therefore, the data from only one gauge station (y = 2.95 ft.) are plotted in this graph.

5.3. Shallow Water Test Results

5.3.1. General

The resistance of a ship in shallow water is greater than in deep water due to the following reasons:

(a) In shallow water the pressures created by the ship's motion are higher than those in deep water, and these higher pressures cause larger waves in shallow water.

(b) The lengths of the waves in shallow water are also greater than those in deep water for the same speed of the ship (Taylor, 60). This also attributes to the increased wave-resistance of the ship in shallow water.

(c) The flow conditions around the ship's hull also change in shallow water, contributing to a small increase in the skin friction resistance.

The shallow water effects on the increase of ship resistance have been evaluated by Taylor (60) as a function of the parameter $\frac{V}{\sqrt{L}}$ where L is the length of the ship in feet and V is the speed in knots. For slow and moderate speed vessels, Taylor obtained an empirical relationship giving the critical point at which the ship resistance starts to increase. The relationship has been stated by Johnson (27). No information was, however, available from Taylor's data on the characteristics of the waves.

The pattern of waves generated in shallow water, i.e., finite water depth, was predicted by Havelock (11), and Inui (26) re-calculated the shapes of the wave fronts for the super-critical speeds. Sorensen (55) conducted investigations on the characteristics of the waves produced by ship motion in shallow water, both for subcritical and super-critical speeds. His data from stereophotographs on the pattern of waves and the discussion of the results provide valuable information on this problem. The data presented are, however, for a parabolic model.

In the present studies, both the Mariner and the Cruiser models were tested in shallow water at various subcritical speeds. The test particulars for different runs are presented in Table 4 for the Mariner model and in Table 5 for the Cruiser model. Water depths of 4 1/8 inches were maintained in the basin in tests with both models. The results obtained from both series of tests are presented and

discussed below.

5.3.2. Test Results

The data obtained from the two sets of experiments with the Mariner model are presented in Table 4, and those with the Cruiser model are presented in Table 5. The values of maximum wave heights Hm and the corresponding half-period T/2 were obtained from the wave records at different gauge stations. The values of the square of the maximum wave height, Hm^2, are plotted as a function of distance from the sailing line with the Froude number as a parameter in Fig. 31 for the Mariner model and in Fig. 32 for the Cruiser model. The results of Hay (20) for the Mariner model with the same water depth of 4 1/8" were also recalculated and are included in Fig. 31. These graphs provide information on the magnitude of the peak energy in the wave train as a function of distance from the sailing line.

The non-dimensional values of $(Hm/d)^2$ have been plotted as a function of y/L with Froude number as a parameter on log-log graphs in Figs. 33 to 37 for both of the models. The results of Hay (20), wherever available, have also been incorporated. Each graph is for a particular Froude number or for Froude numbers not significantly different from each other.

One can observe the following trends in the graphs: In Fig. 33 are plotted the results for the Mariner and the Cruiser models at a Froude number of 0.65 and the results of Hay (20) for a Froude number of 0.672 with the Mariner model. The non-dimensional peak wave energy $(Hm/d)^2$ due to the Mariner model is about 10 times higher than due to the Cruiser model. The energy or the maximum wave height, Hm ,

reduces much faster with distance from the sailing line with the Cruiser model as compared to that of the Mariner model. The relationship for the Mariner model would be approximately $(Hm/d)^2 = C(y/L)^m$, where C is a coefficient and the exponent m in this plot being about equal to -0.82. The results of Hay (20) are for a slightly higher Froude number; as such the values of Hm are higher. In Fig. 34 are the data for a Froude number of 0.72 for both of the models. The data for the Mariner model appear to be more scattered and no such power relationship is apparent. In Fig. 35 the data for a Froude number of 0.75 are plotted for both the models, including those of Hay, for the Mariner model. The power relationship for the data of the Mariner model appears to fit quite well with the value of the exponent m being equal to $-0.665 \simeq -2/3$. A similar condition can be seen in Figs. 36 and 37 for Froude numbers of 0.78 and 0.80. In Figs. 38, 39, and 40 the rapid decrease of $(Hm/d)^2$ as a function of y/L for the Cruiser model is also evident.

The non-dimensional cusp elevations (Hm/d) at distances y/L = 0.5 and 1.5 are plotted in Figs. 41 and 42 as a function of Froude number for the results of tests with the Mariner model. The results of the Cruiser model for y/L = 0.725 are shown in Fig. 43. These plots indicate the increase of maximum wave height at a particular distance from the sailing line as the ship speed is increased.

The half-periods T/2 corresponding to the maximum wave height Hm , obtained from the wave records for both of the models, are plotted in Fig. 44 as a function of the Froude number. The range of Froude numbers in the tests is from 0.58 to 0.96. This figure can be compared

with Fig. 11 of Johnson (27). His results were obtained for model A_L with a length of 3.32 ft., draft of 0.13 ft., and a water depth of 0.52 ft. The results are from a gauge located 3 ft. away from the sailing line with a depth to draft ratio of 3.96. The results are interesting from the point that the half-period reaches a maxima near the critical Froude number and then decreases rapidly as the speed or the Froude number increases in the super-critical range. The increase to the critical value in the subcritical range is at a much faster rate than the decrease in the super-critical range. Although the results of the present tests are limited to the subcritical range only, they compare well with those of Johnson (27).

The dimensionless cusp elevations, Hm/d , are plotted as a function of Froude number with the relative distance y/L as a parameter for the Mariner model in Fig. 45, and for the Cruiser model in Fig. 46. The graphs for the Mariner model show a rapid increase of the wave-making potential beyond a Froude number of 0.75. This Froude number corresponds to a prototype ship speed of 14.5 knots. This increase in the case of the Cruiser model is less rapid and the transition occurs at a Froude number of about 0.86, which corresponds to a prototype ship speed of 6.8 knots. The critical speed apparently is reached between the Froude numbers of 0.9 and 0.94. For higher speeds or Froude numbers, the wave-making resistance or the maximum wave amplitude decreases. This increase of wave height with ship speed confirms the observations of Johnson (27) and Lewis (33). Since the wave energy per unit surface area is proportional to the square of the wave height, the energy associated with this maximum wave will be

serious in the erosion damage of the banks of navigation canals if these are unlined.

5.4. Results of Sorensen Scale Effects Studies

Besides the results of this investigation, the data of Sorensen (55) obtained from studies on scale effects were also recalculated and presented to show the variation of the maximum wave energy as a function of distance from the sailing line for various Froude numbers and for the five different models used by him.

In order to investigate the scale effects, Sorensen conducted a series of tests on five geometrically similar models. The form and dimensions of the models used by him in the scale effects tests were as follows:

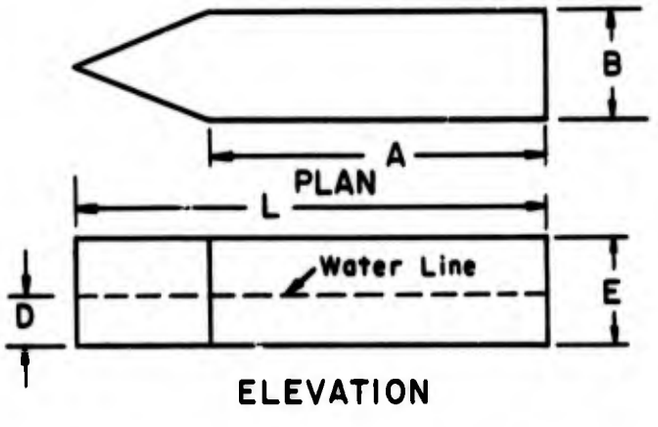

MODEL	L	B	D	A	E	WATER DEPTH USED (d)
A	18	3	1.5	13.5	3	4.5
B	24	4	2.0	18.0	4	6.0
C	30	5	2.5	22.5	5	7.5
D	36	6	3.0	27.0	6	9.0
E	48	8	4.0	36.0	8	12.0

All dimensions in inches.

Sorensen conducted 81 runs with these five models at various depth Froude numbers between 0.4 to 0.9. The time histories of the water surface were obtained with wave gauges located at four positions on a line normal to the sailing line. The gauges were located at ship length ratios (y/L) of 0.5, 1.5, 2.5, and 3.5. Each time history of the surface as the model approached and passed the wave gauge line showed a maximum wave height, i.e., the vertical distance between the trough and the following crest. This generally has been defined as a representative wave height (Johnson, 27; Sorensen, 55; Hay, 20; Bidde, 1). The values of the maximum wave height, Hm, from all the records of the test runs, were presented as a dimensionless wave height, Hm/d, where d is the water depth used in the test run. The data presented in Appendix D (pp. 136-139), of Sorensen's report were used to compute Hm^2 and the values of Hm^2 as a function of distance from sailing line (y) were plotted on a normal graph with Froude number as a parameter for the results of the five models in Figs. 47 to 51. Since the total energy per unit surface area in a sinusoidal wave is directly proportional to the product of the square of the wave height, these plots show the distribution of the peak energy in the wave train generated by the motion of the ship as a function of distance from the sailing line with Froude number as a parameter. No scale effect is observed in models B, C, D, and E, but it is evident for the smallest model (Model A); that is, the maximum wave heights are much smaller for the model at the same relative distance y/L as compared to other models. This effect also was observed by Sorensen (55).

The values of $(Hm/d)^2$ have been computed from the results of

Sorensen and are plotted as a function of distance y/L for various Froude numbers in Figs. 52 to 55 on log-log paper. Each figure corresponds to Froude numbers which do not differ significantly. A power relationship between the parameters $(Hm/d)^2$ and y/L is suggested from these plots. The exponents in the power relationship vary between -0.48 to -0.60, twice the power of y/L in the plots of Hm/d versus y/L made by Sorensen in his Figs. 24-A,B to 27-A,B.

Havelock (11) and Ursell (52) have predicted that the amplitudes of successive diverging wave crests at the cusp locus line will decrease at a rate that is inversely proportional to the cube root of the distance from the point of disturbance, i.e.,

$$hc_d \propto (y)^{-1/3}$$

or

$$hc_d^2 \propto (y)^{-2/3}$$

The scale effects results of Sorensen show that the exponent varies between -0.48 to -0.60 for the tests in deep water, and this would vary between -0.63 to -0.78 in shallow water.

The results of the present investigation with the Mariner model in deep water apparently do not suggest any such relationship due to larger scatter in the values of $(Hm/d)^2$ than in the values of (Hm/d) themselves. The log-log plots of Hm/d versus y/L for these conditions, however, show an approximate power relationship with the exponent varying widely from -0.214 to -0.594.

The shallow-water test results with the Mariner model show the

power relationship between either Hm/d or $(Hm/d)^2$ and y/L to exist for some Froude numbers, but appears to be non-existent at certain other Froude numbers as described earlier. The shallow-water results with the Cruiser model do not show the existence of any such relationship. It may, therefore, appear that the variation of the diverging wave heights with respect to ship speed at a given distance from the sailing line, depend upon the form and size of the ship hull. In these tests, the size of the Mariner model was 5.9 ft. long and that of the Cruiser model was 4.06 ft. long. Their hull forms were, however, significantly different (see Figs. 1, 2, and 3).

In Fig. 56 the values of Hm^2 are plotted as a function of distance from the sailing line for the Cruiser model in deep water ($d = 25''$) with Froude number as a parameter. In Fig. 57 the prototype values of Hm^2 for the Cruiser under shallow-water conditions are plotted as a function of its speed in knots. The values have been obtained from test results by the application of model laws. The values represent the peak wave energy at a distance of 250 ft. from the sailing line with a water depth of 5.5 ft. in the channel.

VI. SUMMARY AND CONCLUSIONS

The main conclusions that can be drawn from these limited studies are summarized as follows:

1. The literature review on the method of calculation of a ship's wave making resistance shows that the method is based on the evaluation of the total wave energy produced by the ship per unit of time. The energy expended in maintaining the waves generated due to the ship's motion must come from the ship. Therefore, that portion of the ship's resistance which is absorbed in raising and maintaining a train of waves is called the wave resistance. The methods proposed by Havelock (13,16), Eggers (5), Sharma (51,50) and others using the concept of a free wave system provide a means of computing the flow of energy either across transverse or longitudinal planes, and thus, evaluate the ship's wave resistance. This can, therefore, be effectively used to compare the wave resistance of different ships or equivalently the wave energy in the wave train produced by different ships in a given channel. The wave resistance will, however, be independent of distance of the sections, where wave profiles are given, as there is no energy loss between sections except for viscous dissipation, which is negligibly small. Since the purpose of this investigation was to determine the variation of peak energy or the variation of energy density, i.e. the energy per unit surface area with distance from the sailing line, the wave resistance was not calculated by using the methods presented in the literature that were reviewed.

2. The wave records taken on tape and plotted on the computer for both the Mariner and the Cruiser models (Figs. 58 to 64) show the profiles of the waves to be significantly different in shallow and in deep water. In shallow water near the sailing line (i.e. 2.95 ft.) there is a deep and wide trough following the first bow wave. The first bow wave is absent in the profile. The stereophotographs of Sorenson (55) in shallow water presented in his Figs. 29-30 for Froude numbers of 0.85 and 0.91 show that the first bow wave extends approximately to a half ship length away from the sailing line. The location of a wave gauge close to the sailing line will show the first bow wave.

3. The long surge ahead of the ship and the deep wide trough present under shallow water conditions at the first gauge location show considerable contribution to energy density at the low frequency range in the Fourier analysis method done with the first set of eight results. This contribution at low frequency, corresponding to a long wave period defined in terms of record length, is absent at the other gauge locations.

4. The Fourier analysis method showed little contribution to energy density at low frequency range, the deep wide trough being absent under these conditions.

5. The variation of energy density or the mean square wave height in wave trains of equal length with distance from the sailing line is shown in Fig. 15 as obtained from the first

set of 8 test runs. This provides information on the rate of decrease of the energy per unit of surface area of the wave train as the waves are dispersed away from the point of generation. The results are not sufficient to arrive at any definite conclusion. The second set of data taken on tape could not be processed due to certain changes made by the Computer Center in the Long Blok program. However, from the point of view of possible erosive action of the wave train, the energy of the maximum wave and its orientation are perhaps more important. Stereophotographs of the waves with a coverage of a larger area would provide the desired information.

6. The main conclusions drawn from the results of the second set of tests with the Mariner model in shallow and deep water and the Cruiser model in shallow water are the following: (Havelock (11) and Ursell (62) made the theoretical prediction that the wave elevations along the cusp locus line would decrease at a rate inversely proportional to the cube root of the distance from the point of wave generation, i.e. $hc_d \propto y^{-1/3}$. The results of Sorensen (55) from the parabolic model tests confirmed the prediction quite well. The results of the present investigation with the Mariner model in deep water showed the power to vary from -0.214 to -0.594 with a wide scatter in the results. The variation of $(\frac{Hm}{d})^2$ as a function of distance do not show the existence of any power relationship.

The shallow-water test results with the Mariner model show the exponent m in the relation $(\frac{Hm}{d})^2 \propto (y/L)^m$ to vary between -0.665 to -0.820 for some Froude numbers and for some other Froude numbers the results are too scattered to suggest any power relationship. The rate of decrease of the peak wave elevations at the cusp locus line is more rapid for the Cruiser model as compared to that with the Mariner model and no power relationship appears to fit the data. These results, therefore, lead to the conclusion that the variation of the maximum wave elevations at the cusp locus line with distance from the point of wave generation depend on the form of the ship's hull.

7. From the test results with the Mariner model in deep water in the Froude number range of 0.27 to 0.64, the relationship between the peak wave elevation and the Froude number was of the form $(\frac{Hm}{d}) = C\ (F_{r_d})^m$. The coefficient of proportionality C varies with the distance from the sailing line. The value of the exponent m is found to be approximately constant and is equal to 2.8 for y/L = 0.5.

   The shallow-water test results indicate the value of the exponent m to be much higher in the range of Froude numbers in which the tests were conducted.

8. The increase of peak wave elevation at a distance from the point of wave generation with the increase of Froude number or the speed of the ship is more rapid in case of shallow water than with deep water. The results of tests with the Mariner model both in deep water and shallow water and the

results of the Cruiser model in shallow water confirm this.

9. The peak elevations increase very rapidly after a Froude number of about 0.75 has been reached in the case of the Mariner model in shallow water. For the Cruiser model, the increase in peak wave elevations with ship speed is less rapid and the transition occurs at a Froude number of about 0.86. This suggests the dependence of the wave characteristics on the hull form.

10. The half-period corresponding to the maximum wave height increases with Froude number both in shallow and deep water. The increase is more rapid in the case of shallow water. The peak value of the half-period was not reached as the Froude numbers were in the subcritical range. Johnson (27) found the half-period to increase to a peak value with increase in Froude number and with further increase in speed or the Froude number in the super-critical range, the half-period decreased. The half-period was found to be independent of the distance from the point of wave generation.

VII. SUGGESTIONS FOR FUTURE STUDY

On the basis of this preliminary investigation, the following studies are suggested for future investigations:

1. The design of banks of navigable canals against erosive action of the ship waves involves the knowledge of the magnitude and the angle of incidence of the waves on the banks. The wave elevations are a function of the distance from the point of wave generation, i.e. the distance from the sailing line. Further, the wave elevation at a given distance as a function of ship speed is dependent on the ship's form and size. Therefore, the waves generated by different ship forms and sizes should be measured to be able to relate the model results to prototype conditions.
2. The stereophotogrammetric method might be used to measure the wave configurations to determine the energy density and peak energy as a function of distance from the sailing line.
3. Tests with models of different shape and size may be made in order to predict squat and backflow in navigable canals to design bank revetment.

ACKNOWLEDGMENT

This study was the continuation of a project supported by a contract with the U. S. Army, Corps of Engineers, Coastal Engineering Research Center, Washington, D. C. The author is grateful to Professor J. W. Johnson for his valuable guidance, suggestions, and encouragement throughout the study. Thanks are also due to Professors J. Wehausen and R. L. Wiegel for their valuable suggestions and comments. Mr. Jim Allison, Electronic Technician, contributed greatly in his invaluable assistance in maintaining the electronic equipment in operation, and for his assistance in obtaining data on magnetic tape. The writer is also thankful to Mr. Harry Nichandros, a graduate student, who assisted in the early part of the study and who also conducted preliminary tests to calibrate the model towing system.

REFERENCES

1. Bidde, D.D., Ship Waves in Shoaling Water. Hyd. Eng. Lab., Univ. of California, Berkeley. Report no. HEL-12-6. January, 1968.

2. Birkhoff, G., B.V. Korvin - Kroukovsky, and J. Kotik, Theory of Wave Resistance of Ships. Society of Naval Architects and Marine Engrs., Vol. 62, 1954, pp. 359-384.

3. Carlson, E.J., Gravel Blanket Required to Prevent Wave Erosion. Jour., Hydraulic Division, Amer. Soc. Civil Engrs., May 1959, pp. 109-145.

4. DeBruyn, H.C.P. and A.G. Maris, Form of Cross Section and System of Bank Protection to be Adopted on Canals and Rivers. 16th International Congress of Navigation, Brussels, 1st Section, 1st Communication, Paper 39, 1935, pp. 1-24.

5. Eggers, K., Uber die Ermittlung des Wellenwiderstandes eines Schiffsmodells durch Analyse seines Wellensystems (Teil 1 und 2), Schiffstechnik 9 (No. 46): 79-84, 85 (1962); 10 (No. 52): 93-106 (1963).

6. Franzius, O., Waterways Engineering. The Technology Press, Mass. Inst. of Tech., Cambridge, 1936, p. 431.

7. Froude, R.E., On the Leading Phenomena of the Wave-Making Resistance of Ships. Trans., Inst. of Naval Arch., Vol. 22, 1881, pp. 221-224.

8. Froude, W., On Experiments Upon the Effect Produced on the Wave-Making Resistance of Ships by Length of Parallel Middle Body. Trans., Royal Inst. of Naval Arch., Vol. 18, 1877, pp. 77-87.

9. Gadd, G.E. and Hogben, N., An Appraisal of the Ship Resistance Problem in the Light of Measurements of the Wave Pattern. International Seminar on Theoretical Wave-Reistance, University of Michigan, Vol. 1, August, 1963, pp. 273-349.

10. Guilloton, R.S., The Waves Generated by a Moving Body. Trans., Royal Inst. of Naval Arch., Vol. 102, 1960, pp. 157-173.

11. Havelock, T.H., The Propagation of Groups of Waves in Dispersive Media, with Application to Waves on Water Produced by a Travelling Disturbance. Proc., Royal Soc. of London, Series A, 1908, pp. 398-430.

12. Havelock, T.H., The Propagation of Disturbances in Dispersive Media, Cambridge University Press, 1914, p. 4.

13. Havelock, T.H., Some Aspects of the Theory of Ship Waves and Wave Resistance. Proc., Royal Soc. of London, Series A, Vol. 108, 1925, pp. 3-18.

14. Havelock, T.H., Ship Waves: The Calculation of Wave Profiles. Proc., Royal Soc. of London, Series A, Vol. 135, 1931, pp. 1-13.

15. Havelock, T.H., Ship Waves: Their Variation with Certain Systematic Changes of Form. Proc., Royal Soc. of London, Series A, Vol. 136, 1932, pp. 465-471.

16. Havelock, T.H., The Calculation of Wave Resistance. Proc., Roy. Soc. (London) Ser. A, 1934, 144:514-521.

17. Havelock, T.H., Ship Waves: The Relative Efficiency of Bow and Stern. Proc., Royal Soc. of London, Series A, Vol. 149, 1935, pp. 417-426.

18. Havelock, T.H., Wave Patterns and Wave Resistance. Trans., Inst. of Naval Architects, Vol. 76, 1934, pp. 430-442.

19. Havelock, T.H., Wave Resistance Theory and Its Application to Ship Problems. Trans., Society of Naval Architects and Marine Engrs., Vol. 59, 1951, pp. 13-24.

20. Hay, Duncan, Ship Waves in Navigable Waterways. Hyd. Eng. Lab., University of California, Berkeley. Report No. HEL-12-5. September, 1967.

21. Hertzberg, R., Wave-Wash Control on Mississippi River Levees. Trans. Amer. Soc. Civil Engrs., Vol. 119, 1954, pp. 625-638.

22. Hogner, E., A Contribution to the Theory of Ship Waves. Arkiv for Matematik, Astronomi och Fysik, band 17, No. 12, 1922-23, pp. 1-50.

23. Hovgaard, W., Diverging Waves. Trans., Inst. of Naval Arch., Vol. 51, 1909, pp. 251-261.

24. Hulman, L.G., Erosion on Riprapped Embankments by Oblique Waves. M.S. Thesis, Univ. of Iowa, Aug. 1967.

25. Inui, Teturo, On Deformation, Wave Patterns and Resonance Phenomena of Water Surface Due to a Moving Disturbance. Proc., Physico-Mathematical Soc. of Japan, Vol. 18, No. 2, 1936, pp. 60-98.

26. Inui, Takao, Wave-Making Resistance of Ships. Trans., Soc. of Naval Arch. and Marine Engrs., Vol. 70, 1962, pp. 283-353.

27. Johnson, J.W., Ship Waves in Navigation Channels. Proc., Sixth Conf. on Coastal Engr., Chap. 40, Berkeley, Calif., 1958, pp. 666-690.

28. Johnson, J.W., Waves in Shoaling Waters. Proc. of 11th Conf. on Coastal Engineering. London, Sept., 1968. Vol. 2, Part 4, pp. 1488-1498.

29. Krey, H., Fahrt der Schiffe auf beschranktem Wasser. Schiffbau. Berlin, 1913.

30. Krey, H. and R. Winkel, Experiments on Models of Canals. Hydraulic Laboratory Practice, Amer. Soc. of Mech. Engrs., 1929, pp. 262-264.

31. Lacmann, O., Die Photogrammetrie in ihrer Anwendung auf Nicht-Topographischen Gebieten. Hirzel Verlag, Leipzig, 1950.

32. Lamb, Sir. H., Hydrodynamics. Dover Publications, Sixth Ed., New York, 1932, pp. 433-440, 623-624.

33. Lewis, William H., The Foreshore Erosion Problem in the Lower Reaches of the Mississippi River. Shore and Beach, Vol. 24, No. 1, 1956, pp. 13-15.

34. Lighthill, M.J., Group Velocity. J. Inst., Maths. Applics. 1, pp. 1-28.

35. Lord Kelvin (Sir William Thomson), Stationary Waves in Flowing Water. Philosophical Magazine, Vol. 22, 1886.

36. Lord Kelvin (Sir William Thomson), On Ship Waves. Proc., Inst. of Mech. Engrs., 1887, pp. 409-433.

37. Lord Kelvin (Sir William Thomson), Deep-water Ship Waves. Proc., Royal Soc. of Edinburg, 1904.

38. Lunde, J.K., On the Linearized Theory of Wave Resistance for Displacement of Ships in Steady and Accelerated Motion. Trans., Society of Naval Architects and Marine Engrs., Vol. 59, 1951, pp. 25-76.

39. Marriner, W.W., Deductions from Recent Experiments on the Influence of the Depth of Water on Speed. Trans., Inst. of Naval Arch., Vol. 47, 1905, pp. 344-346.

40. Marussi, A., Stereophotogrammetric Apparatus for the Study of Waves Generated by Ship Models. International Shipbuilding Progress, Vol. 2, No. 15, Rotterdam, 1955, pp. 537-538.

41. Mizuno, T. and Wehausen, J.V., Determination of a Ship's Wave Resistance in a Canal from Measurements of Wave Profiles. Hyd. Eng. Lab., Univ. of California, Berkeley, Report No. HEL-12-4. December, 1966.

42. Morison, J.R., Measurement of Wave Heights by Resistance Elements. Bull., Beach Erosion Board, Corps of Engineers, U.S. Army, Vol. 3, No. 3, 1949, pp. 16-22.

43. Newman, J.N., The Determination of Wave Resistance from Wave Measurements Along a Parallel Cut. Proc. International Seminar on Theoretical Wave Resistance, Ann Arbor, Michigan, Aug. 1963, pp. 353-376, 379.

44. Peters, A.S., A New Treatment of the Ship Wave Problem. Comm. on Pure and Applied Math., Vol. 2, 1949, pp. 123-148.

45. Pien, P.C., and Moore, W.L., Theoretical and Experimental Study of Wave-Making Resistance of Ships. Proc. International Seminar on Theoretical Wave Resistance, Ann Arbor, Michigan, Aug. 1963, pp. 133-182, 188.

46. Rankine, W.J.M., On Waves Which Travel Along with Ships. Trans., Inst. of Naval Arch., Vol. 9, 1968, pp. 275-281.

47. Robb, A.M., Theory of Naval Architecture. Charles Griffen and Co., Ltd., London, 1952.

48. Rosik, J., Form of Cross-Section and System of Bank Protection to be Adopted on Canals and Rivers. 16th International Congress of Navigation, Brussels, 1st Section, 1st Communication, Paper 40, 1935, p. 4.

49. Schijf, J.B., Protection of Embankments [illegible] in Inland and Maritime Waters, and in Overflow or Weirs. XVII International Navigation Congress, Lisbon, Section I, 1949, pp. 61-78.

50. Sharma, S.D., An Attempted Application of Wave Analysis Techniques to Achieve Bow-Wave Reduction. 6th Symposium Naval Hydrodynamics, Washington, D.C. ACR-136. Office of Naval Research, Department of the Navy.

51. Sharma, S.D., A Comparison of the Calculated and Measured Free-Wave Spectrum of an Inuid in Steady Motion. Proc. International Seminar on Theoretical Wave Resistance, Ann Arbor, Michigan, Aug. 1963, pp. 201-257, 270.

52. Sharma, S.D., Untersuchungen uber den Zahigkeits- und Wellenwiderstand mit besonderer Berucksichtigung ihrer Wechselwirkung. Institut fur Schiffbau der Universitat Hamburg, Report 138, Dec. 1964, pp. 442-451.

53. Sharma, S.D., Zur Problematik der Aufteilung des Schiffswiderstandes in zahigkeits- und wellenbedingte Anteile. Jahrbuch STG, 59:458-504, 1965.

54. Shor, S.W.W., A Fourier Transform Method for Calculating Wave-Making Resistance from Wave Height on a Line Parallel to a Ship's Track. Proc., International Seminar on Theoretical Wave Resistance, Ann Arbor, Michigan, Aug. 1963, pp. 601-615.

55. Sorensen, R.M., "Ship Waves," Technical Report HEL-12-2, Hyd. Eng. Lab., Univ. of Calif., Berkeley, 1966.

56. Sorensen, R.M., Investigation of Ship-Generated Waves. Jour., Waterways and Harbors Div., Proc., Amer. Soc. Civil Engrs., Vol. 93, No. WW1, Feb. 1967.

57. Sorensen, R.M., Stereophotogrammetric Analysis of Wave Surfaces. Journal of Hyd. Div., ASCE, Vol. 94, HY1, Jan. 1968, pp. 181-194.

58. Sorensen, R.M., Waves Generated by Model Ship Hull. Journal Waterways and Harbors Div., ASCE, No. WW4, Nov. 1969, pp. 513-538.

59. Takahei, T., A Study on the Waveless Bow (Parts 1 and 2). J. SNA Japan. 108: 289-297 (1960); 109: 203-217 (1961).

60. Taylor, D.W., The Speed and Power of Ships. U.S. Govt. Printing Office, Washington, D.C., 1943, pp. 26-28.

61. Tothill, J.T., Ships in Restricted Channels -- A Correlation of Model Tests, Field Measurements and Theory. National Research Council, Ottawa, Canada. Div. of Mech. Engr. Ship Section. Report No. MB-264, Jan. 1966.

62. Ursell, F., On Kelvin's Ship-Wave Pattern. Jour. Fluid Mech., Vol. 8, Part 3, 1960, pp. 418-431.

63. Wiegel, R.L., Parallel Wire Resistance Wave Meter. Proc., First Conference on Coastal Engineering Instruments. Council on Wave Research, Berkeley, Calif., 1956, pp. 39-43.

64. Wortman, H., Construction of Navigation Canals Affording Operation at High Speed. 6th International Congress of Navigation, 1st Question, Paper 2, 1894, p. 5.

APPENDIX I

COMPARISON OF PEAK ENERGY OF A MARINER CARGO SHIP AND A CRUISER UNDER PROTOTYPE CONDITIONS

The test results obtained with the Mariner model in shallow water (d = 4 1/8") and those with the Cruiser model in deep water (d = 24 7/8") can be used to compare the peak wave energy at any particular distance from the sailing line for both ships under prototype conditions by using the scales of the models. Since the Cruiser model was not available when the second set of tests were performed, sufficient results with this model in deep water are not available for a wide range of Froude numbers. A typical numerical example is shown below for the available data. The numerical example shows that the peak wave energy at a distance of 500 ft. from the sailing line due to the passage of the Mariner cargo ship at a speed of 15 knots in a water depth of 33 ft., can be as high as 473 times that due to the Cruiser moving at a speed of 9.5 knots at the same distance from the sailing line and at the same water depth. Unfortunately, there are no data for the Cruiser model at a speed of 15 knots in deep water to compare the energies at the same speed of 15 knots for the Mariner model.

Another comparison has been made between the maximum wave energies due to the Mariner at a speed of 11.5 knots and due to the Cruiser at a speed of 9.5 knots. These are almost equal (i.e. ratio = 0.88).

The peak wave energies due to the Cruiser at a distance of 250 ft. from the sailing line and at a water depth of 5.5 ft. for

different speeds are taken from Figs. 33 to 40 and presented in Table A.

Numerical Example

(a) Cruiser model tests in deep water:

$d_{Model} = 25''$

$d_{Prototype} = \frac{25}{12} \times 16 = \underline{33.3 \text{ ft.}}$

$V_{Model} = 4.0 \text{ ft./sec.}$

$V_{Prototype} = 4.0 \times 4 = 16.0 \text{ ft./sec.} = \underline{9.5 \text{ knots}}$

The peak energy which is proportional to the square of the maximum wave height is obtained from Fig. 56.

$(Hm^2)_{Model}$ at a distance of 31.25 ft. from the sailing line by extrapolation

$= 3.5 \times 10^{-4} \text{ ft.}^2$.

$(Hm^2)_{Prototype} = (3.5 \times 10^{-4}) \times 16^2 = \underline{896 \times 10^{-4} \text{ ft.}^2}$

at a distance of $31.25 \times 16 = 500$ ft. from sailing line.

(b) Mariner model tests in shallow water:

$d_{model} = 4\ 1/8''$

$d_{prototype} = \frac{33}{8 \times 12} \times 96 = 33 \text{ ft.}$

$V_{prototype} = 15 \text{ knots}$ - $V_{Model} = 2.58 \text{ ft./sec.}$

Prototype distance = 500 ft. -- Model distance = 5.21 ft.

From Fig. 36.

By interpolation.

$\left(\frac{Hm}{d}\right)^2_{model} = 390 \times 10^{-4} \text{ ft.}^2$ at $y/L = 0.88$ or $y_{model} = 5.21$

TABLE A. CRUISER MODEL IN SHALLOW WATER

y_{model} = 15.625 ft. d_{model} = 4 1/8"

$y_{prototype}$ = 250 ft. $d_{prototype}$ = 5.5 ft.

Model Speed ft/sec	Prototype Ship Speed Knots	F_{r_d}	$(\frac{Hm}{d})_{Model}$ $\times 10^{-4}$ ft^2	$(Hm^2)_{Prototype}$ $\times 10^{-4}$ ft^2	$(Hm^2)_{Prototype}$ $\times 10^{-4}$ ft^2
3.10	7.35	0.94	270.0	32.0	8180.
2.96	7.0	0.90	300.0	35.6	9110.
2.90	6.85	0.87	100.0	11.9	3220.
2.80	6.75	0.85	37.0	3.4	870
2.60	6.15	0.78	5.0	0.59	151.
2.50	5.90	0.75	1.9	0.22	56.5
2.40	5.70	0.72	0.75	0.09	22.8
2.15	5.10	0.65	0.09	0.01	2.6

$(Hm)^2_{model} = 46 \times 10^{-4}$ ft.^{2}

$(Hm)^2_{prototype} = 46 \times (96)^2 \times 10^{-4}$ ft.^{2} at $y_{prototype} = 500$ ft.

(c) Prototype comparison:

The ratio of the peak energies for the two vessels under the above prototype conditions - namely, at 500 ft. from the sailing line, water depth of 33 ft., with the Cruiser speed being 9.5 knots and the Mariner speed being 15 knots is

$$\frac{(Hm) \text{ Prototype for Mariner}}{(Hm^2) \text{ Prototype for Cruiser}} = \frac{46 \times (96)^2 \times 10^{-4}}{3.5 \times (16)^2 \times 10^{-4}} = 473$$

Another comparison between the Cruiser and the Mariner is made as follows when the Mariner speed is 11.5 knots instead of 15 knots:

$V_{model} = 1.97$ ft./sec.

$V_{prototype} = 11.5$ knots

$(Hm^2)_{model} = 0.086 \times 10^{-4}$ ft.^{2} at 5.21 ft.

$(Hm^2)_{prototype} = 0.086 \times (96)^2 \times 10^{-4}$ ft.^{2} at 500 ft.

$= 792 \times 10^{-4}$ ft.^{2}

or the ratio of energies is:

$$\frac{(Hm^2) \text{ Prototype for Mariner}}{(Hm^2) \text{ Prototype for Cruiser}} = \frac{792 \times 10^{-4}}{3.5 \times 16^2 \times 10^{-4}}$$

$$= \frac{792}{895} = 0.88$$

) Prototype peak energy of Cruiser

Using Fig. 57, the peak energy at a distance of 250 ft. from the sailing line with the Cruiser moving at different speeds in water 5.5 ft. deep is presented in the following

table:

TABLE B. Hm^2 AT DIFFERENT SPEEDS OF THE CRUISER IN SHALLOW WATER:

SPEED OF CRUISER (KNOTS)	Hm^2 $Ft.^2 \times 10^{-4}$
5.0	1.6
6.0	90.0
7.0	900.0

TABLE 3a. RESULTS OF MARINER MODEL TESTS IN DEEP WATER

Mariner Model
Scale = 1:96
Length = 5.90 ft.

Deep Water
Water Depth d = 21-7 8"
Date: Nov. 21, 1969, set 2

RECORD NO.	RUN NO.	SPEED OF SHIP FT SEC	Fr_d	y/L = 0.5 Hm FT × 10^{-2}	Hm^2 FT^2 × 10^{-4}	Hm d × 10^{-2}	(Hm d)^2 × 10^{-4}	T 2 SEC	y/L = 1.5 Hm FT × 10^{-2}	Hm^2 FT^2 × 10^{-4}	Hm d × 10^{-2}	(Hm d)^2 × 10^{-4}	T 2 SEC	y/L = 2.5 Hm FT × 10^{-2}	Hm^2 FT^2 × 10^{-4}	Hm d × 10^{-2}	(Hm d)^2 × 10^{-4}	T 2 SEC	y/L = 3.5 Hm FT × 10^{-2}	Hm^2 FT^2 × 10^{-4}	Hm d × 10^{-2}	(Hm d)^2 × 10^{-4}	T 2 SEC
35	1	1.80	0.59	12.50	156.0	6.03	36.4	0.40	11.1	123.0	5.35	28.6	0.40	10.0	100.0	4.81	23.2	0.40	9.2	84.6	4.41	19.7	0.40
36	2	1.1	0.63	12.6	159.0	6.07	36.8	0.40	11.0	121.0	5.30	28.1	0.40	10.2	104.0	4.91	24.1	0.40	9.2	84.6	4.41	19.7	0.40
37	3	1.0	0.61	12.50	156.0	6.03	36.4	0.40	11.4	130.0	5.50	30.1	0.40	10.0	100.0	4.81	23.2	0.40	9.2	84.6	4.41	19.7	0.40
38	4	1.0	0.61	12.40	154.0	5.97	35.7	0.40	11.8	139.1	5.70	32.5	0.40	10.3	106.0	4.96	24.6	0.40	9.2	84.6	4.41	19.7	0.40
39	5	5.25	0.61	12.50	156.0	6.03	36.4	0.40	11.3	128.0	5.45	29.7	0.40	10.0	100.0	4.81	23.2	0.40	9.4	89.4	4.51	20.6	0.40
40	6	5.0	0.61	11.20	125.5	5.40	29.2	0.40	9.4	88.4	4.54	20.6	0.40	8.50	72.3	4.10	16.8	0.40	7.8	60.8	3.76	14.1	0.40
41	7	1.8	0.59	10.40	108.0	5.01	25.1	0.34	7.5	56.3	3.62	13.1	0.36	6.50	42.3	3.14	9.9	0.40	6.2	38.4	3.0	9.0	0.40
42	8	1.72	0.58	10.0	100.0	4.81	23.2	0.34	8.0	64.0	3.86	14.9	0.38	6.50	42.3	3.14	9.9	0.40	6.3	39.7	3.04	9.2	0.40
43	9	1.8	0.59	10.0	100.0	4.81	23.2	0.36	7.8	60.8	3.76	14.1	0.40	6.40	41.0	3.08	9.5	0.40	6.2	38.4	3.0	9.0	0.40
44	10	1.8	0.59	10.1	102.0	4.86	23.7	0.36	7.6	57.7	3.66	13.4	0.40	6.30	39.7	3.04	9.2	0.40	6.3	39.7	3.01	9.2	0.40
45	11	1.1	0.42	3.5	12.25	1.69	2.86	0.32	3.2	10.2	1.54	2.4	0.30	1.80	3.24	0.87	0.75	0.30	1.5	2.25	0.72	0.5	0.30
46	12	0.46	0.43	4.0	16.0	1.93	3.7	0.24	3.2	10.2	1.54	2.4	0.30	2.10	4.41	1.01	1.02	0.30	1.5	2.25	0.72	0.5	0.30
47	13	0.1	0.42	4.0	16.0	1.93	3.7	0.24	3.4	11.6	1.64	2.7	0.30	2.0	4.0	0.96	0.92	0.30	1.7	2.89	0.82	0.67	0.30
48	14	0.5	0.43	4.0	16.0	1.93	3.7	0.24	3.1	9.6	1.50	2.2	0.30	2.30	5.3	1.11	1.23	0.30	1.9	3.61	0.92	0.67	0.30
49	15	1.0	0.37	1.7	2.89	0.82	0.7	0.20	1.3	1.69	0.63	0.4	0.20	0.90	0.81	0.43	0.18	0.20	0.8	0.64	0.40	0.16	0.20
50	16	OUT OF SCALE																					
51	17	1.17	0.51	6.0	36.0	2.9	8.4	0.30	6.0	36.0	2.90	8.4	0.30	4.7	22.0	2.26	5.1	0.30	4.6	21.2	2.22	4.9	0.30
52	18	1.20	0.51	6.0	36.0	2.9	8.4	0.30	5.8	33.6	2.80	7.8	0.30	5.2	27.1	2.50	6.2	0.30	4.7	22.1	2.26	5.1	0.30
53	19	1.20	0.51	6.0	36.0	2.9	8.4	0.30	5.7	32.5	2.74	7.5	0.30	4.8	23.0	2.32	5.4	0.30	4.6	21.2	2.22	4.9	0.30
54	20	0.8	0.44	4.6	21.2	2.21	4.9	0.30	4.3	18.5	2.06	4.2	0.30	3.7	13.7	1.78	3.2	0.30	3.7	13.7	1.78	3.2	0.30
55	21	0.6	0.44	4.6	21.2	2.21	4.9	0.30	4.3	18.5	2.06	4.2	0.30	3.7	13.7	1.78	3.2	0.30	3.7	13.7	1.78	3.2	0.30
56	22	0.62	0.44	4.7	22.1	2.26	5.1	0.30	4.4	19.4	2.12	4.5	0.30	3.7	13.7	1.78	3.2	0.30	3.8	14.4	1.83	3.3	0.30
57	23	0.60	0.44	4.8	23.05	2.30	5.3	0.30	4.2	17.6	2.02	4.1	0.30	3.5	12.25	1.68	2.8	0.30	3.8	14.4	1.83	3.3	0.30
58	24	2.76	0.34	1.9	3.61	0.90	0.8	0.20	1.4	1.96	0.67	0.45	0.20	1.0	1.0	0.48	0.23	0.20	1.0	1.0	0.48	0.23	0.20
59	25	2.80	0.34	1.8	3.24	0.87	0.75	0.20	1.4	1.96	0.67	0.45	0.20	1.0	1.0	0.48	0.23	0.20	0.8	0.64	0.38	0.14	0.20
60	26	2.75	0.34	1.8	3.24	0.87	0.75	0.20	1.4	1.96	0.67	0.45	0.20	1.0	1.0	0.48	0.23	0.20	1.0	1.0	0.48	0.23	0.20
61	27	2.81	0.35	1.8	3.24	0.87	0.75	0.20	1.6	2.56	0.77	0.59	0.20	1.0	1.0	0.48	0.23	0.20	0.90	0.81	0.43	0.18	0.20
62	28	2.30	0.28	0.80	0.64	0.38	0.14	0.18	0.6	0.36	0.29	0.08	0.18	0.25	0.06	0.12	0.01	0.18	0.20	0.04	0.09	0.008	0.18
63	29	2.21	0.27	0.85	0.72	0.41	0.16	0.18	0.4	0.16	0.19	0.04	0.18	0.20	0.04	0.09	-	0.18	0.15	0.02	0.07	0.005	0.18
64	30	2.25	0.28	0.75	0.56	0.36	0.13	0.18	0.4	0.16	0.19	0.04	0.18	0.25	0.06	0.12	0.01	0.18	0.15	0.02	0.07	0.005	0.18
65	31	2.21	0.27	0.80	0.64	0.38	0.14	0.18	0.4	0.16	0.19	0.04	0.18	0.25	0.06	0.12	0.01	0.18	0.15	0.02	0.07	0.005	0.18
66	32	3.15	0.39	2.40	5.76	1.15	1.25	0.2	1.9	3.61	0.90	0.80	0.2	1.0	1.0	0.48	0.28	0.20	0.95	0.9	0.45	0.19	0.20
67	33	3.10	0.38	2.40	5.76	1.15	1.25	0.2	1.7	2.89	0.82	0.70	0.2	0.9	0.81	0.43	0.18	0.20	0.90	0.81	0.43	0.18	0.20
68	34	3.16	0.39	2.40	5.76	1.15	1.25	0.2	1.8	3.24	0.87	0.75	0.2	0.9	0.81	0.43	0.18	0.20	1.0	1.0	0.48	0.23	0.20
69	35	3.15	0.39	2.5	6.25	1.20	1.30	0.2	1.7	2.89	0.82	0.70	0.2	1.0	1.0	0.48	0.23	0.20	0.90	0.81	0.43	0.18	0.20

TABLE 3b. RESULTS OF CRUISER MODEL TESTS IN DEEP WATER

Cruiser Model - Deep Water d = 25" - July 18, 1969, set 1

RECORD NO.	RUN NO.	SPEED OF SHIP FT SEC	Fr_d	y/L = 0.725 2.95' Hm FT × 10^{-2}	Hm^2 FT^2 × 10^{-1}	Hm d × 10^{-2}	(Hm d)^2 × 10^{-4}	T 2 SEC	y/L = 8.8' Hm FT × 10^{-2}	Hm^2 FT^2 × 10^{-1}	Hm/d × 10^{-2}	(Hm/d)^2 × 10^{-4}	T/2 SEC	y/L = 14.7' Hm FT × 10^{-2}	Hm^2 FT^2 × 10^{-4}	Hm d × 10^{-2}	(Hm d)^2 × 10^{-4}	T 2 SEC
35	2	1.80	0.19	7.3	53.3	3.50	12.2	0.26	1.0	16.0	1.92	3.7	0.26	3.5	12.2	1.7	2.9	0.26
36	3	3.90	0.17	6.25	39.1	3.00	9.0	0.24	4.58	21.0	2.2	1.8	0.24	3.8	14.4	1.8	3.2	0.24
37	1	3.38	0.11	1.2	17.6	2.02	1.1	0.20	2.9	8.4	1.4	2.0	0.20	2.4	5.8	1.1	1.2	0.20

TABLE 1 RESULTS OF MARINER MODEL TESTS IN SHALLOW WATER

Mariner Model
Scale = 1:96
Length = 5.90 ft.
λ = 2.43

Shallow Water
Water Depth d = 4-1 ft
Date July 16, 1969, set 1

RECORD NO.	RUN NO.	SPEED OF SHIP FT SEC	F_{nd}	y L = 0.5				y L = 1.5				y L = 2.5				y L = 3.5			
				Hm FT x 10^{-2}	Hm^2 FT^2 x 10^{-1}	Hm d x 10^{-2}	$(Hm\ d)^2$ x 10^{-3}	T/2 SEC	Hm FT x 10^{-2}	Hm^2 FT^2 x 10^{-3}	Hm d x 10^{-2}	$(Hm.d)^2$ x 10^{-3}	T/2 SEC	Hm FT x 10^{-2}	Hm^2 FT^2 x 10^{-3}	Hm d x 10^{-2}	$(Hm\ d)^2$ x 10^{-4}	T 2 SEC	Hm FT x 10^{-2}	Hm^2 FT^2 x 10^{-3}	Hm d x 10^{-2}	$(Hm\ d)^2$ x 10^{-4}	T 2 SEC
21	1	2.44	0.71	1.5	2.25	4.36	19.0	1.1 ,0.2	1.1	1.21	3.52	12.4	0.20	0.90	0.81	2.62	6.86	0.2					
22	2	2.38	0.70	1.2	1.44	3.50	12.25	1.3 ,0.18	0.7	0.49	2.04	4.2	0.18	0.50	0.25	1.45	2.1	0.2					
26	3	3.66	0.80	5.0	25.0	14.55	212.0	0.5 ,0.24	3.7	13.7	19.8	116.6	0.24	2.1	4.41	6.1	37.2	0.24					
27	4	3.66	0.80	4.8	23.0	14.0	196.0	0.5 ,0.24	3.1	9.6	9.0	81.0	0.24	1.5	2.25	4.3	19.4	0.24					
28	5	3.62	0.79	3.0	9.0	8.73	76.2	0.56,0.24	0.7	0.49	2.04	4.2	0.20	0.4	0.16	1.15	1.32	0.2	AMPLIFIER DID NOT WORK				
29	6	3.58	0.77	3.0	9.0	8.73	76.2	0.5 ,0.24	1.0	1.0	2.91	8.4	0.20	0.6	0.36	1.74	3.02	0.2					
30	7	3.71	0.83	6.0	36.0	17.5	306.0	0.5 ,0.24	4.9	24.0	14.2	202.0	0.24	3.8	11.4	11.05	122.0	0.24					
32	9	3.80	0.85	6.5	72.2	24.9	620.0	0.48,0.24	5.6	31.4	16.3	266.0	0.24	4.0	16.0	11.6	134.6	0.24					
				Mariner Model											Date: Nov. 20, 1969, set 2								
23	1	2.45	0.73	2.5	6.25	7.27	52.9	0.2	1.0	1.0	2.91	8.46	0.2	0.9	0.81	2.72	7.4	0.2	0.7	0.49	2.04	4.16	0.2
24	2	2.40	0.72	1.8	3.24	5.24	27.4	0.2	1.2	1.44	3.49	12.2	0.2	1.1	1.21	3.20	10.2	0.2	0.65	0.42	1.89	3.57	0.2
25	3	2.46	0.71	1.9	3.61	5.52	30.4	0.2	1.25	1.56	3.64	13.2	0.2	1.2	1.44	3.49	12.2	0.2	0.80	0.64	2.32	5.5	0.2
26	4	2.59	0.72	2.0	4.0	5.82	33.8	0.2	1.0	1.0	2.91	8.5	0.2	1.0	1.0	2.91	8.5	0.2	0.60	0.36	1.75	3.04	0.2
28	5	2.53	0.71	2.0	4.0	5.82	33.8	0.2	1.0	1.0	2.91	8.5	0.2	1.0	1.0	2.91	8.5	0.2	0.7	0.49	2.04	4.1	0.2
27	6	2.20	0.66	1.2	1.44	3.49	12.2	0.2	0.5	0.25	1.45	2.1	0.2	0.45	0.20	1.31	1.72	0.2	0.4	0.16	1.16	1.25	0.2
29	7	2.33	0.71	1.8	3.24	5.24	27.4	0.2	1.40	1.96	4.06	16.5	0.2	1.0	1.0	2.91	8.5	0.2	0.8	0.64	2.32	5.1	0.2
30	8	2.36	0.71	1.8	3.24	5.24	27.4	0.2	1.30	1.69	3.78	14.3	0.2	1.35	1.82	3.92	15.4	0.2	0.8	0.64	2.32	5.1	0.2
31	9	NO VELOCITY		2.6	6.75	7.55	57.0	0.2	1.70	2.89	4.94	24.4	0.2	1.3	1.69	3.78	14.3	0.2	0.9	0.81	2.62	6.9	0.2
32	10	2.46	0.77	5.3	28.10	15.40	237.0	0.2	2.80	7.85	8.15	66.5	0.2	2.0	4.0	5.82	33.8	0.2	1.95	3.8	5.67	32.0	0.2
33	11	2.47	0.71	2.0	4.0	5.82	33.8	0.2	1.10	1.21	3.20	10.2	0.2	0.8	0.64	2.32	5.4	0.2	0.6	0.36	1.75	3.01	0.2
34	12	2.38	0.68	1.4	1.96	4.06	16.5	0.2	0.80	0.64	2.32	5.4	0.2	0.8	0.64	2.32	5.4	0.2	0.65	0.42	1.89	3.6	0.2
35	13	2.31	0.65	1.0	1.0	2.91	8.5	0.2	0.65	0.42	1.89	3.6	0.2	0.6	0.36	1.74	3.0	0.2	0.45	0.20	1.31	1.7	0.2
36	14	2.21	0.65	1.2	1.44	3.49	12.2	0.2	0.60	0.36	1.75	3.1	0.2	0.5	0.25	1.45	2.1	0.2	0.45	0.20	1.31	1.7	0.2
37	15	2.35	0.71	1.8	3.24	5.24	27.4	0.2	1.20	1.44	3.49	12.2	0.2	0.9	0.81	2.72	7.4	0.2	0.85	0.72	2.47	6.1	0.2
38	16	2.42	0.72	1.45	2.10	4.21	17.7	0.2	0.90	0.81	2.62	6.9	0.2	0.55	0.30	1.60	2.6	0.2	0.50	0.25	1.45	2.1	0.2
39	17	2.07	0.62	0.80	0.64	2.32	5.4	0.2	0.45	0.20	1.31	1.7	0.2	0.2	0.04	0.58	0.35	0.2	0.15	0.02	0.43	0.18	0.2
40	18	2.22	0.65	0.90	0.81	2.62	6.9	0.2	0.80	0.64	2.32	5.4	0.2	0.75	0.56	2.18	4.75	0.2	0.50	0.25	1.45	2.1	0.2
41	19	2.08	0.62	0.5	0.25	1.45	2.1	0.18	0.35	0.12	1.02	1.0	0.18	0.15	0.02	0.43	0.18	0.18	-	-	-	-	0.18
42	20	1.92	0.59	0.5	0.25	1.45	2.1	0.18	0.15	0.02	0.43	0.18	0.18	-	-	-	-	0.18	-	-	-	-	0.18
43	21	2.52	0.75	7.6	57.7	22.1	489.0	0.22	5.7	32.4	16.6	276.0	0.22	4.5	20.2	13.1	171.0	0.22	2.8	7.85	8.15	66.0	0.22
44	22	2.62	0.79	8.6	74.0	25.0	625.0	0.24	6.5	42.3	18.9	358.0	0.24	5.0	25.0	14.55	212.0	0.22	4.0	16.0	11.6	135.0	0.22
45	23	2.61	0.78	8.8	77.5	25.6	655.0	0.22	6.7	44.9	19.5	380.0	0.24	5.2	27.0	15.1	228.0	0.22	4.0	16.0	11.6	135.0	0.22
46	24	2.60	0.78	8.3	68.8	24.2	586.0	0.22	5.7	32.4	16.6	276.0	0.22	4.8	23.0	13.95	195.0	0.22	3.9	15.2	11.35	128.0	0.22
47	25	2.60	0.78	8.9	79.3	25.8	666.0	0.22	6.1	37.2	17.8	315.0	0.22	5.0	25.0	14.55	212.0	0.22	4.2	17.7	12.2	149.0	0.22
48	26	2.63	0.79	8.8	77.5	25.6	655.0	0.22	8.0	64.0	23.3	544.0	0.22	6.0	36.0	17.5	304.0	0.22	5.5	30.2	16.0	256.0	0.22
49	27	2.65	0.80	10.0	100.0	29.1	846.0	0.22	8.0	64.0	23.3	544.0	0.22	5.6	31.4	16.3	266.0	0.22	5.3	28.1	15.4	237.0	0.22
50	28	2.67	0.80	10.0	100.0	29.1	846.0	0.22	8.2	67.3	23.8	566.0	0.22	6.2	38.4	18.0	324.0	0.22	4.5	20.2	13.1	172.0	0.22
51	29	2.65	0.80	9.2	84.60	26.7	712.0	0.22	8.0	64.0	23.3	544.0	0.22	6.0	36.0	17.5	304.0	0.22	4.7	22.1	13.7	188.0	0.22
52	30	2.63	0.79	8.5	72.2	24.7	610.0	0.24	8.0	64.0	23.2	540.0	0.22	5.6	31.4	16.3	266.0	0.22	5.0	25.0	14.5	210.0	0.22
53	31	2.68	0.80	10.0	100.0	29.1	846.0	0.24	8.0	64.0	23.2	540.0	0.20	6.1	37.2	17.7	314.0	0.24	3.8	14.45	11.05	122.0	0.24
54	32	2.69	0.81	10.0	100.0	29.1	846.0	0.22	7.9	62.4	23.0	530.0	0.24	6.4	40.9	18.6	346.0	0.24	4.6	21.2	13.3	177.0	0.24
55	33	2.67	0.80	10.7	114.50	31.1	966.0	0.22	8.0	64.0	23.2	540.0	0.22	6.0	36.0	17.5	306.0	0.22	5.0	25.0	14.5	210.0	0.22
56	34	2.70	0.81	10.5	110.2	30.5	930.0	0.22	9.7	94.1	28.0	795.0	0.22	6.4	40.9	18.6	346.0	0.22	4.2	17.62	12.2	149.0	0.22

TABLE 5. RESULTS OF CRUISER MODEL TESTS IN SHALLOW WATER

Cruiser Model
Scale = 1:16
Length = 4.06 ft.

Shallow Water
Water Depth d = 4-1/8"
Date: Nov. 18, 1969, set 2

RECORD NO.	RUN NO.	SPEED OF SHIP FT SEC	Fr_d	y/L = 0.725					y/L = 2.18					y/L = 3.62					y/L = 5.01				
				Hm FT x 10^{-2}	Hm^2 FT^2 x 10^{-4}	Hm/d x 10^{-2}	$(Hm/d)^2$ x 10^{-4}	T/2 SEC	Hm FT x 10^{-2}	Hm^2 FT^2 x 10^{-4}	Hm/d x 10^{-2}	$(Hm/d)^2$ x 10^{-4}	T/2 SEC	Hm FT x 10^{-2}	Hm^2 FT^2 x 10^{-4}	Hm/d x 10^{-2}	$(Hm/d)^2$ x 10^{-4}	T/2 SEC	Hm FT x 10^{-2}	Hm^2 FT^2 x 10^{-4}	Hm/d x 10^{-2}	$(Hm\ d)^2$ x 10^{-4}	T/2 SEC
22	1	2.96	0.90	7.40	54.80	21.5	462.0	0.3	5.6	31.4	16.3	266.0	0.3	3.6	12.9	10.4	108.0	0.3	2.3	5.3	6.7	45.0	0.3
23	2	2.80	0.85	7.0	49.0	20.4	416.0	0.3	5.0	25.0	14.55	212.0	0.3	3.2	10.24	9.3	86.5	0.3	1.9	3.61	5.5	30.2	0.3
24	3	2.90	0.87	6.3	39.7	18.3	336.0	0.3	4.5	20.25	13.1	172.0	0.3	2.9	8.41	8.4	70.5	0.3	2.0	4.0	5.8	33.6	0.3
26	5	2.80	0.85	4.8	23.0	13.9	193.0	0.28	3.1	9.6	9.0	81.0	0.3	2.2	4.84	6.4	41.0	0.28	1.6	2.56	4.6	21.2	0.28
27	6	2.96	0.90	12.0	144.0	34.9	1220.0	0.3	9.2	84.6	26.8	718.0	0.3	6.2	38.4	18.0	324.0	0.3	3.4	11.56	9.9	98.0	0.3
28	7	2.95	0.89	11.6	135.0	33.7	1136.0	0.3	9.0	81.0	26.1	680.0	0.3	6.3	39.7	18.3	335.0	0.3	3.7	13.7	10.7	114.2	0.3
29	8	3.0	0.91	12.7	161.1	36.9	1361.0	0.3	8.7	75.7	25.3	640.0	0.3	6.3	39.7	18.3	335.0	0.3	3.9	15.2	11.3	128.0	0.3
30	9	2.92	0.88	12.0	144.0	34.8	1211.0	0.3	8.0	64.0	23.2	538.0	0.3	6.2	38.4	18.0	324.0	0.3	3.4	11.56	9.9	98.0	0.3
31	10	2.96	0.90	12.5	156.4	36.3	1317.0	0.3	9.2	84.6	26.8	718.0	0.3	6.8	46.3	19.8	392.0	0.3	4.0	16.0	11.6	135.0	0.3
32	11	2.96	0.90	10.7	114.6	31.1	966.0	0.3	9.0	81.0	26.1	681.0	0.3	6.5	42.3	18.9	358.0	0.3	4.0	16.0	11.6	135.0	0.3
33	12	3.20	0.96	13.3	177.0	38.6	1512.0	0.44	8.5	72.3	24.7	610.0	0.40	5.9	34.8	17.2	296.0	0.36	3.7	13.7	11.9	141.8	0.4
34	13	3.10	0.94	14.5	210.5	42.1	1773.0	0.42	8.5	72.3	24.7	610.0	0.4	6.0	36.0	17.4	311.0	0.34	3.5	12.26	10.2	104.0	0.38
35	14	3.02	0.92	13.5	182.10	39.2	1537.0	0.3	10.0	100.0	29.1	846.0	0.3	6.3	39.7	18.3	335.0	0.3	3.9	15.2	11.3	128.0	0.3
36	15	3.01	0.92	13.7	188.0	39.8	1582.0	0.28	9.7	94.0	28.2	796.0	0.3	6.5	42.3	18.9	358.0	0.3	4.1	16.8	11.9	141.8	0.3
37	16	3.0	0.91	13.5	182.1	39.2	1537.0	0.3	10.2	104.0	29.6	876.0	0.3	6.3	39.7	18.3	335.0	0.3	3.7	13.7	10.7	114.2	0.3
38	17	2.50	0.75	1.4	1.96	4.06	16.5	0.2	1.0	1.0	2.91	8.5	0.2	0.5	0.25	1.45	2.1	0.2	0.3	0.09	0.87	0.8	0.2
39	18	2.15	0.65	0.4	0.16	1.16	1.35	0.18	0.25	0.0625	0.74	0.55	0.2	0.1	0.01	0.29	0.08	0.2	-	-	-	-	0.2
10	19	2.90	0.87	5.7	32.5	16.5	272.0	0.26	4.5	20.25	13.1	172.0	0.3	3.2	10.24	9.3	86.5	0.3	1.8	3.24	5.2	27.0	0.3
11	20	2.80	0.85	4.0	16.0	11.6	135.0	0.26	3.0	9.0	8.73	76.0	0.28	2.0	4.0	5.82	34.0	0.28	1.3	1.69	3.8	14.0	0.28
12	21	2.60	0.78	2.0	4.0	5.82	34.1	0.24	1.4	1.96	4.06	16.5	0.24	0.8	0.64	2.32	5.4	0.24	0.5	0.25	1.45	2.1	0.24
13	22	2.18	0.75	1.2	1.44	3.48	12.1	0.2	0.8	0.64	2.32	5.4	0.22	0.4	0.16	1.16	1.35	0.24	0.2	0.04	0.58	0.34	0.24

MODEL A
MARINER MODEL BOW

MODEL A
MARINER CLASS CARGO SHIP

FIG 1 MARINER MODEL BOW AND PROFILE

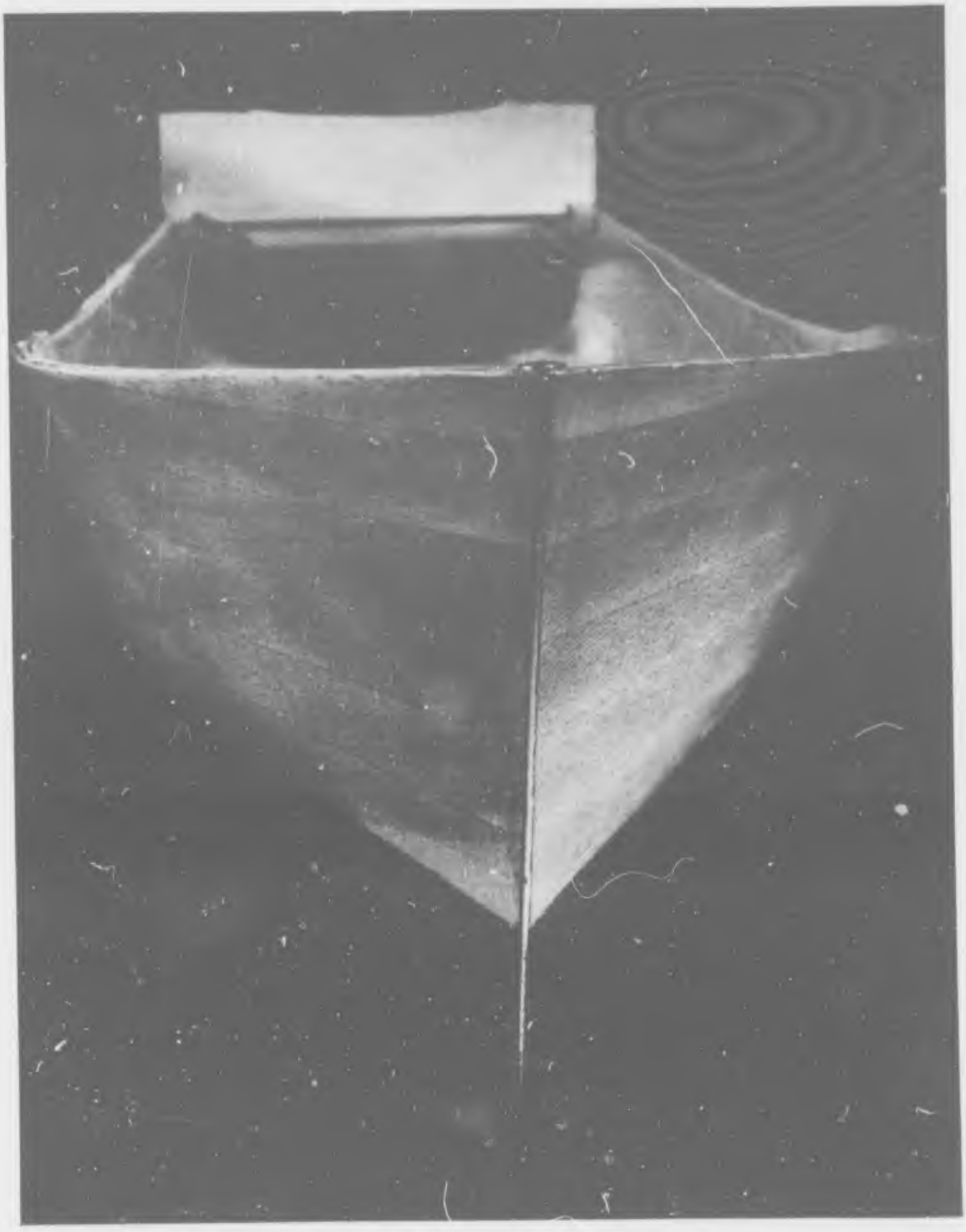

FIG. 2 CRUISER MODEL BOW

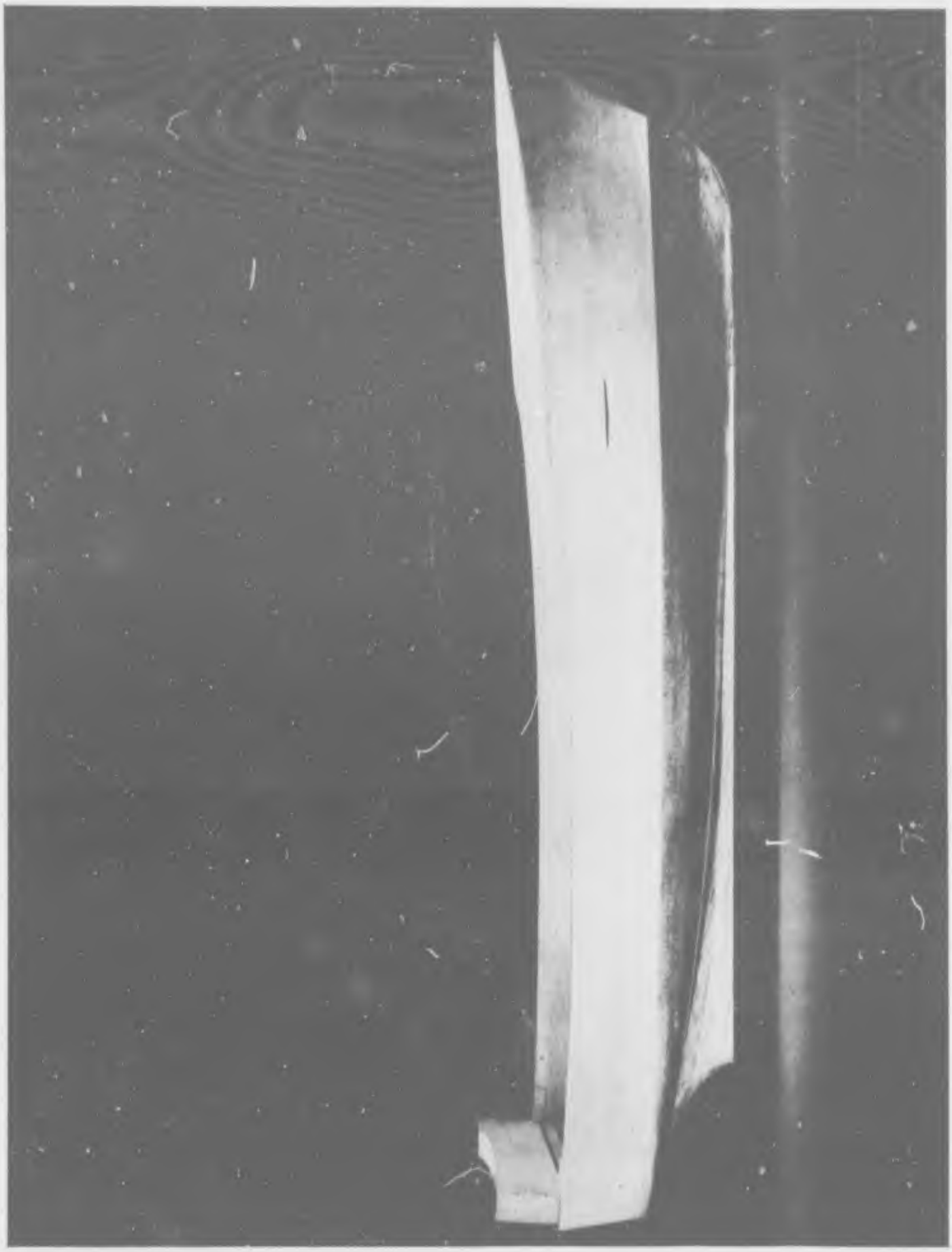

FIG 3 CRUISER MODEL PROFILE

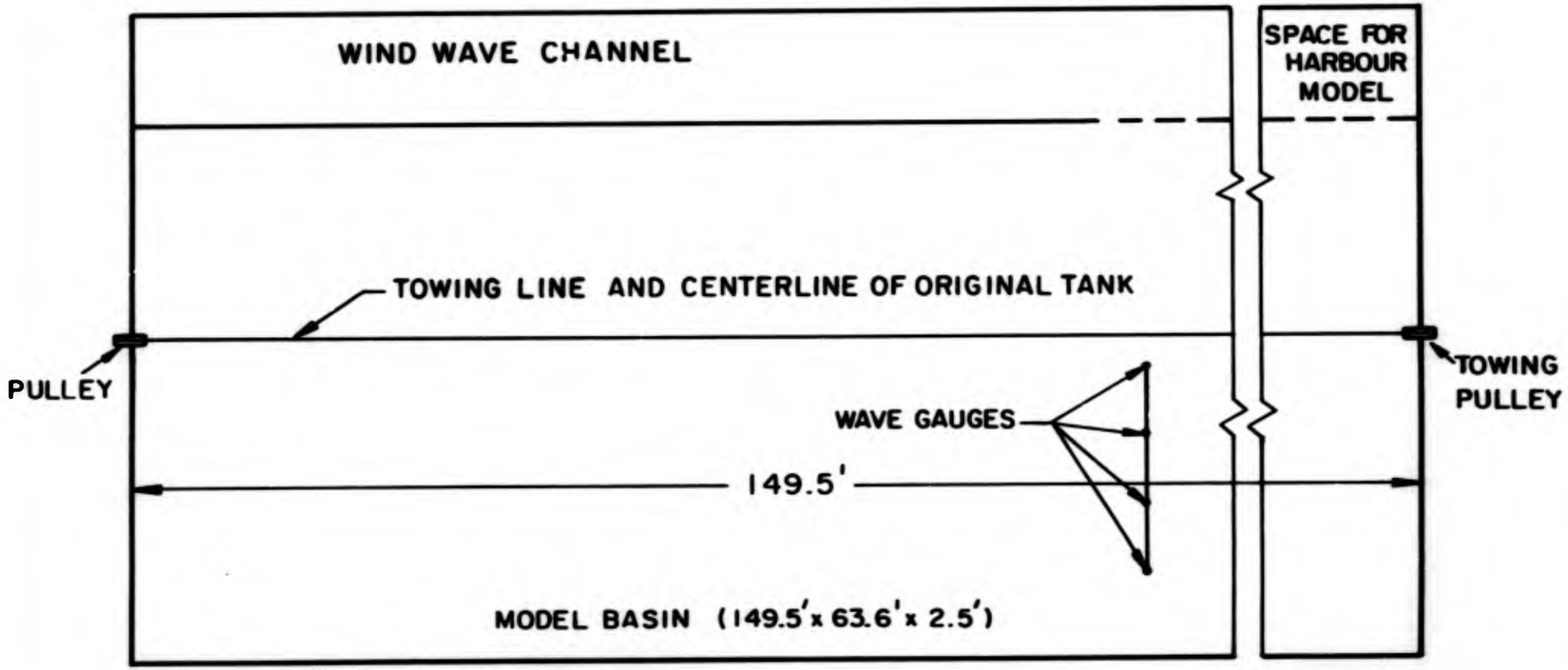

FIG. 4 GENERAL LAYOUT OF EXPERIMENTAL SET-UP

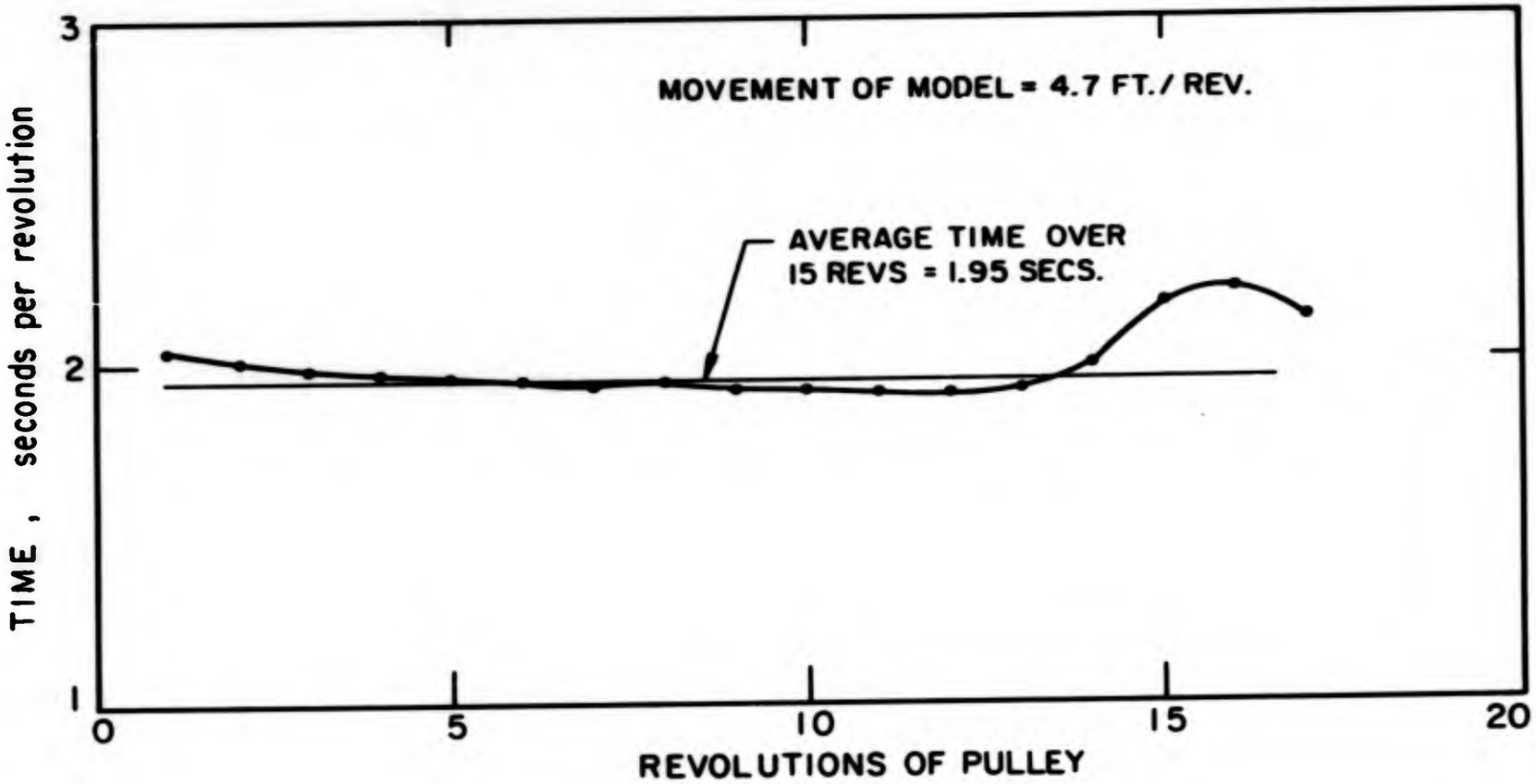

FIG. 5 VARIATION OF TIME PERIOD OF REVOLUTION OF DRIVING PULLEY WITH NUMBER OF REVOLUTION

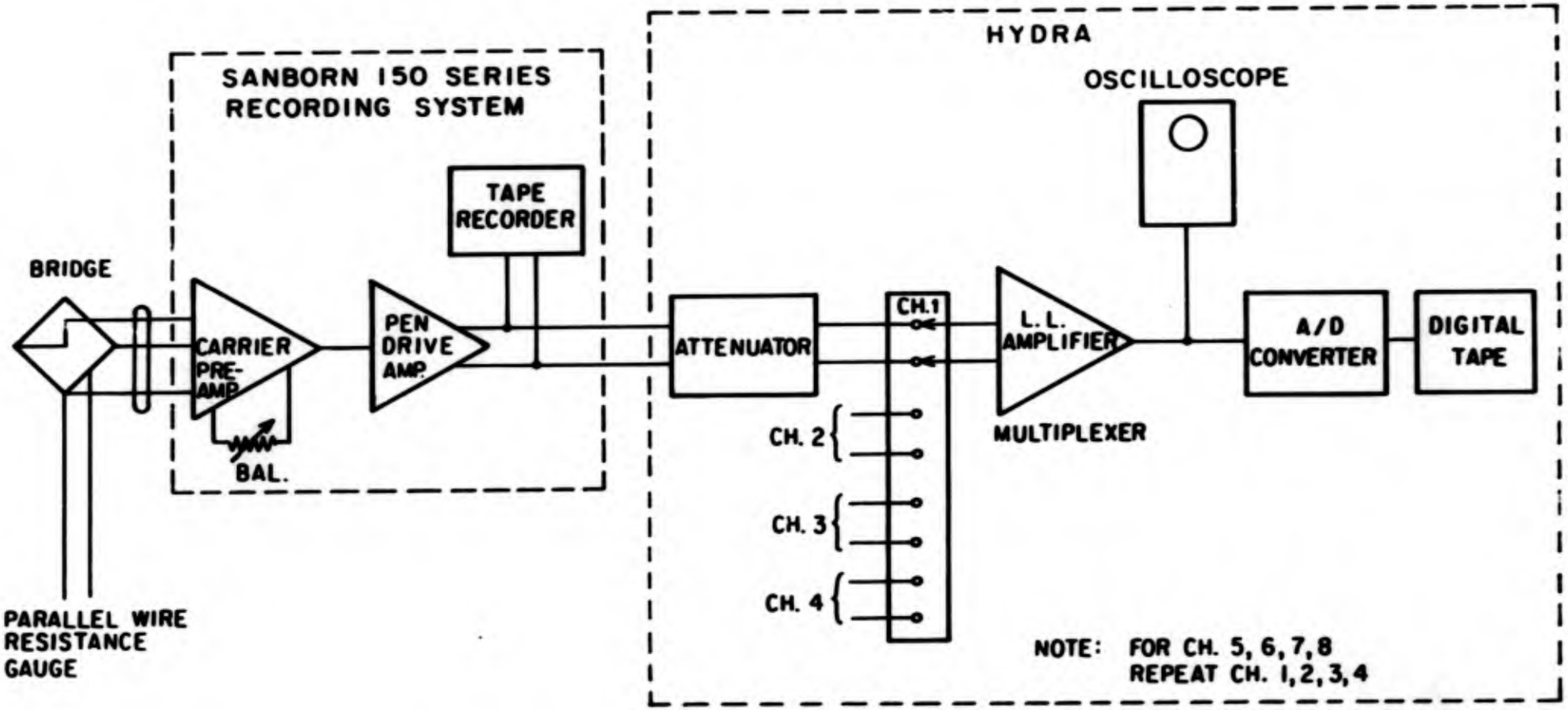

FIG. 6 WAVE HEIGHT RECORDING SYSTEM

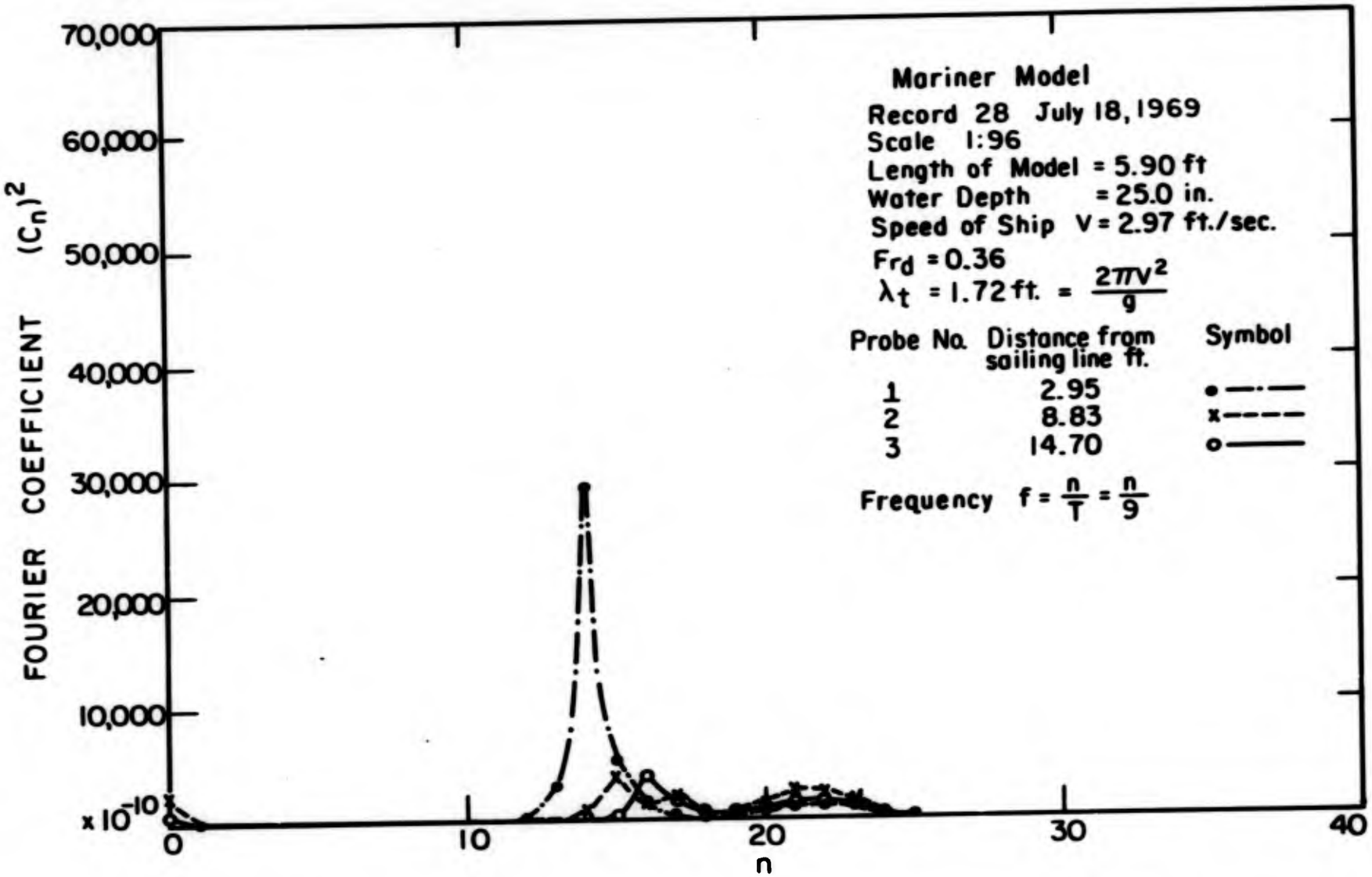

FIG. 7 ENERGY DENSITY AS A FUNCTION OF FREQUENCY IN A LONGITUDINAL WAVE PROFILE FOR MARINER MODEL IN DEEP WATER (d=25")

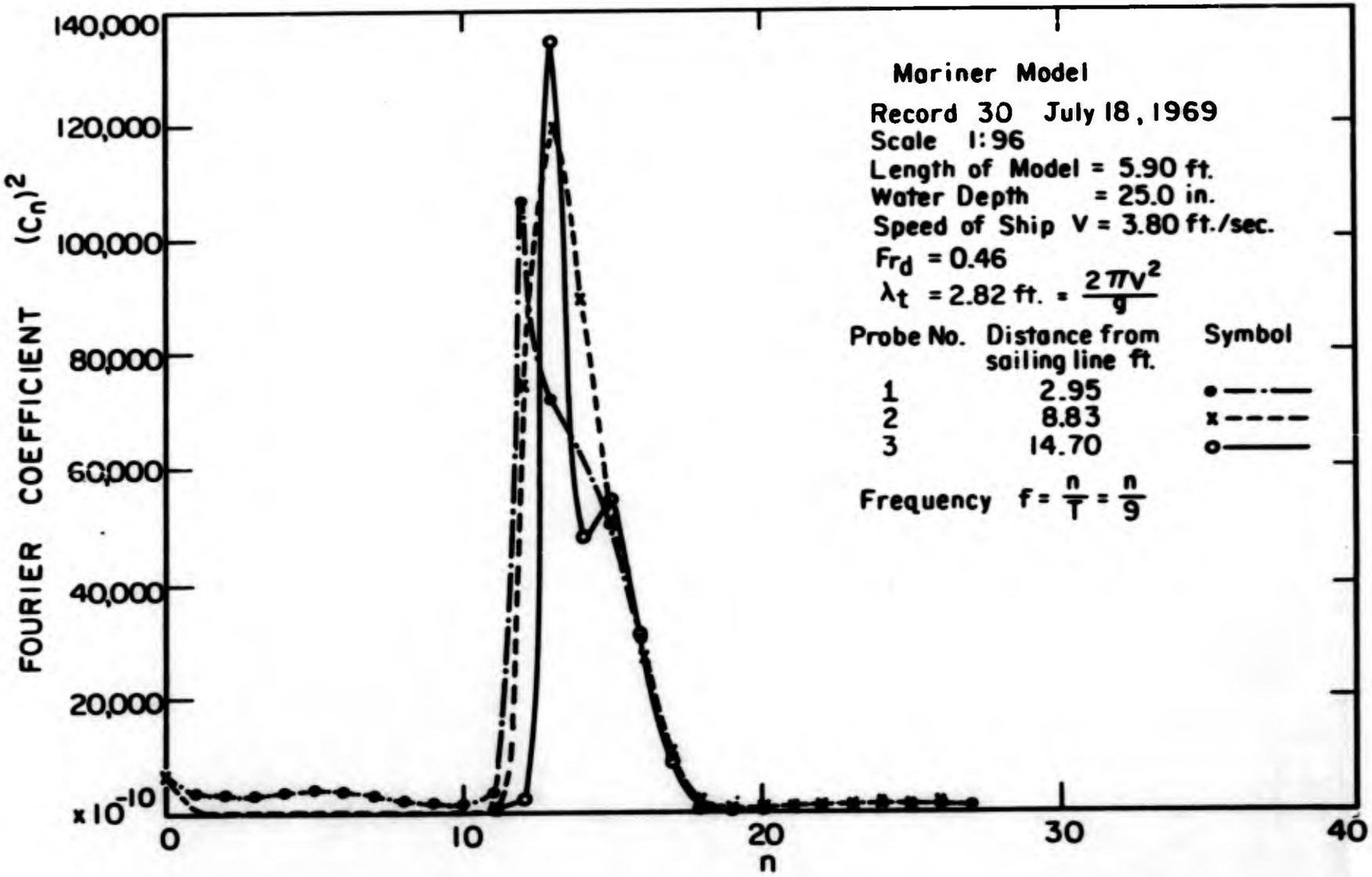

FIG. 8 ENERGY DENSITY IN A LONGITUDINAL WAVE PROFILE FOR MARINER MODEL IN DEEP WATER (d = 25")

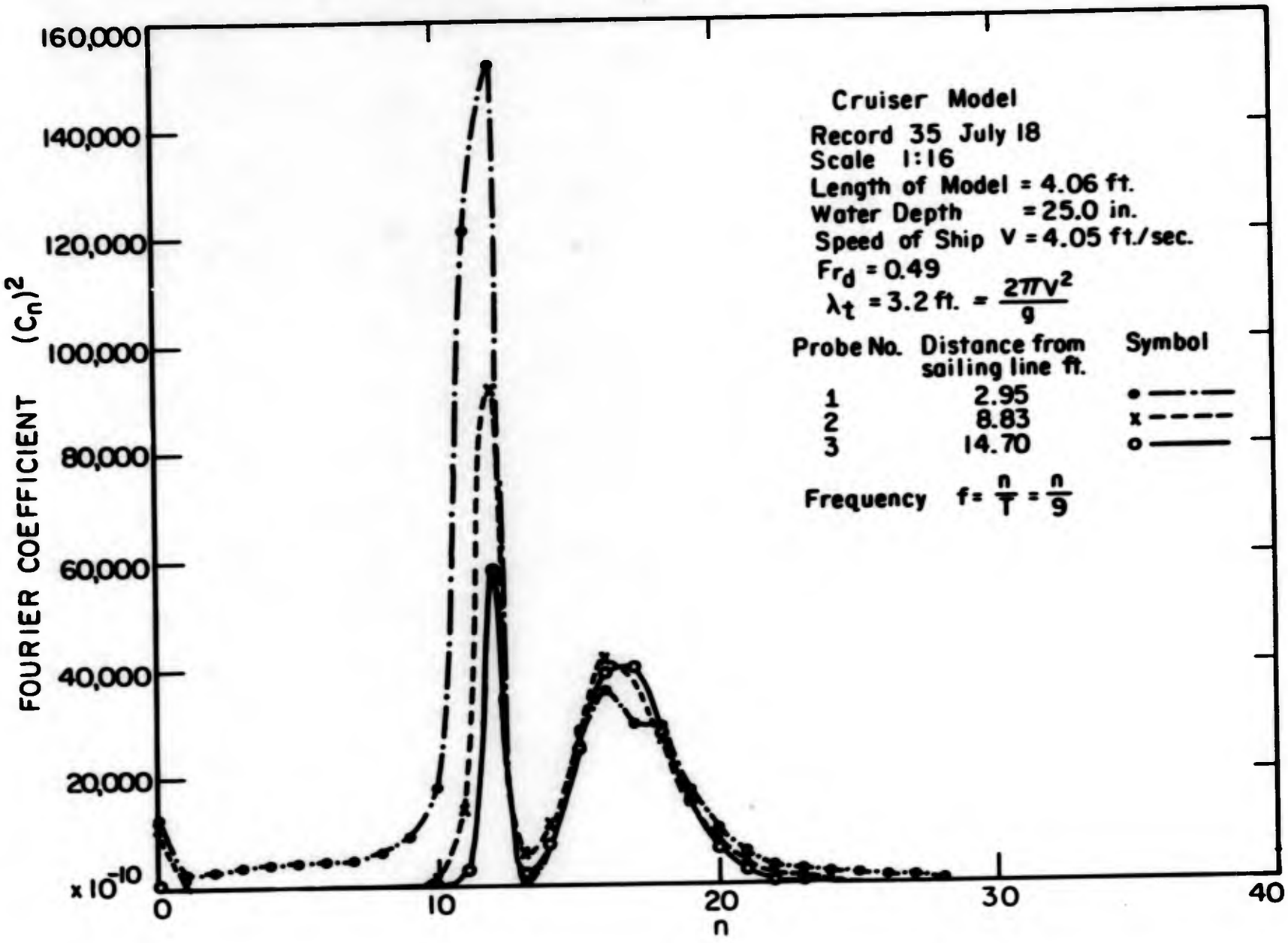

FIG. 9 ENERGY DENSITY IN A LONGITUDINAL WAVE PROFILE FOR MARINER MODEL IN DEEP WATER (d = 25")

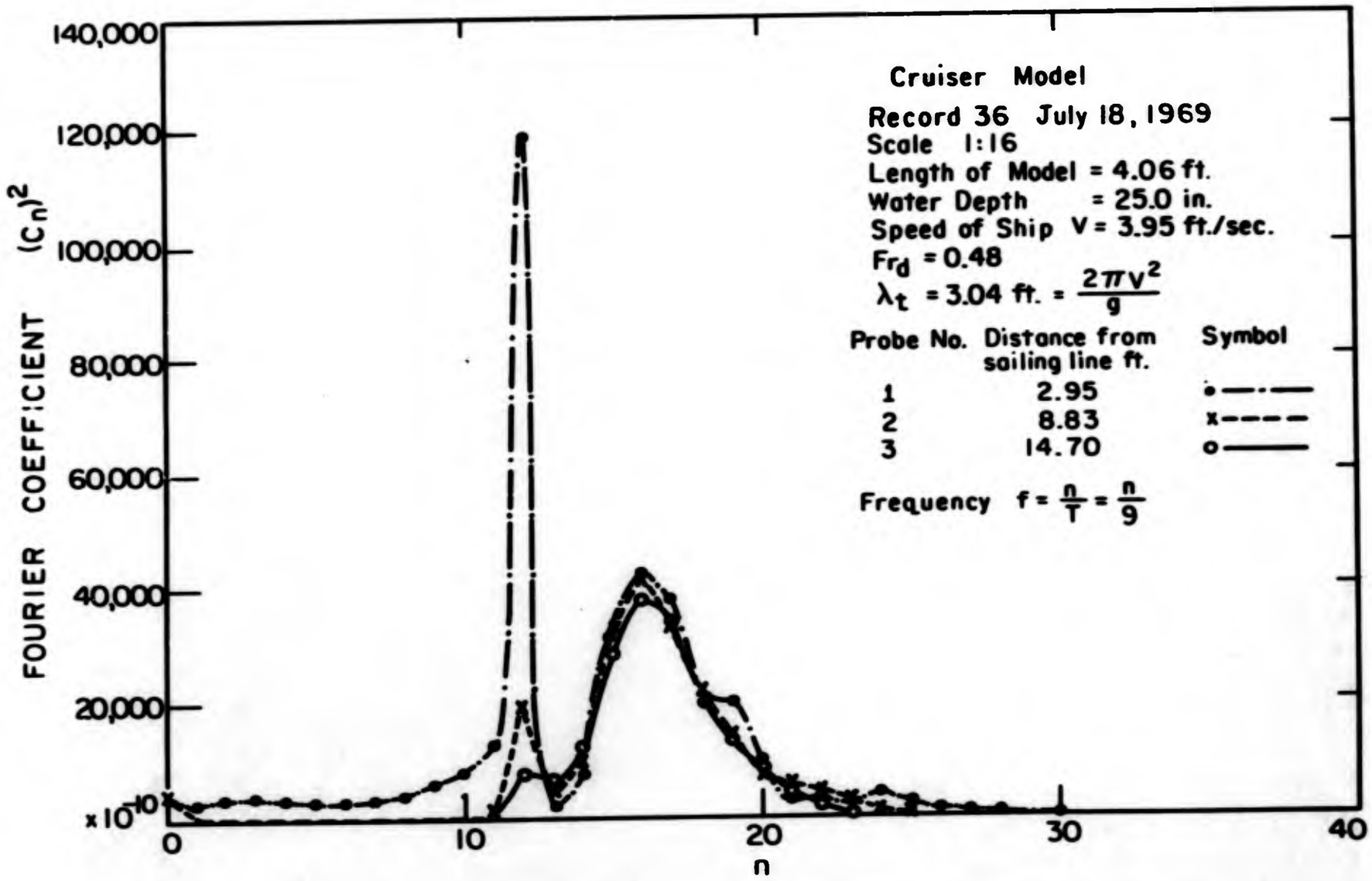

FIG. 10 ENERGY DENSITY IN A LONGITUDINAL WAVE PROFILE FOR CRUISER MODEL IN DEEP WATER (d=25")

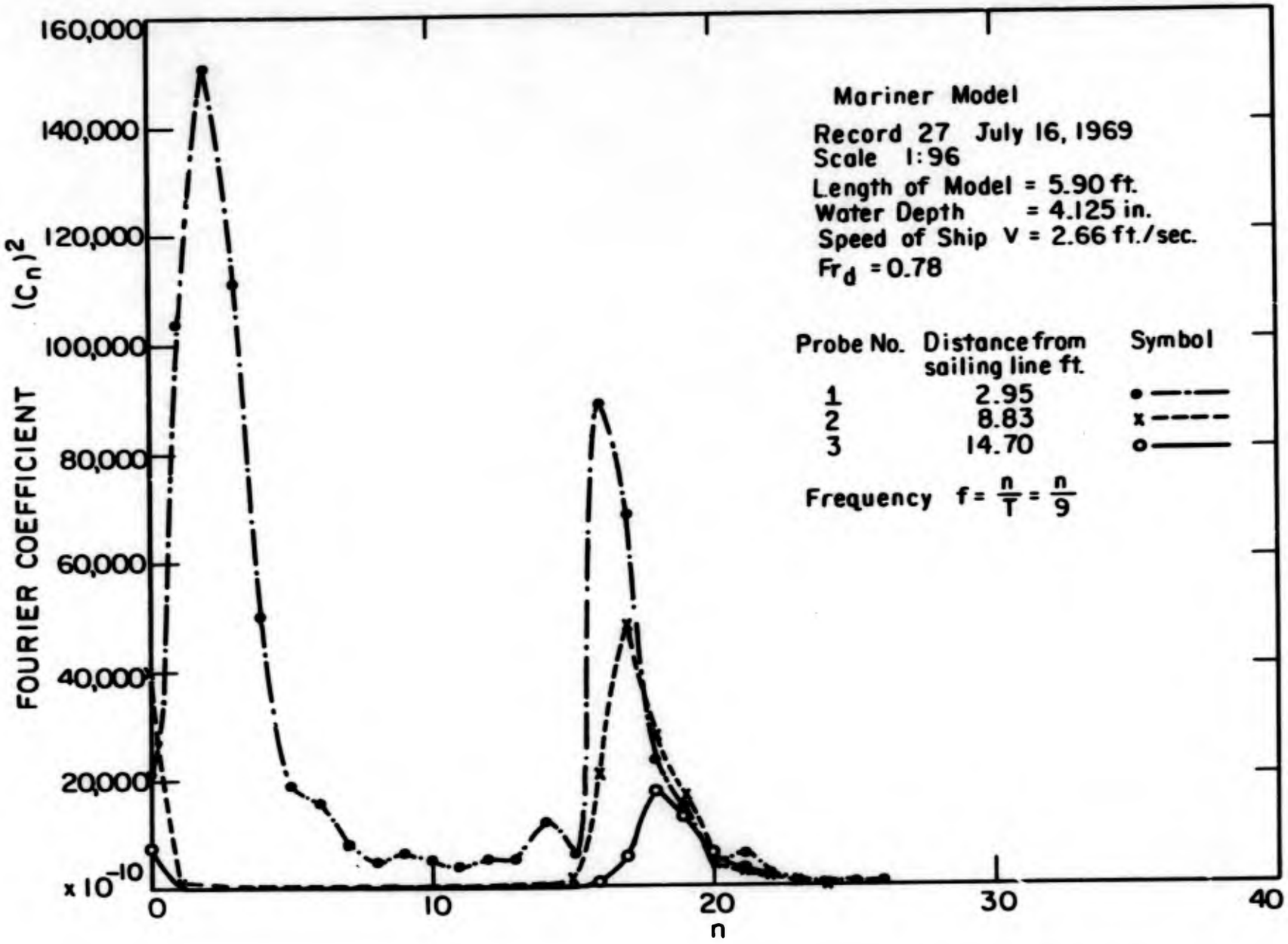

FIG. 11 ENERGY DENSITY IN A LONGITUDINAL WAVE PROFILE FOR MARINER MODEL IN SHALLOW WATER (d = 4.125 IN)

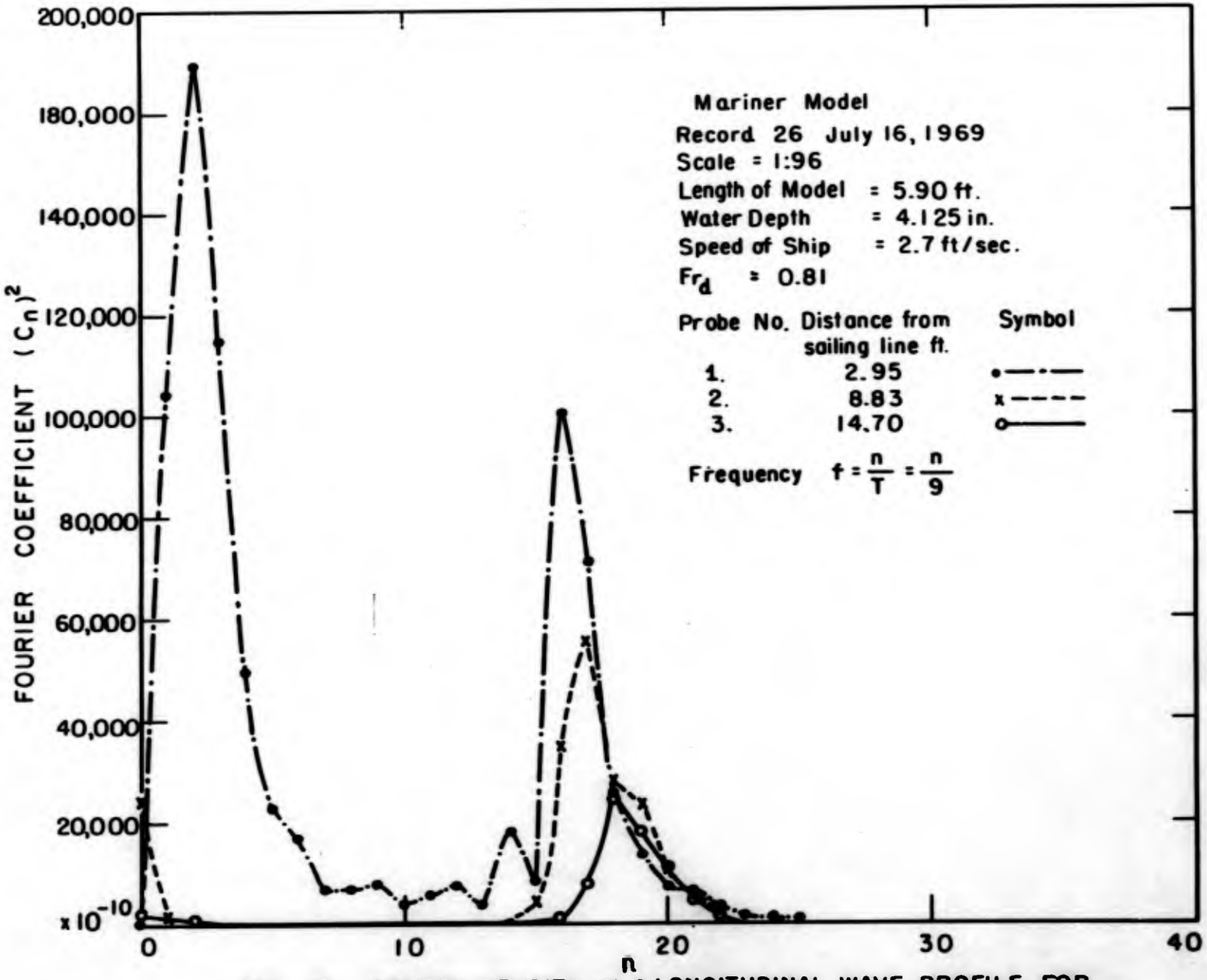

FIG 12 ENERGY DENSITY IN A LONGITUDINAL WAVE PROFILE FOR MARINER MODEL IN SHALLOW WATER (d = 4.125 IN)

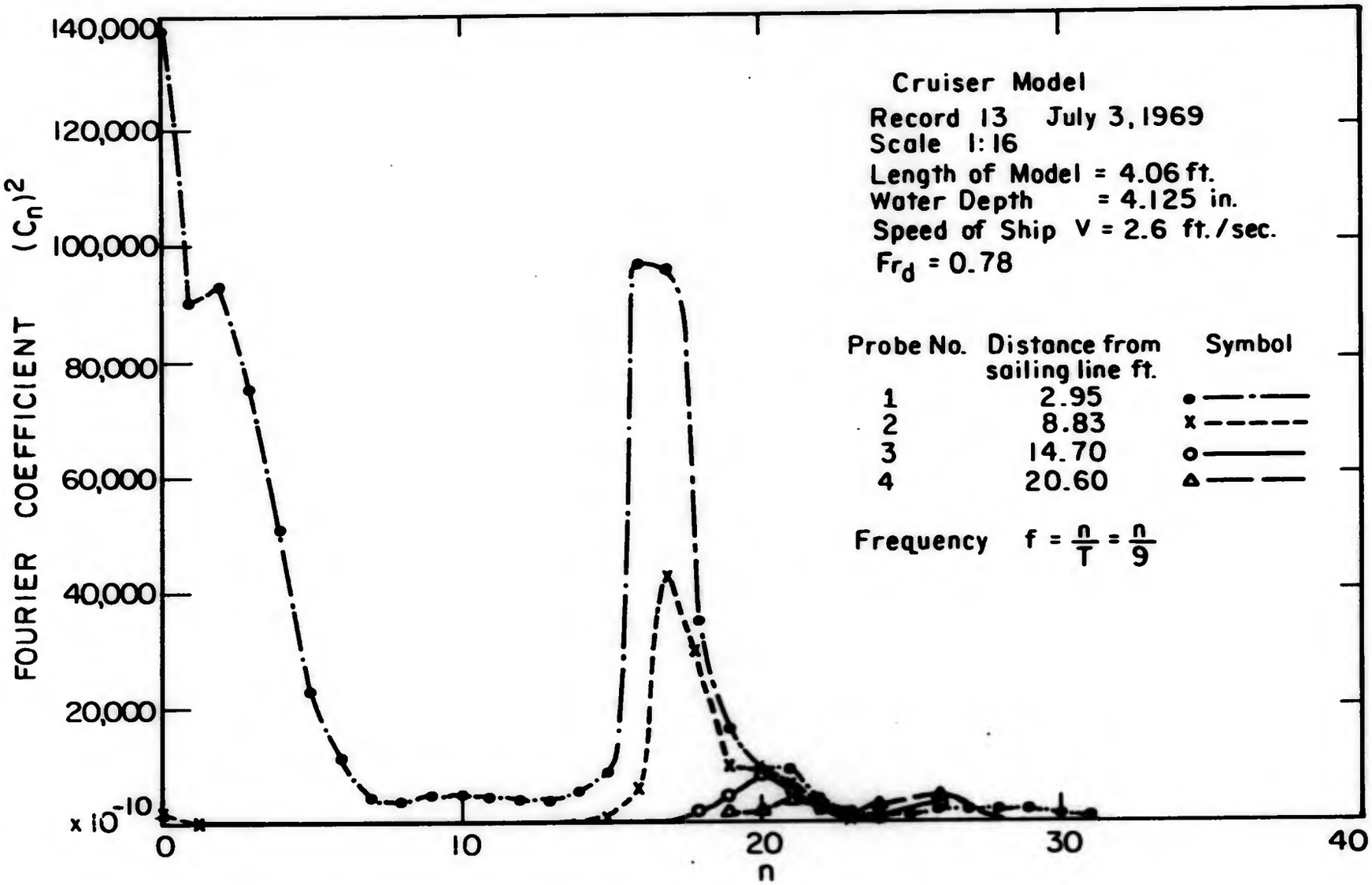

FIG. 13 ENERGY DENSITY IN A LONGITUDINAL WAVE PROFILE FOR CRUISER MODEL IN SHALLOW WATER (d = 4.125 IN)

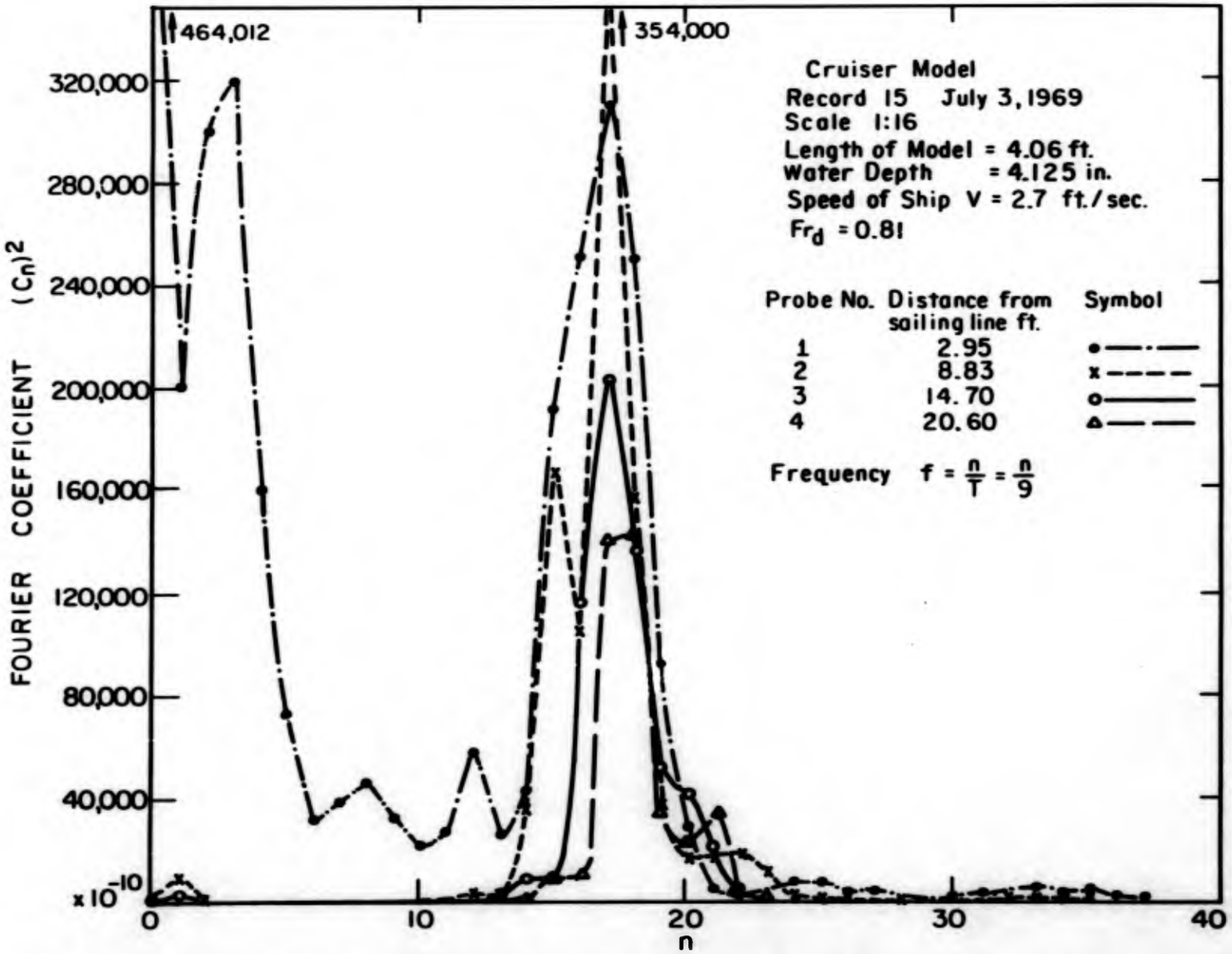

FIG. 14 ENERGY DENSITY IN A LONGITUDINAL WAVE PROFILE FOR CRUISER MODEL IN SHALLOW WATER (d = 4.125 IN)

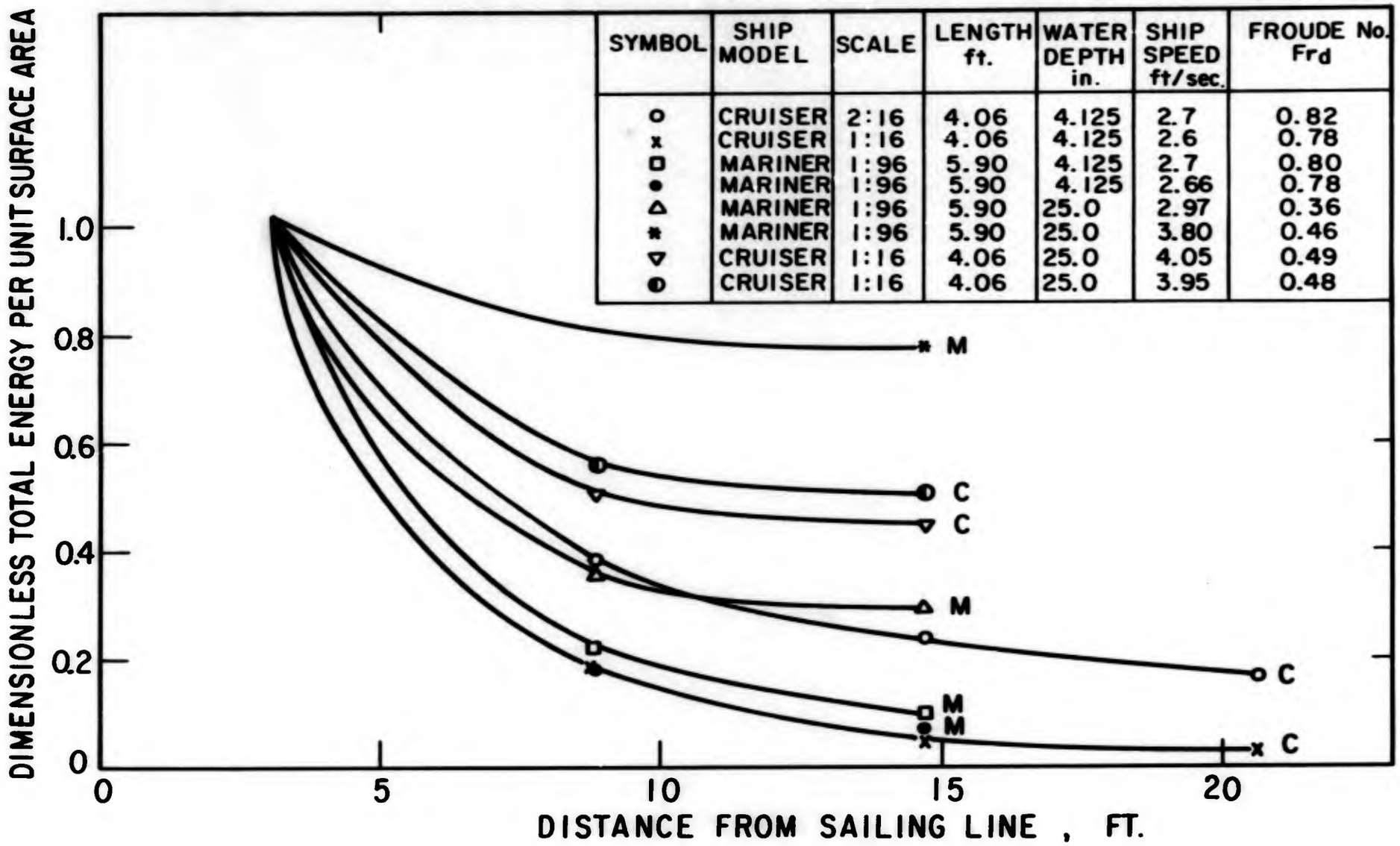

FIG. 15 DIMENSIONLESS TOTAL ENERGY PER UNIT SURFACE AREA AS A FUNCTION OF DISTANCE FROM SAILING LINE.

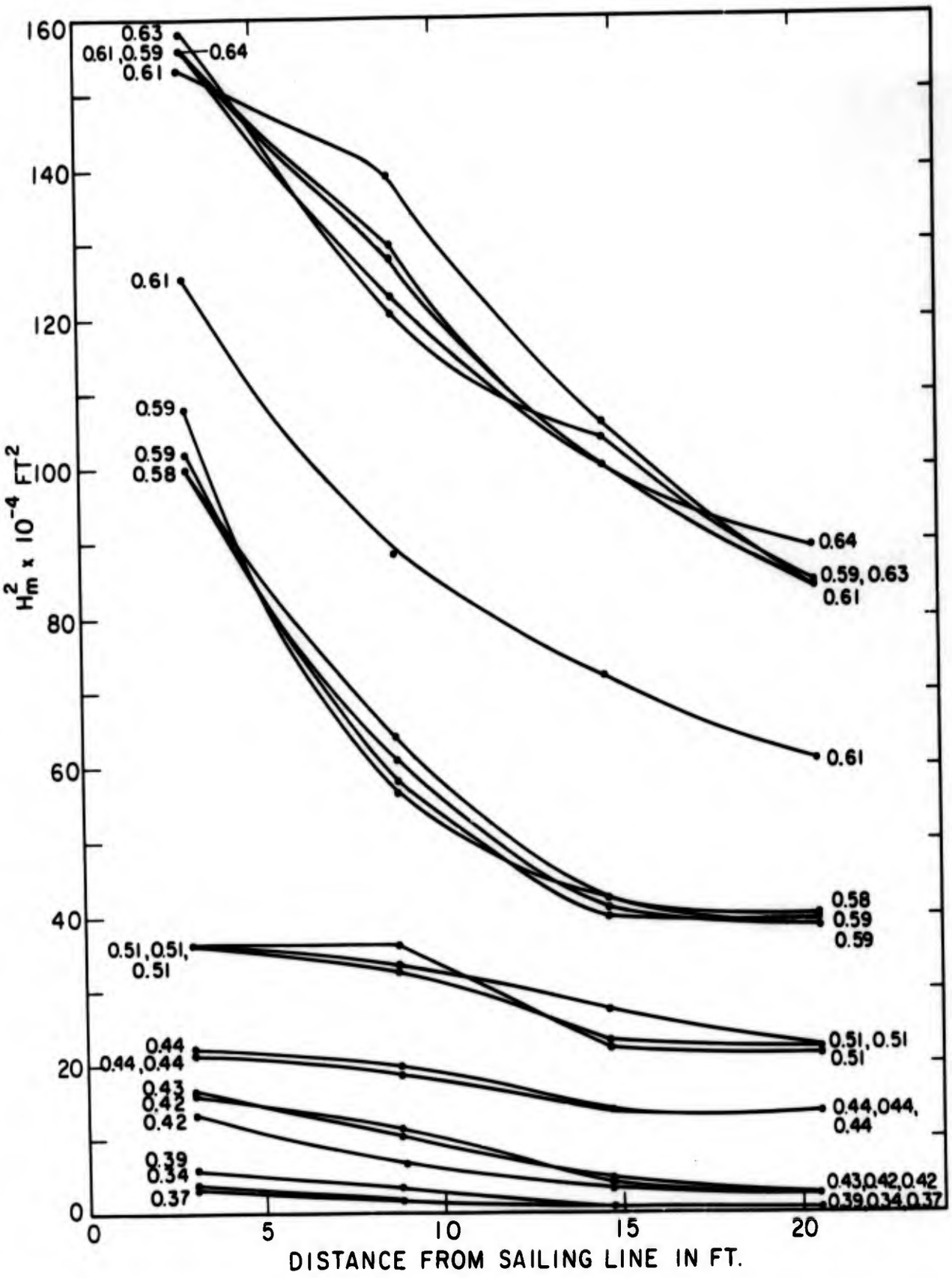

FIG 16 H_m^2 AS A FUNCTION OF DISTANCE FROM SAILING LINE WITH FROUDE NUMBER AS A PARAMETER FOR MARINER MODEL IN DEEP WATER ($d = 24\frac{7}{8}$")

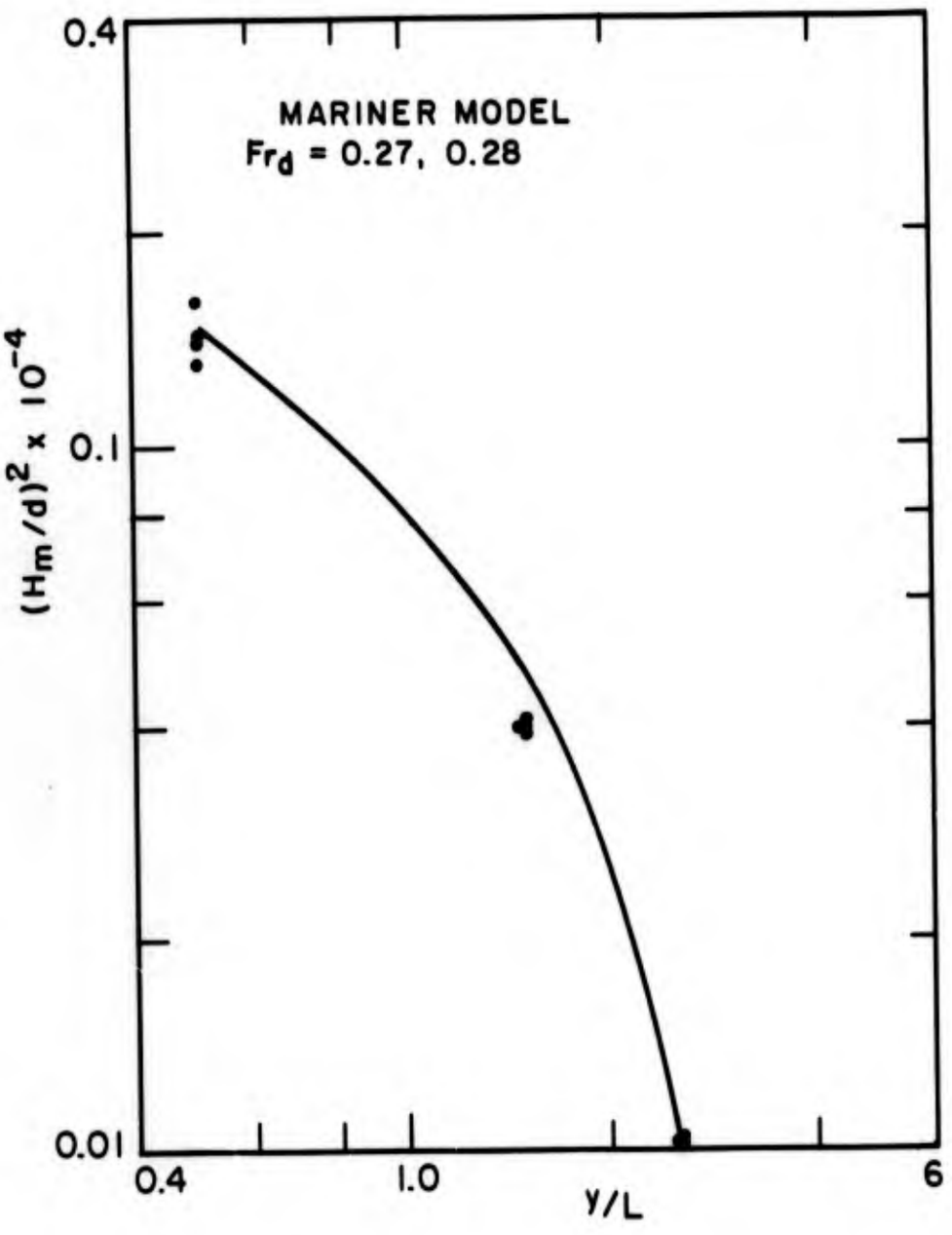

FIG. 17 $(H_m/d)^2$ AS A FUNCTION OF y/L FOR MARINER MODEL IN DEEP WATER ($d = 24\frac{7}{8}$")

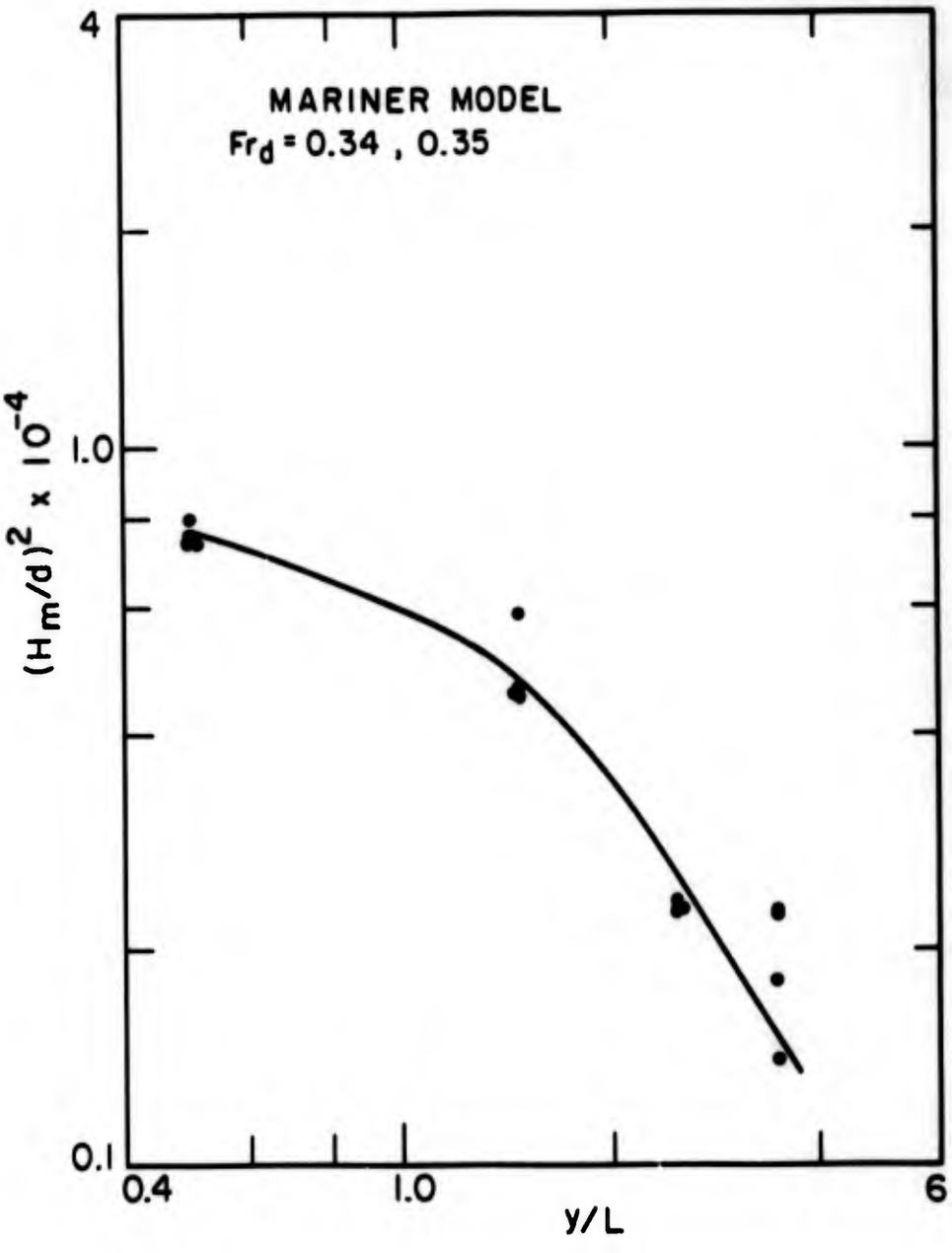

FIG. 18 $(H_m/d)^2$ AS A FUNCTION OF y/L FOR MARINER MODEL IN DEEP WATER ($d = 24\frac{7}{8}"$)

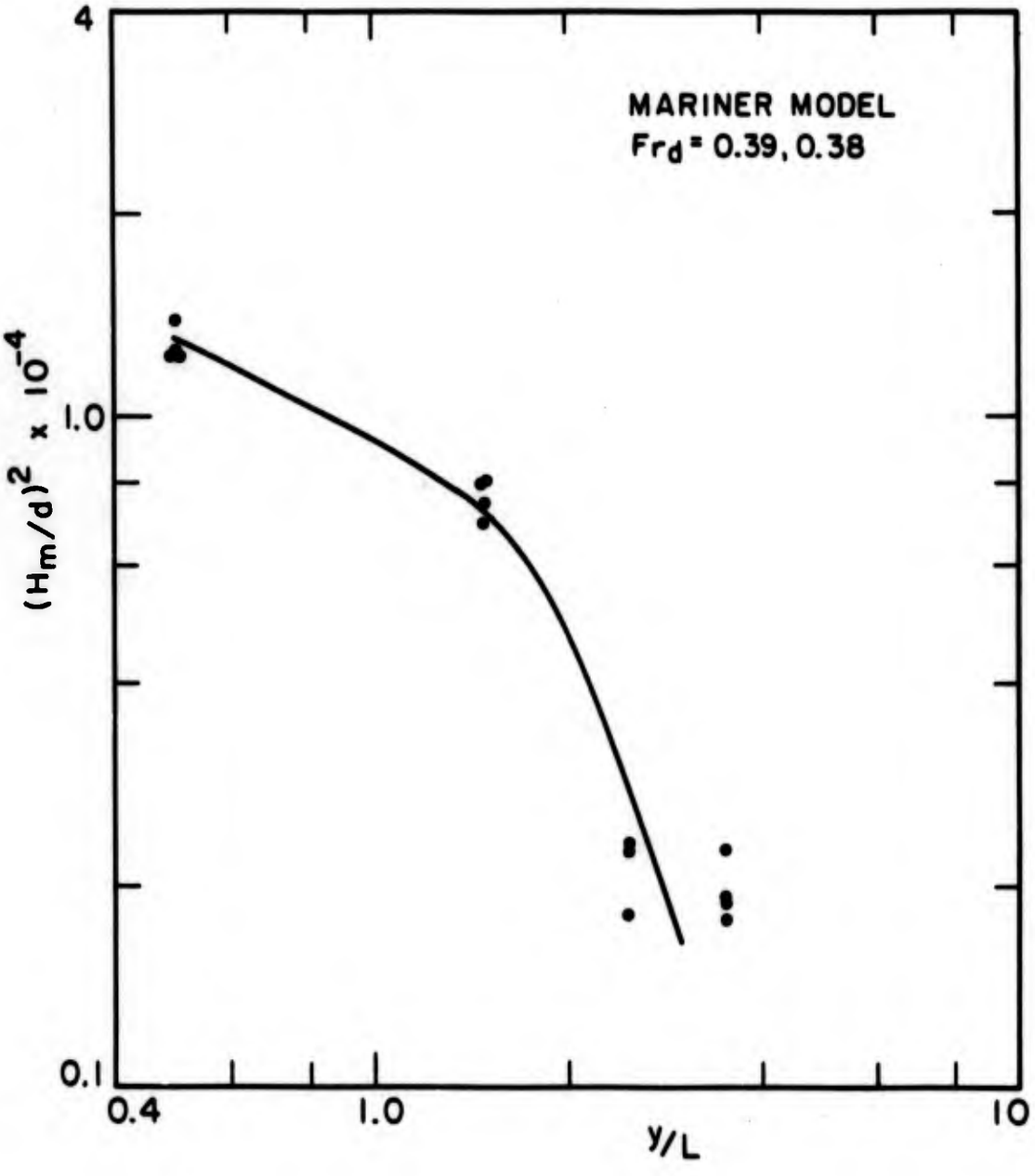

FIG. 19 $(H_m/d)^2$ AS A FUNCTION OF y/L FOR MARINER MODEL IN DEEP WATER ($d = 24\frac{7}{8}$")

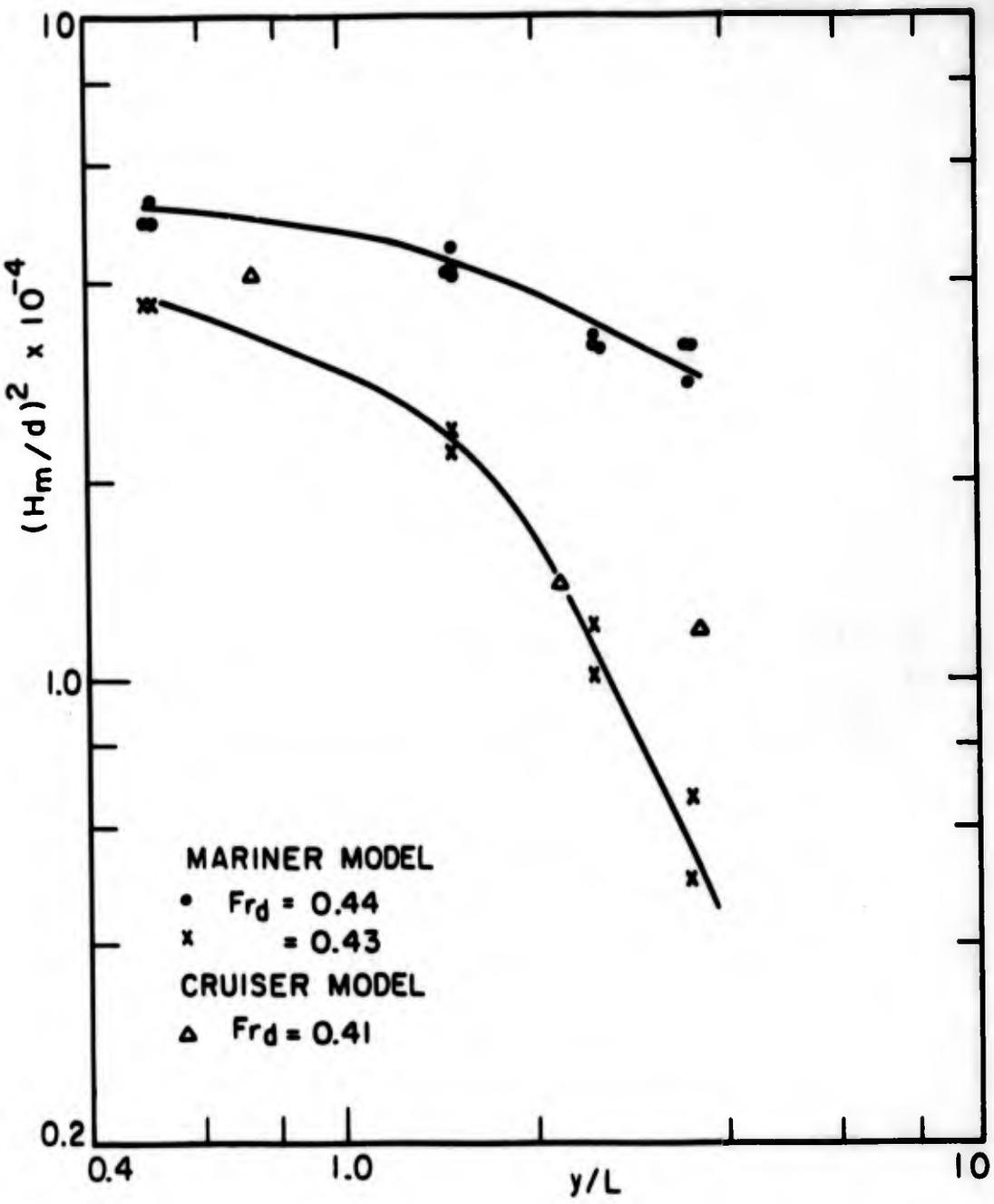

FIG. 20 $(H_m/d)^2$ AS A FUNCTION OF y/L FOR MARINER AND CRUISER MODELS IN DEEP WATER ($d = 24\frac{7}{8}$")

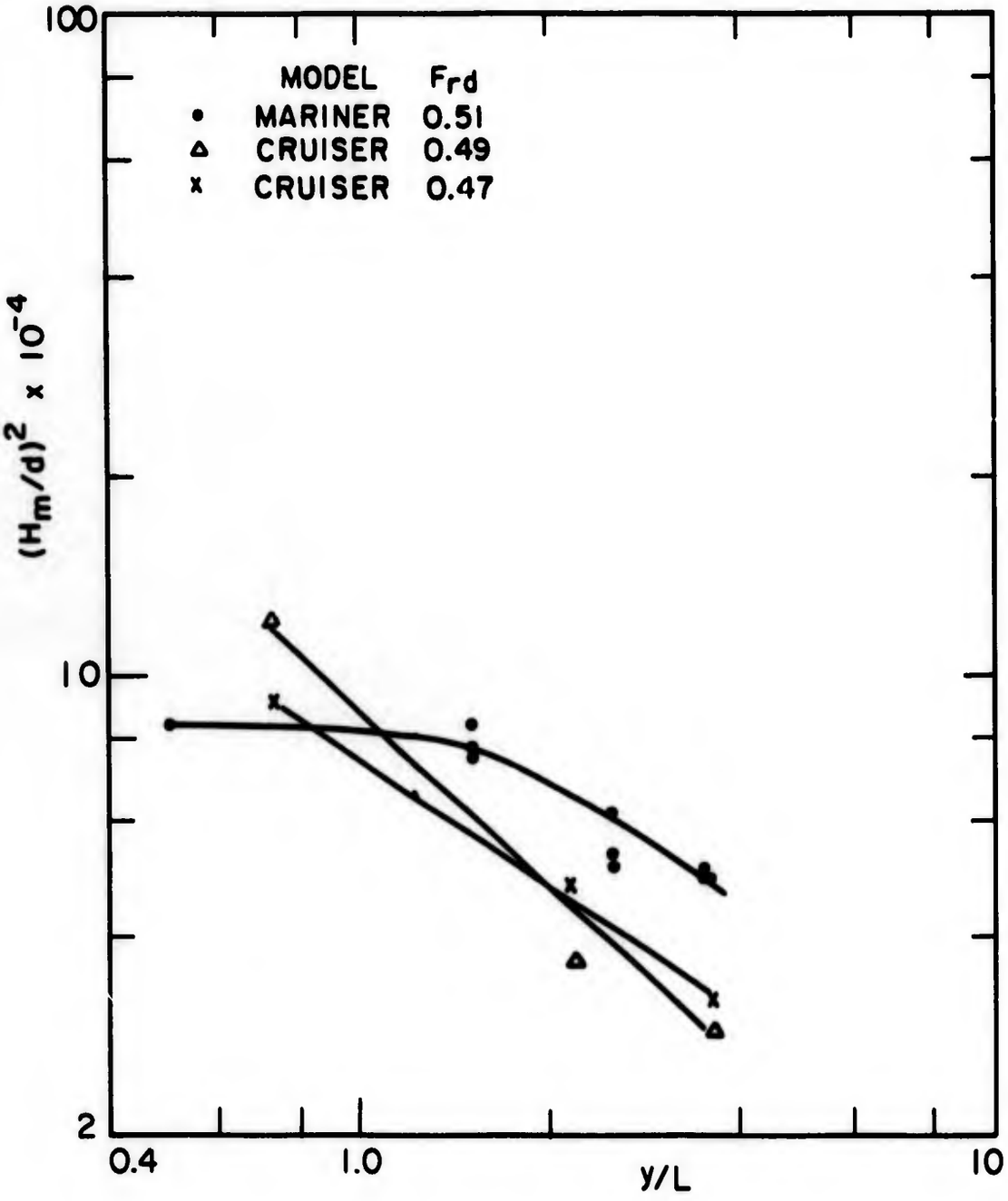

FIG. 21 $(H_m/d)^2$ AS A FUNCTION OF y/L FOR MARINER AND CRUISER MODELS IN DEEP WATER ($d = 24\frac{7}{8}$")

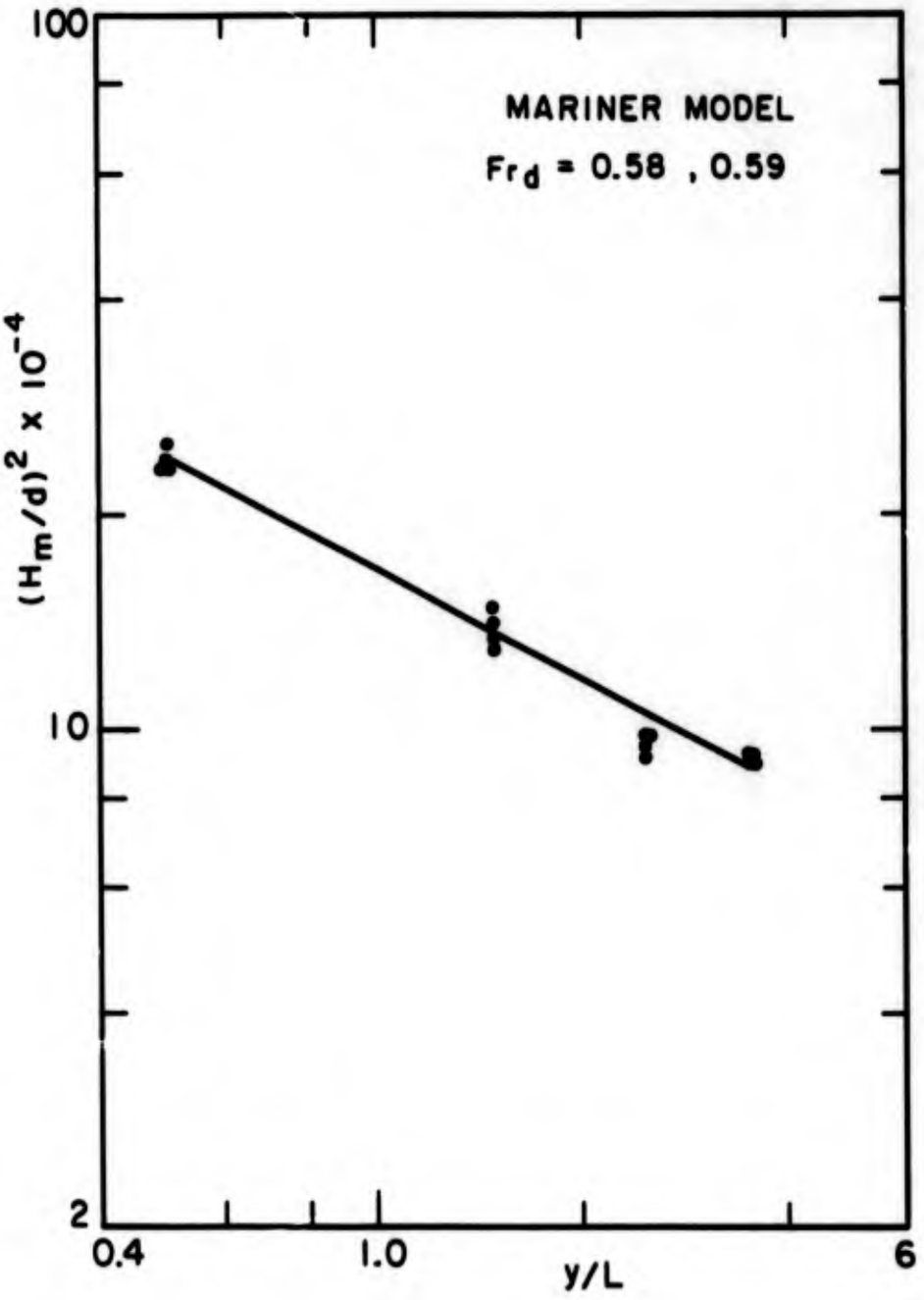

FIG. 22 $(H_m/d)^2$ AS A FUNCTION OF y/L FOR MARINER MODEL IN DEEP WATER ($d = 24\frac{7}{8}$)

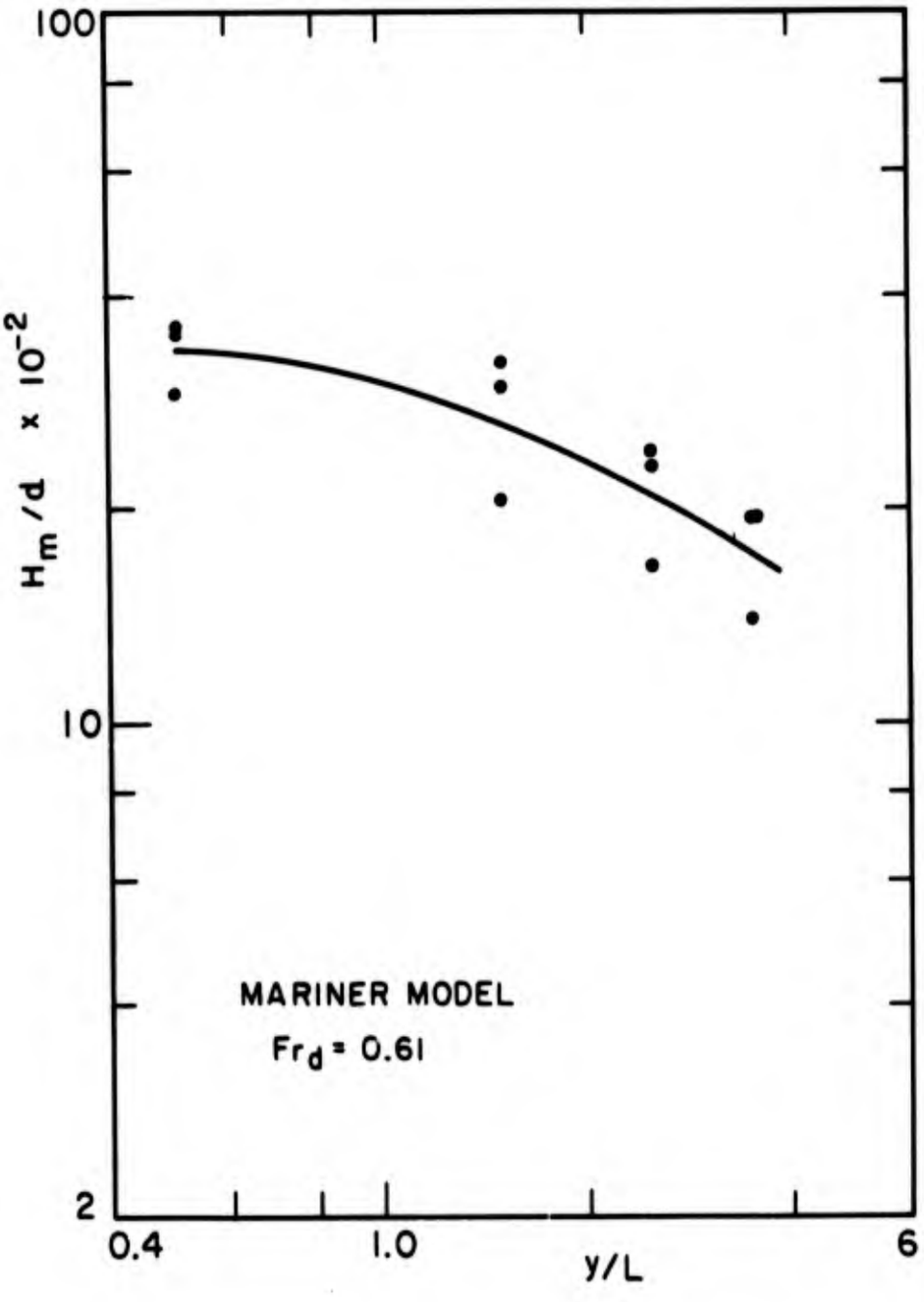

FIG. 23 $(H_m/d)^2$ AS A FUNCTION OF y/L FOR MARINER MODEL IN DEEP WATER ($d = 24\frac{7}{8}"$)

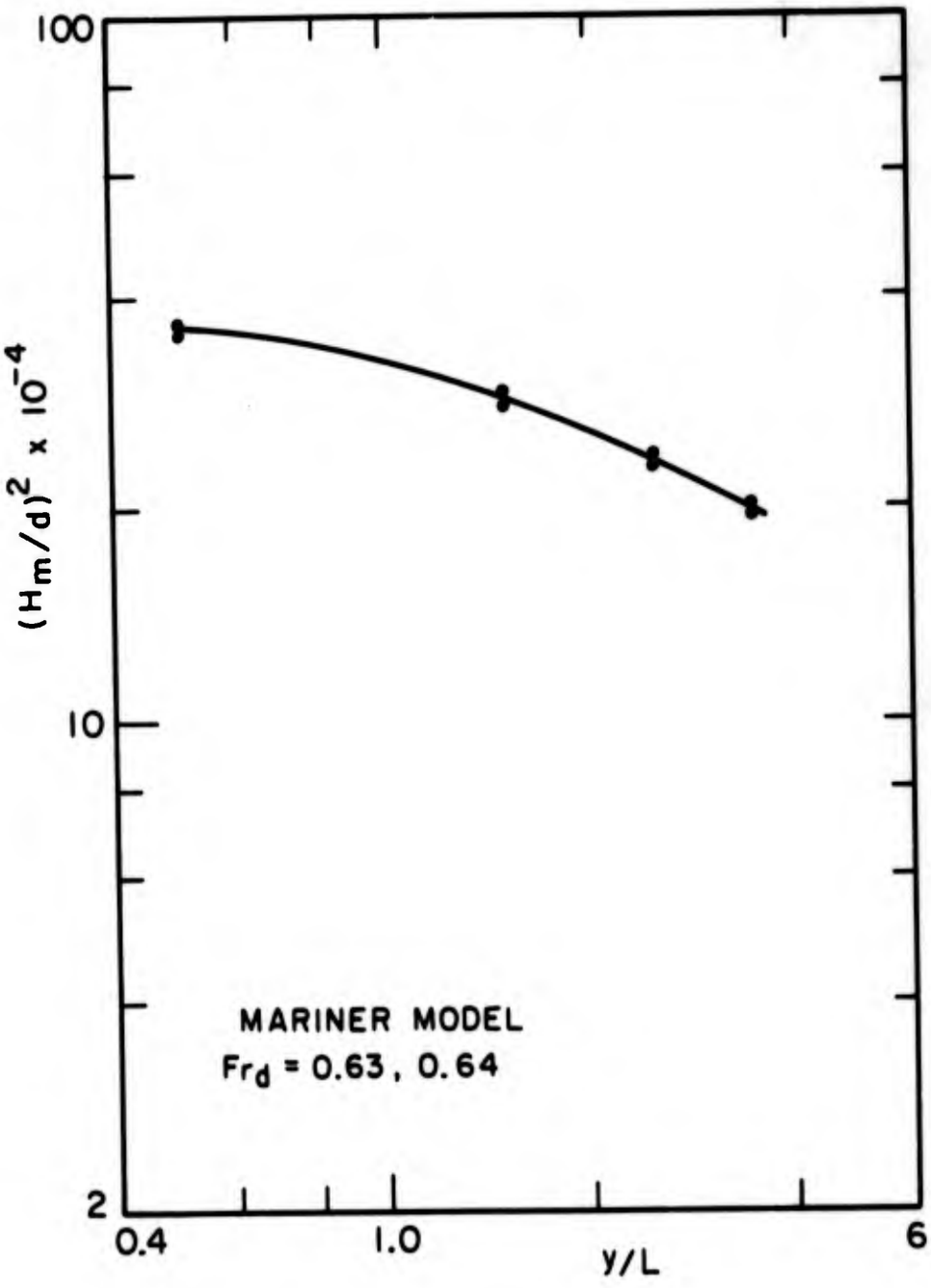

FIG. 24 $(Hm/d)^2$ AS A FUNCTION OF y/L FOR MARINER MODEL IN DEEP WATER ($d = 24\frac{7}{8}$")

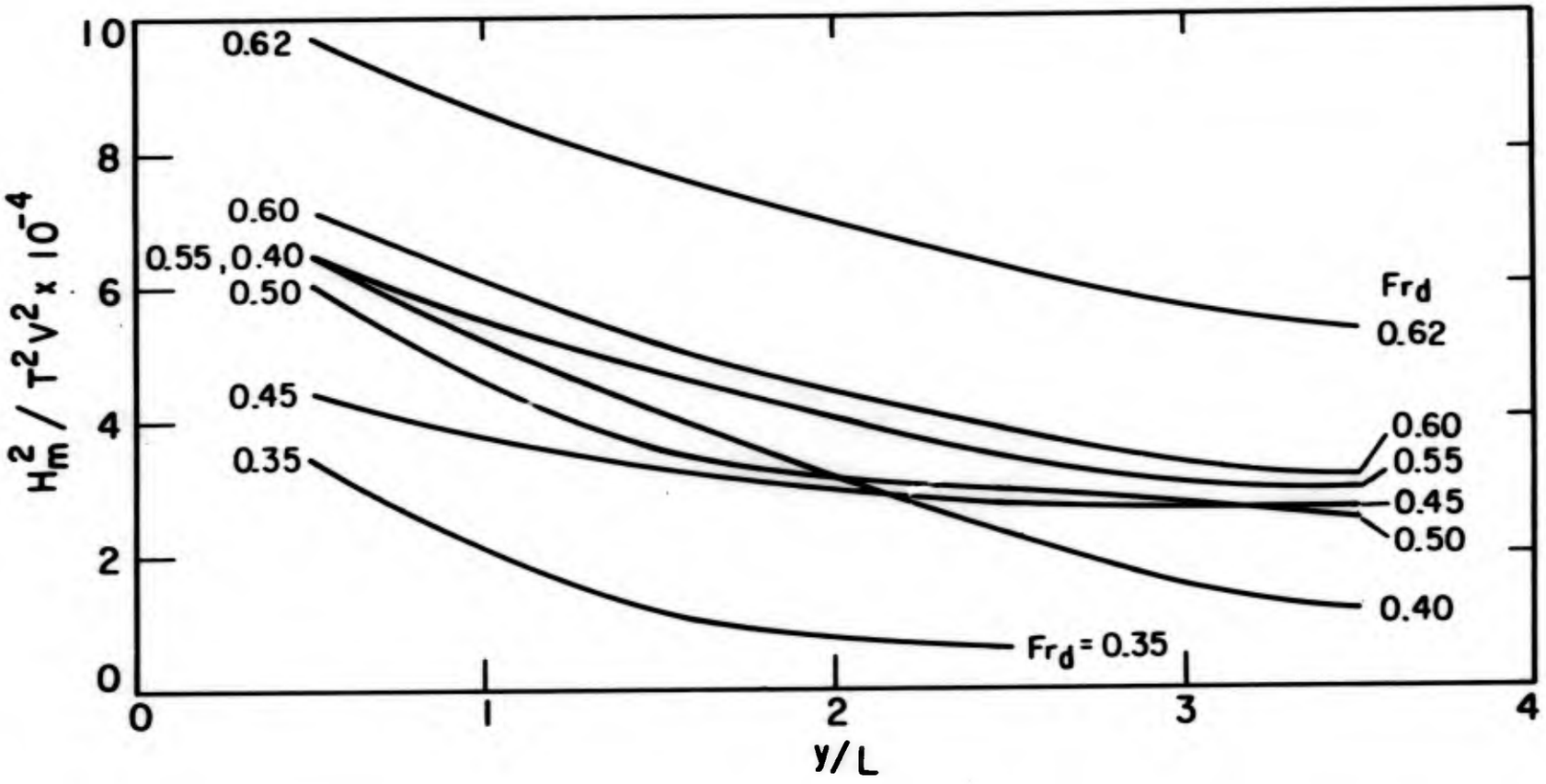

FIG. 25 $H_m^2/T^2 V^2$ AS A FUNCTION OF y/L WITH FROUDE NUMBER AS A PARAMETER FOR MARINER MODEL IN DEEP WATER ($d = 24\frac{7}{8}$)

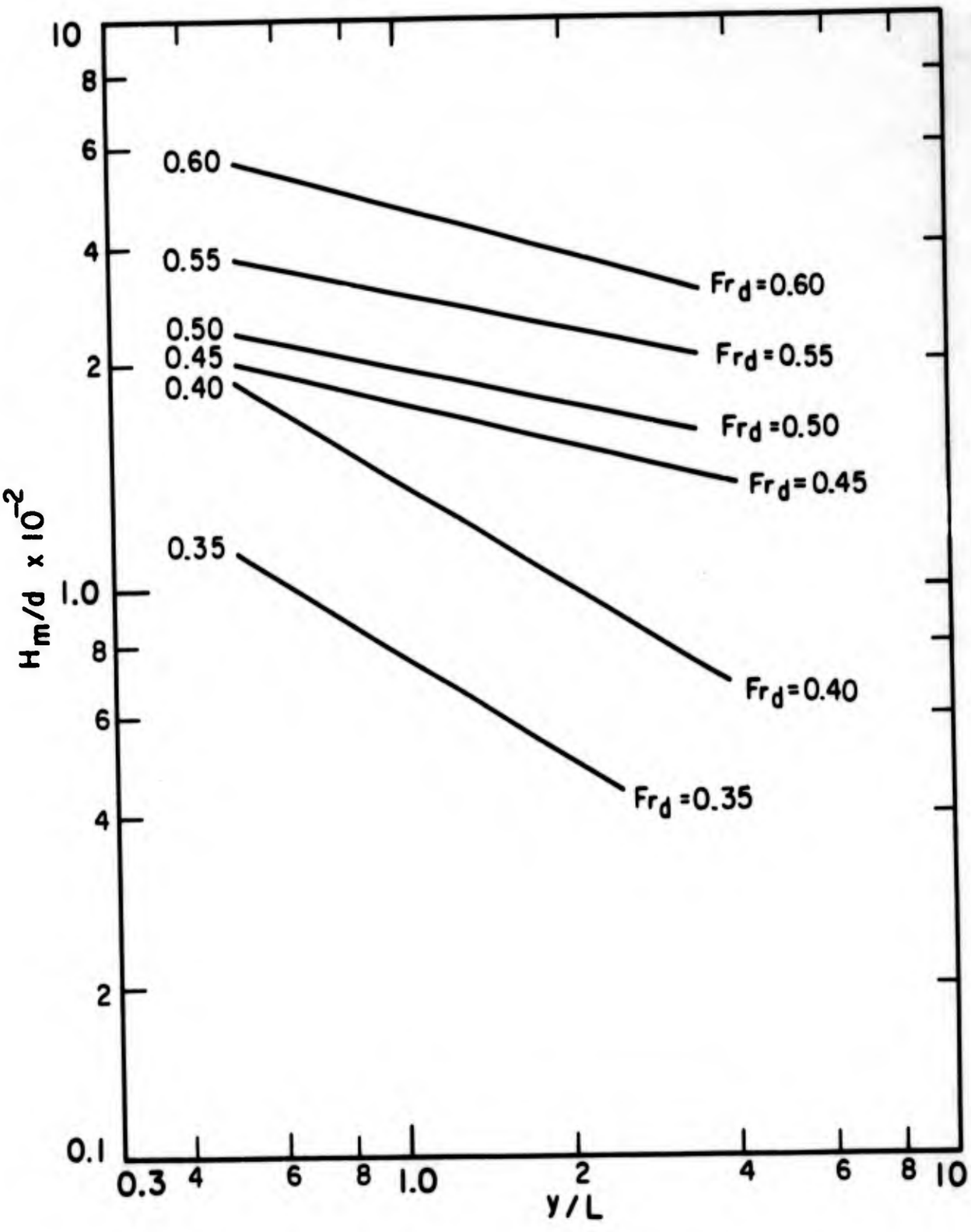

FIG. 26 H_m/d AS A FUNCTION OF y/L FOR VARIOUS FROUDE NUMBERS FOR MARINER MODEL IN DEEP WATER ($d = 24\frac{7}{8}$")

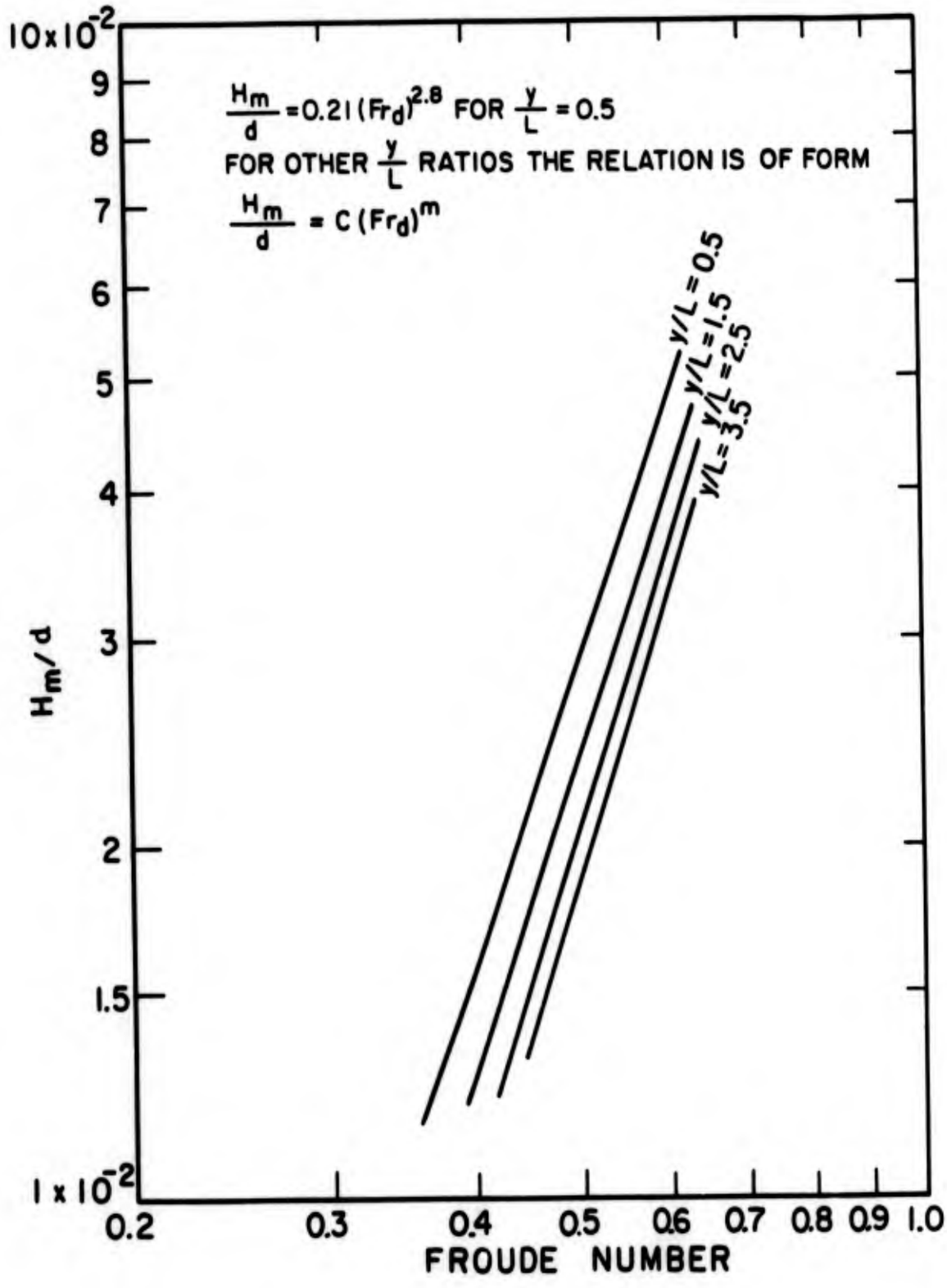

FIG. 27 $\frac{H_m}{d}$ AT DIFFERENT $\frac{y}{L}$ AS A FUNCTION OF FROUDE NUMBER FOR MARINER MODEL IN DEEP WATER ($d = 24\frac{7}{8}$")

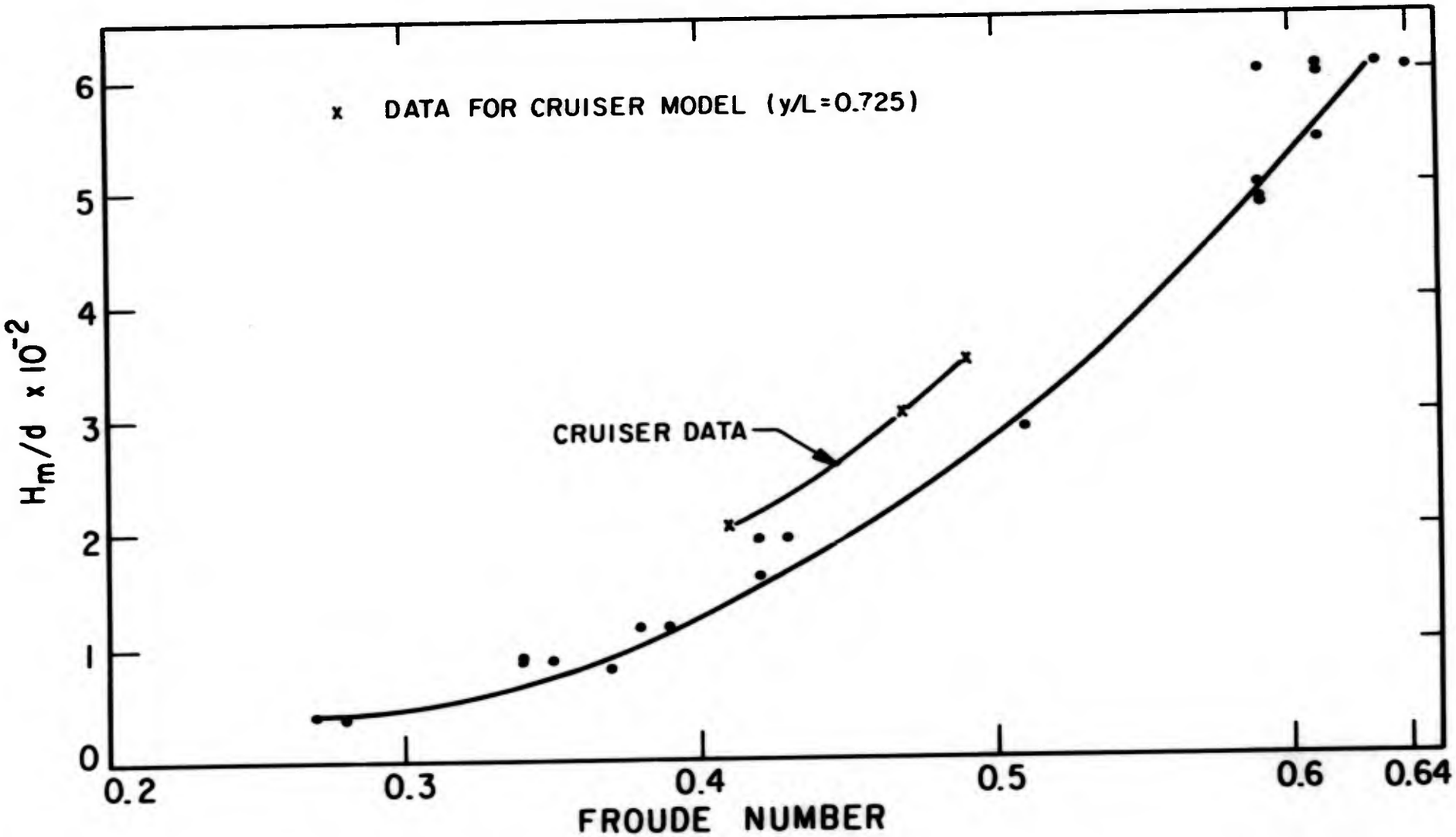

FIG. 28 DIMENSIONLESS MAXIMUM WAVE HEIGHT AS A FUNCTION OF FROUDE NUMBER AT y/L = 0.50 FOR MARINER MODEL IN DEEP WATER ($d = 24\frac{7}{8}$)

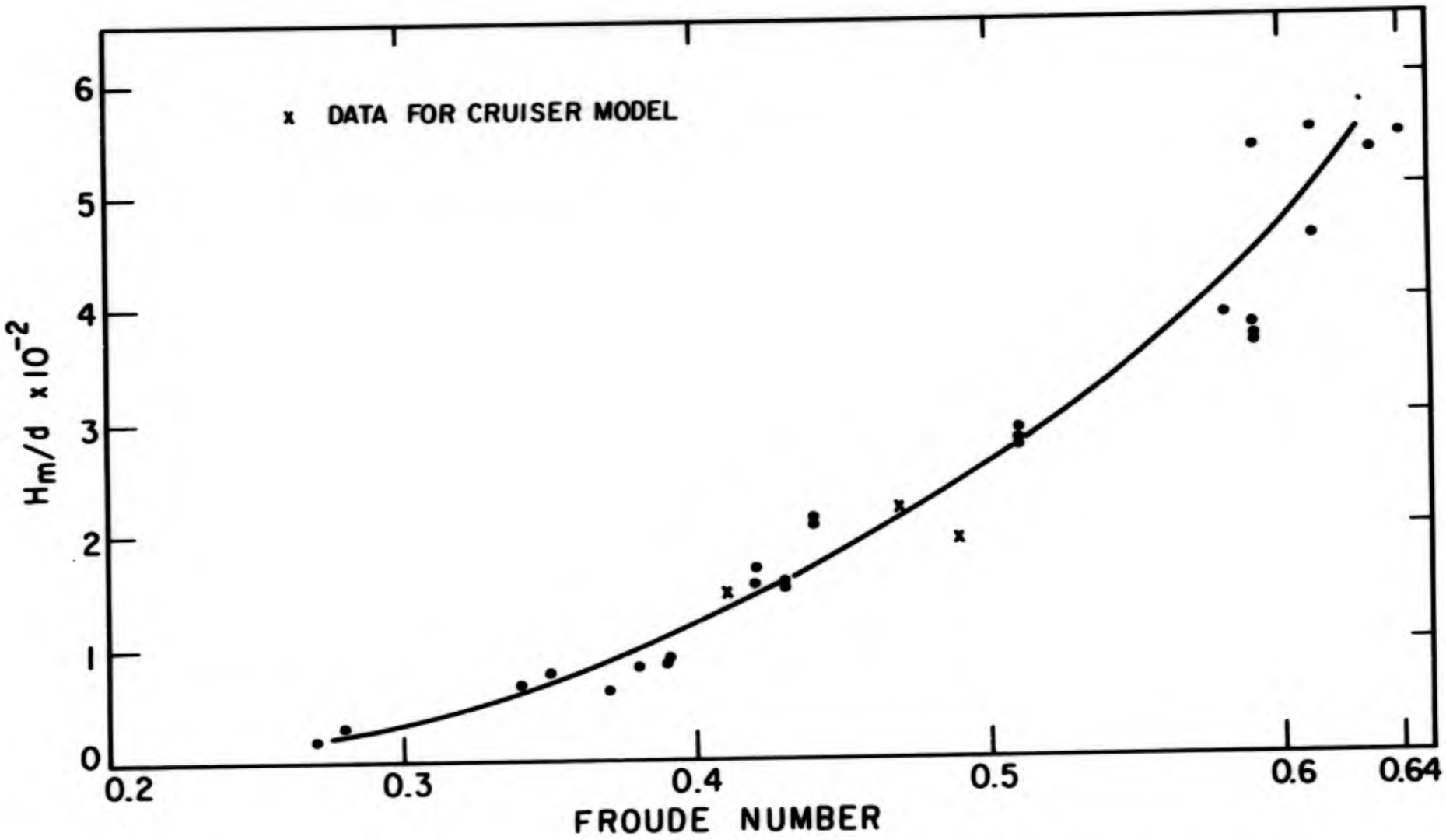

FIG. 29 DIMENSIONLESS MAXIMUM WAVE HEIGHT AS A FUNCTION OF FROUDE NUMBER AT y/L = 1.5 FOR MARINER MODEL IN DEEP WATER ($d = 24\frac{7}{8}$)

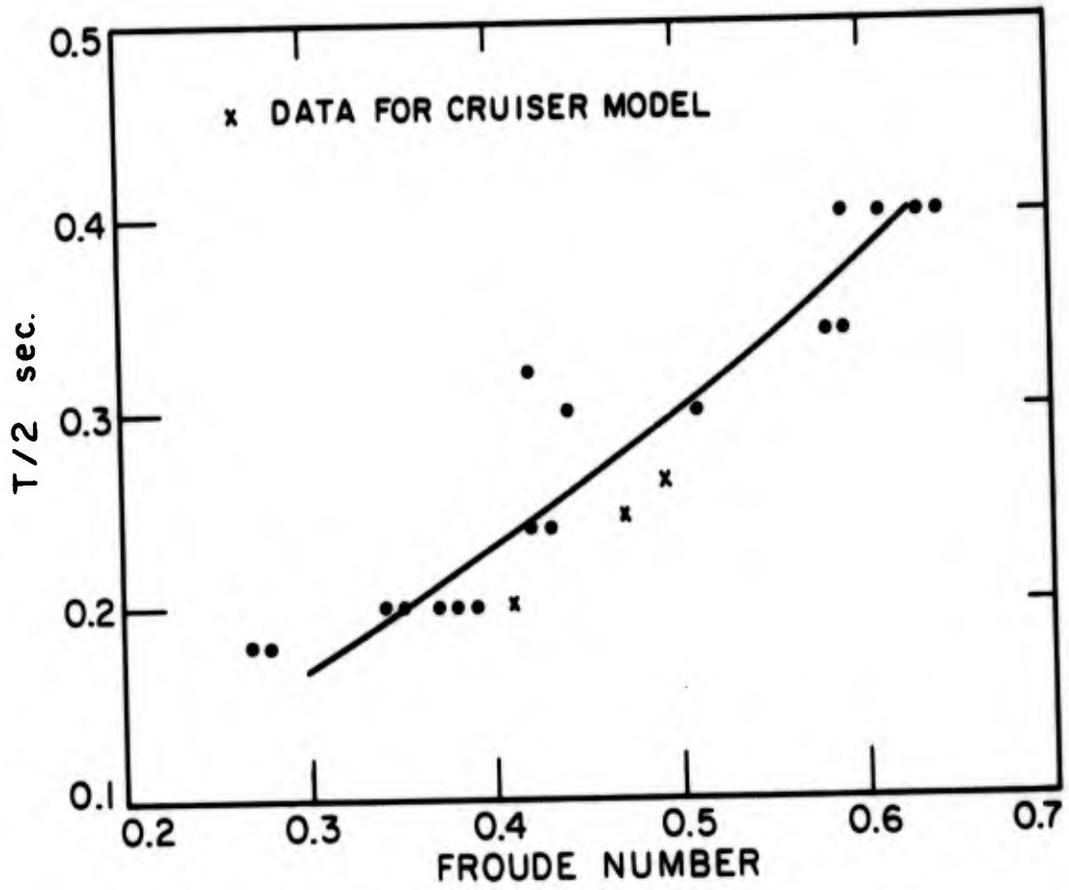

FIG. 30 HALF PERIOD OF HIGHEST WAVE AS A FUNCTION OF FROUDE NUMBER FOR MARINER & CRUISER MODELS IN DEEP WATER ($d = 24\frac{7}{8}$")

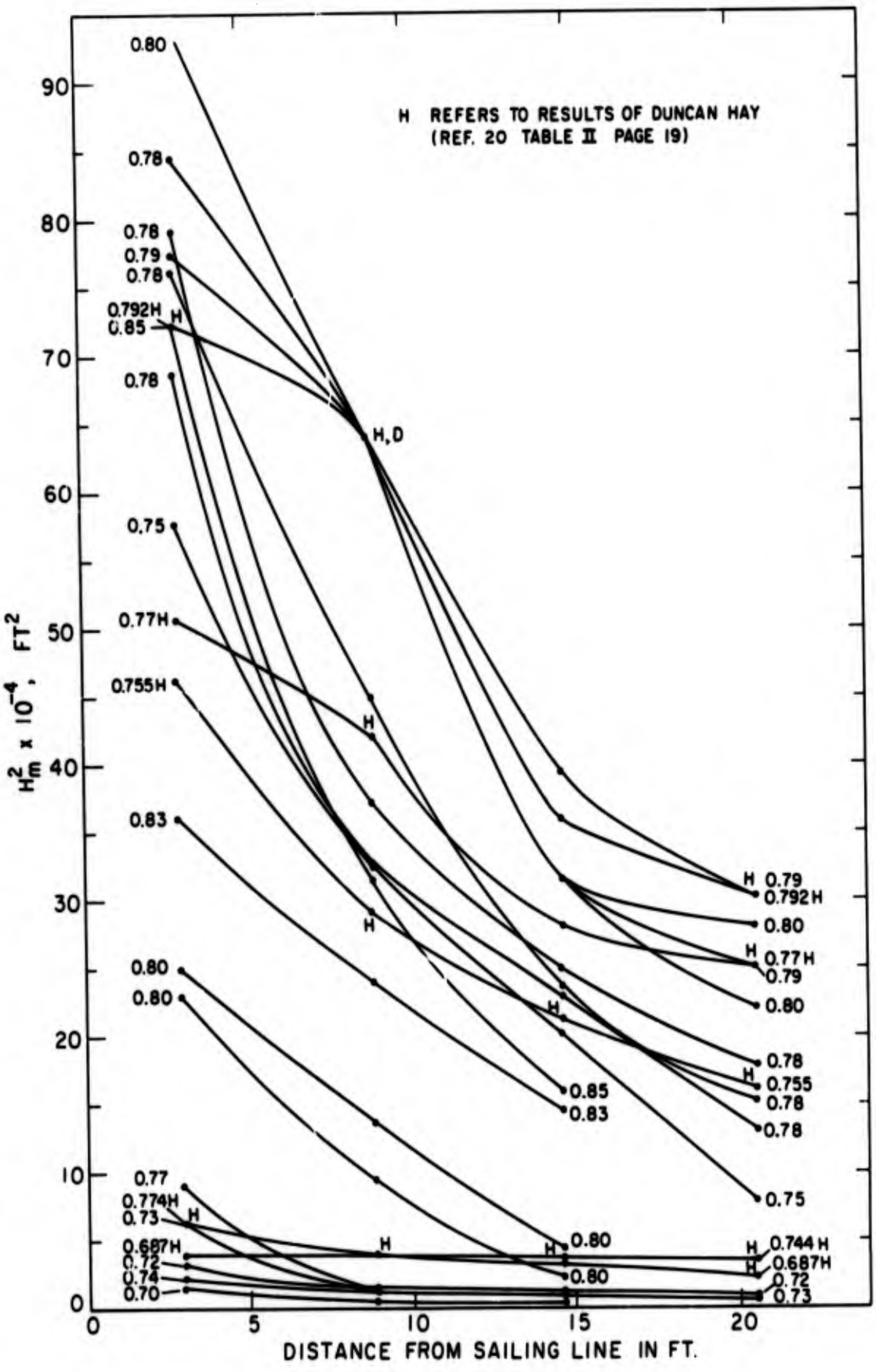

FIG 31 H_m^2 AS A FUNCTION OF DISTANCE FROM SAILING LINE WITH FROUDE NUMBER AS A PARAMETER FOR MARINER MODEL IN SHALLOW WATER ($d = 4\frac{1}{8}$")

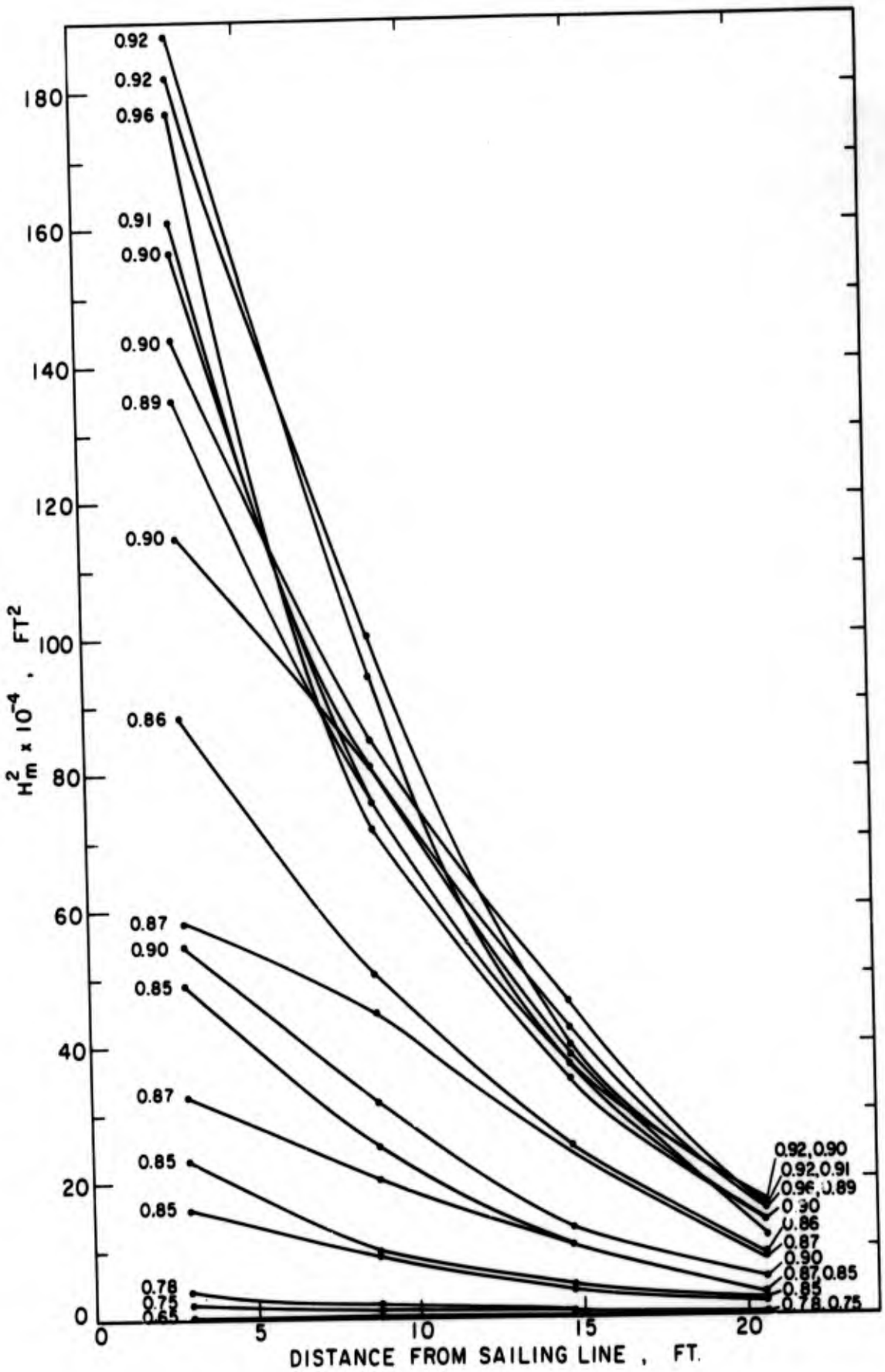

FIG. 32 H_m^2 AS A FUNCTION OF DISTANCE FROM SAILING LINE WITH FROUDE NUMBER AS A PARAMETER FOR CRUISER MODEL IN SHALLOW WATER

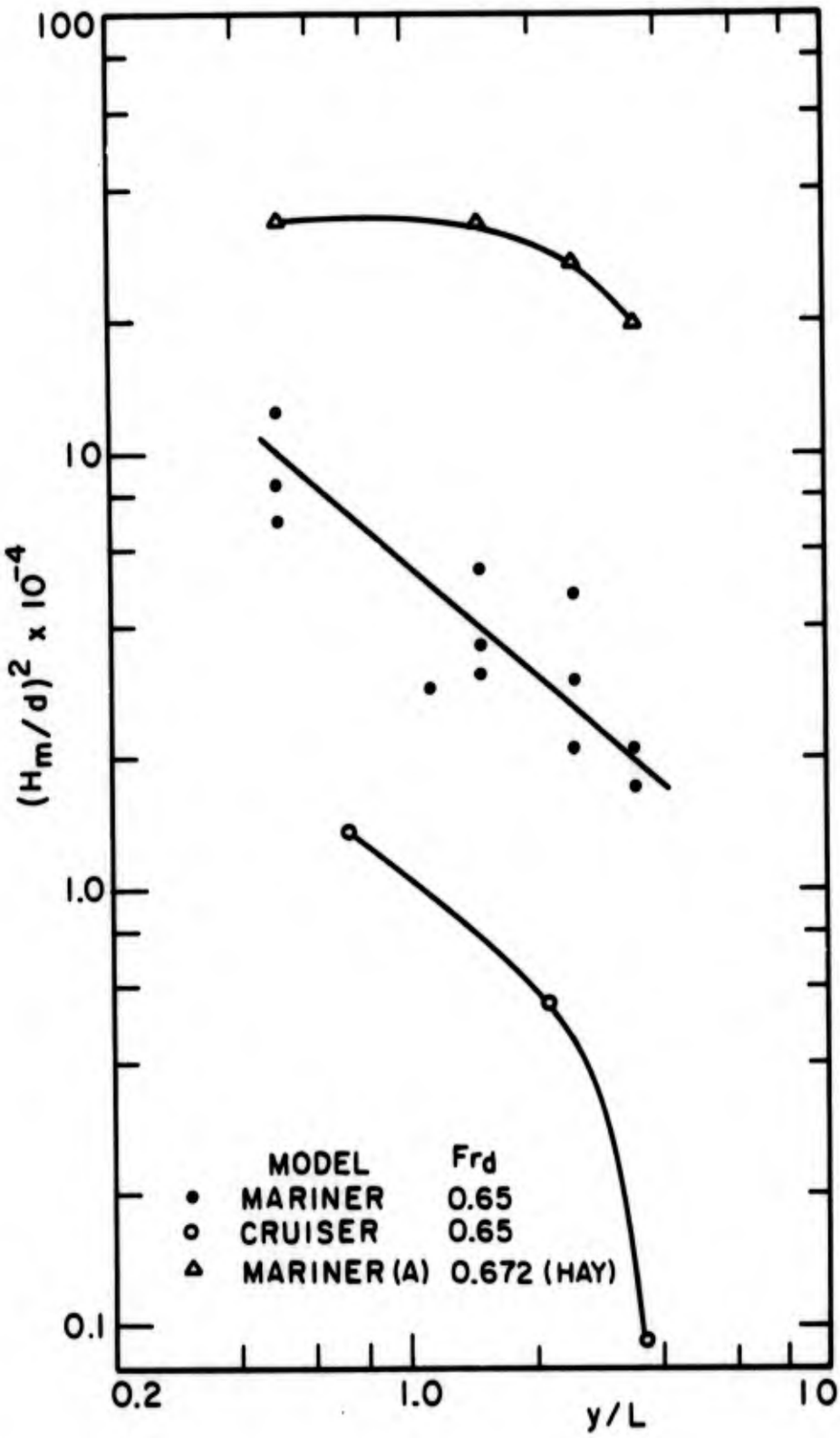

FIG. 33 $(H_m/d)^2$ AS A FUNCTION OF y/L FOR THE MARINER & CRUISER MODELS IN SHALLOW WATER ($d = 4\frac{1}{8}$")

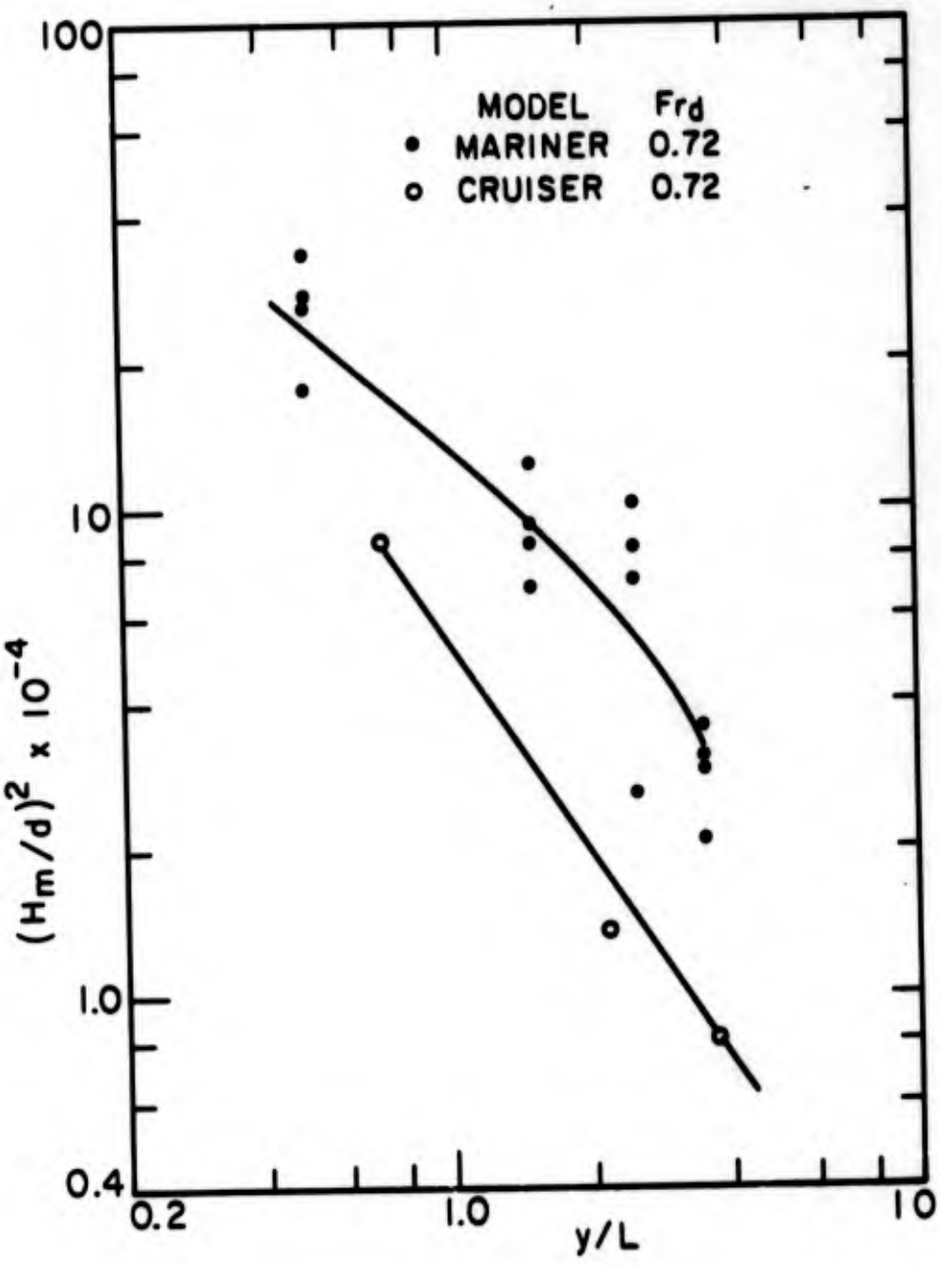

FIG. 34 $(H_m/d)^2$ AS A FUNCTION OF y/L FOR THE MARINER & CRUISER MODELS IN SHALLOW WATER ($d = 4\frac{1}{8}$")

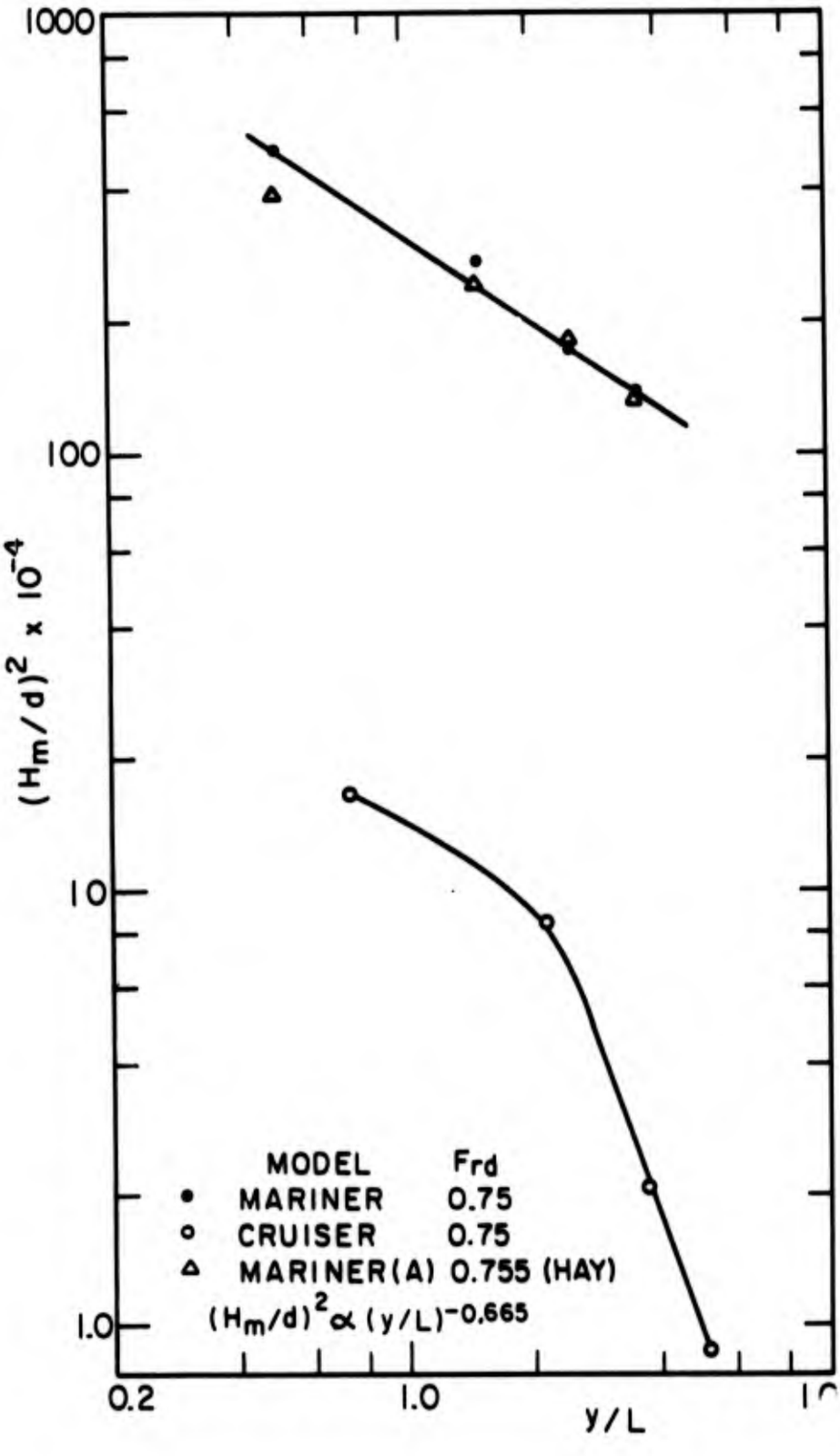

FIG. 35 $(H_m/d)^2$ AS A FUNCTION OF y/L FOR THE MARINER & CRUISER MODELS IN SHALLOW WATER ($d = 4\frac{1}{8}$")

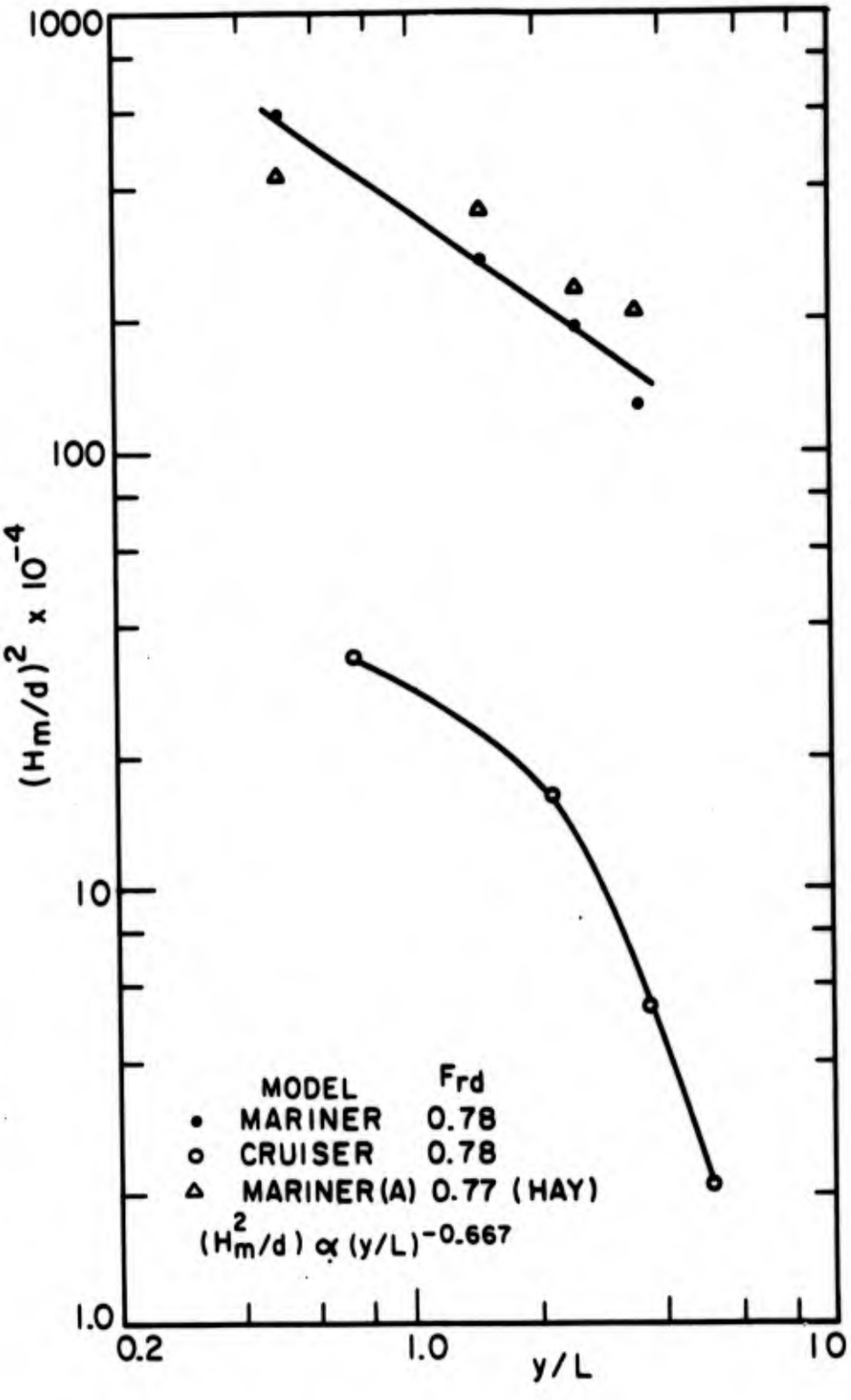

FIG. 36 $(H_m/d)^2$ AS A FUNCTION OF y/L FOR THE MARINER & CRUISER MODELS IN SHALLOW WATER ($d = 4\frac{1}{8}$")

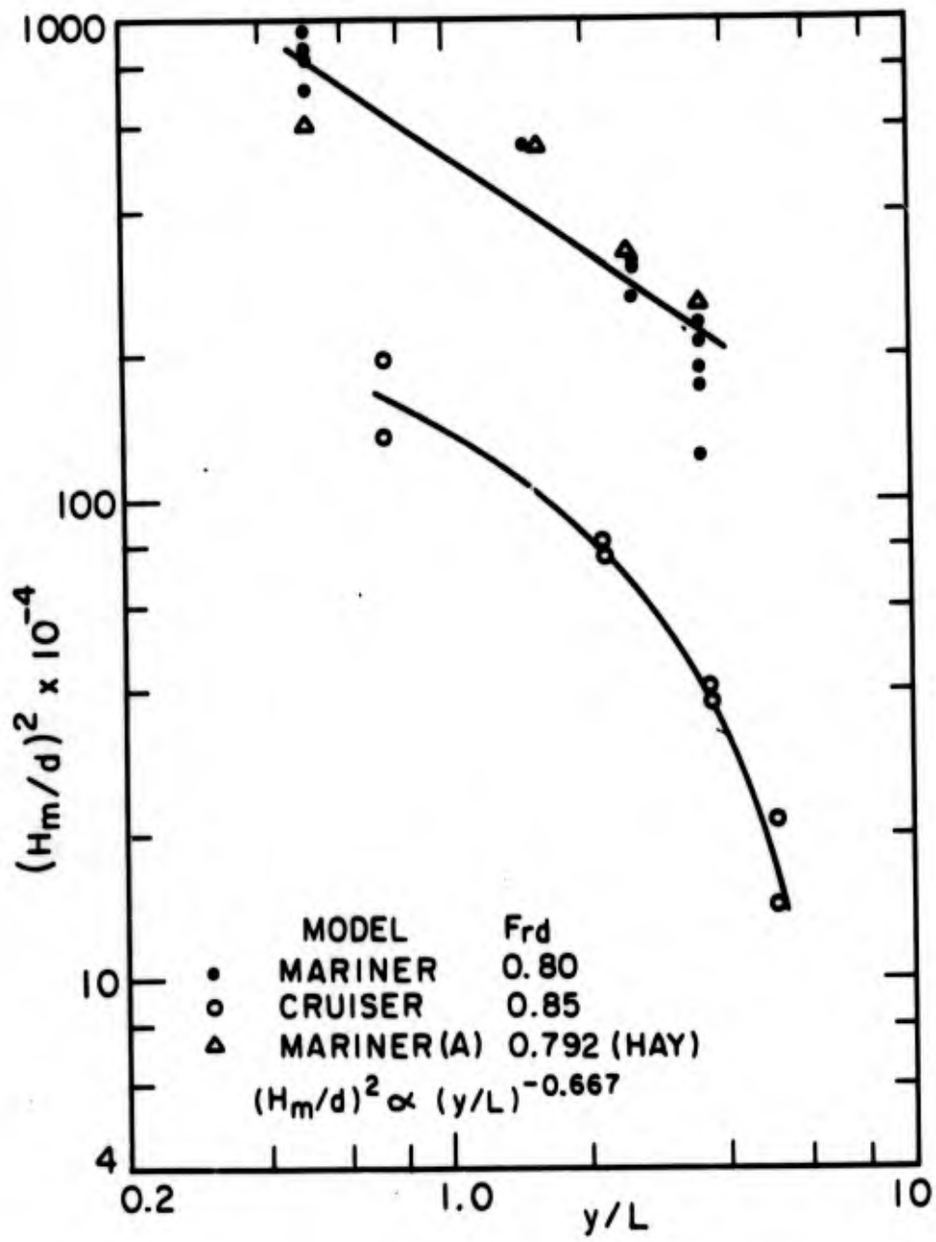

FIG. 37 $(H_m/d)^2$ AS A FUNCTION OF y/L FOR THE MARINER & CRUISER MODELS IN SHALLOW WATER ($d = 4\frac{1}{8}$")

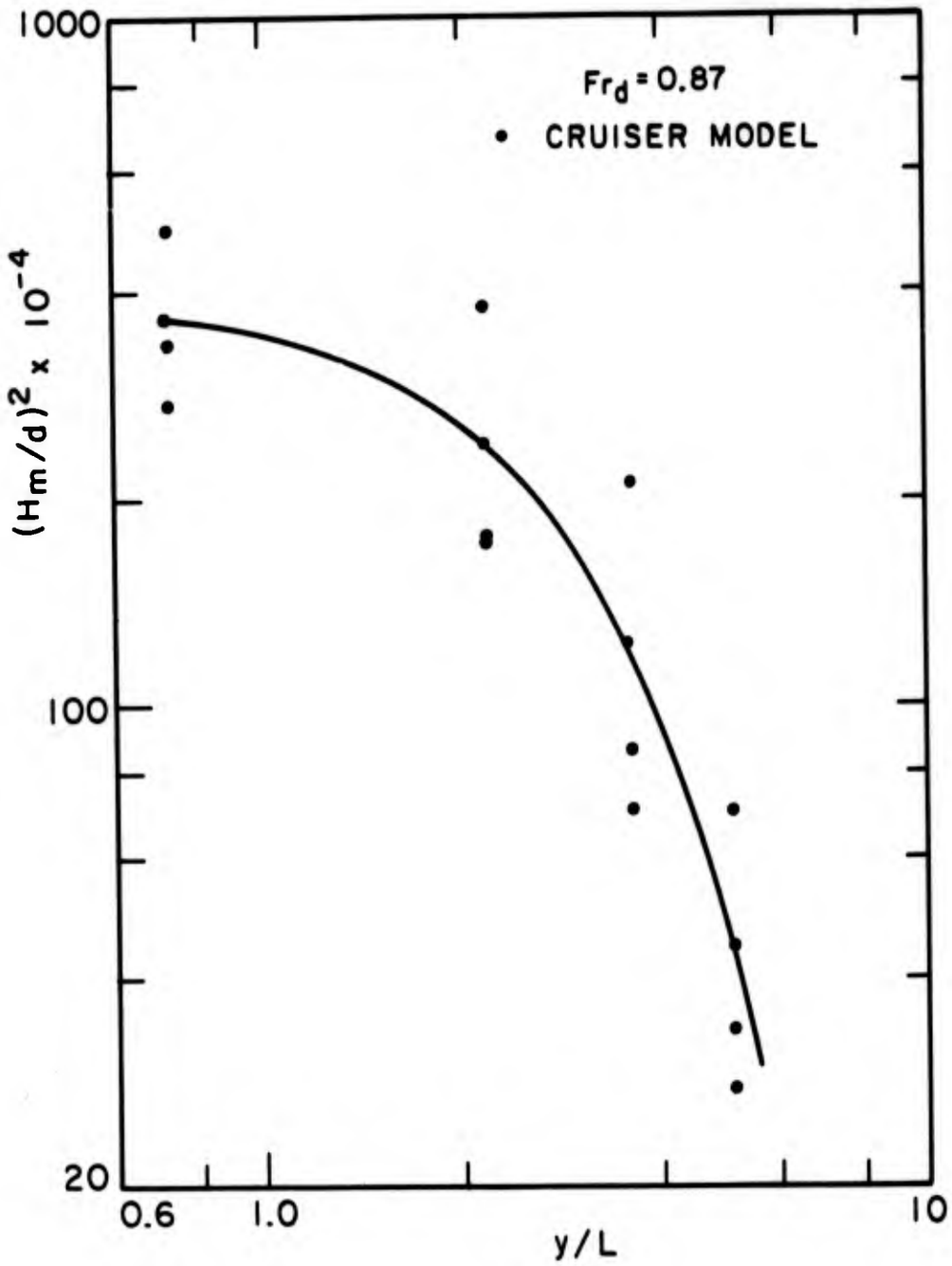

FIG. 38 $(H_m/d)^2$ AS A FUNCTION OF y/L FOR CRUISER MODEL IN SHALLOW WATER ($d = 4\frac{1}{8}"$)

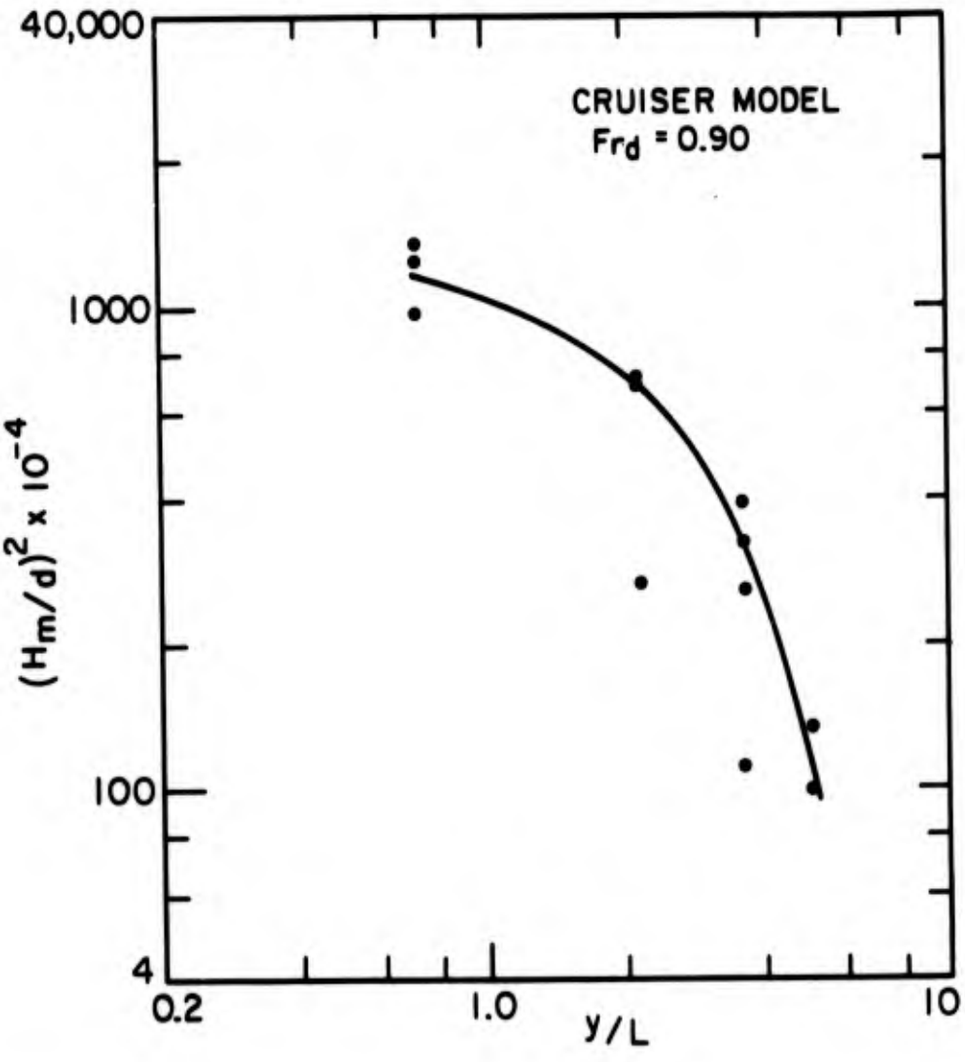

FIG. 39 $(H_m/d)^2$ AS A FUNCTION OF y/L FOR CRUISER MODEL IN SHALLOW WATER ($d = 4\frac{1}{8}$")

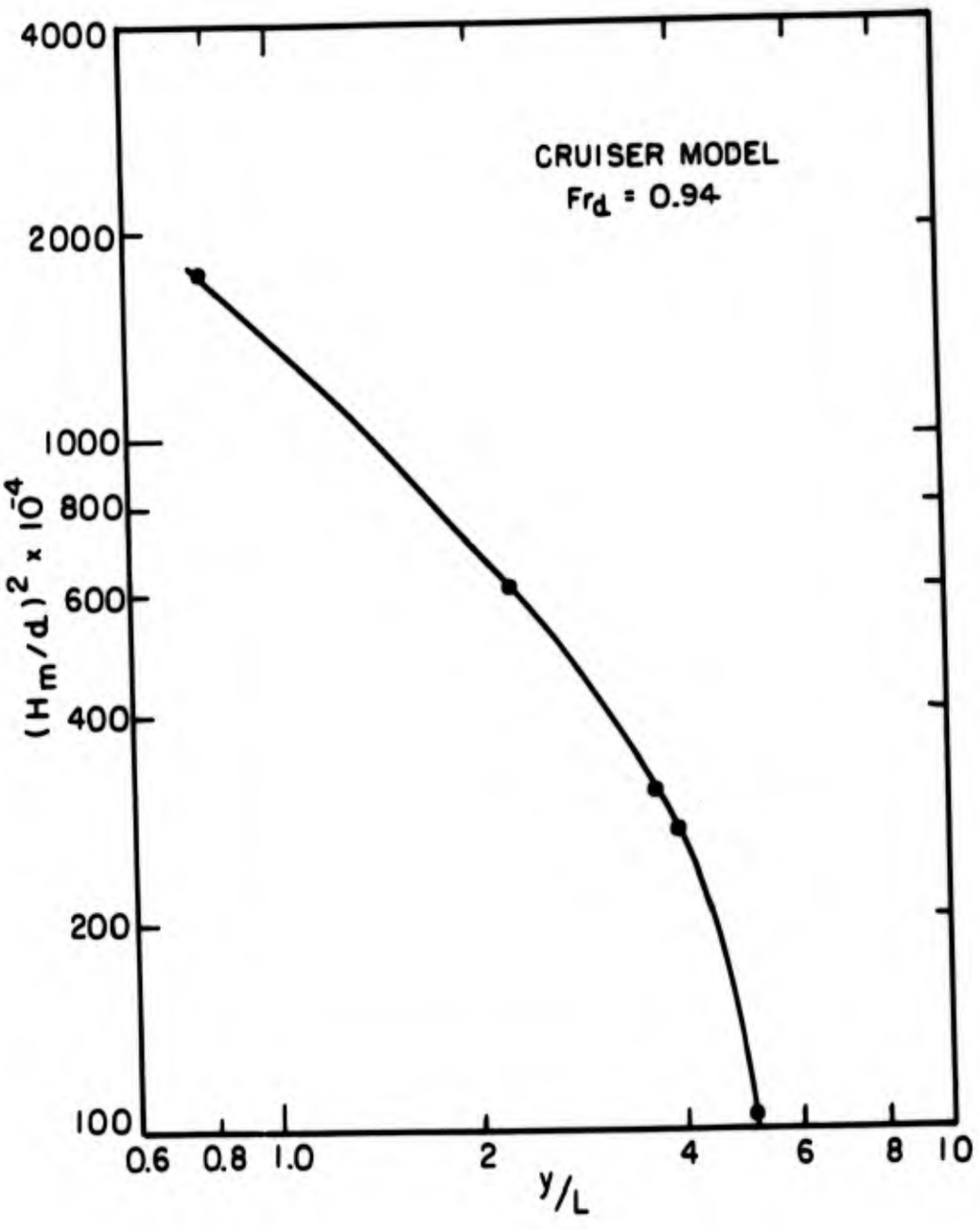

FIG. 40 $\left(\frac{H_m}{d}\right)^2$ AS A FUNCTION OF $\frac{y}{L}$ FOR CRUISER MODEL IN SHALLOW WATER ($d = 4\frac{1}{8}$")

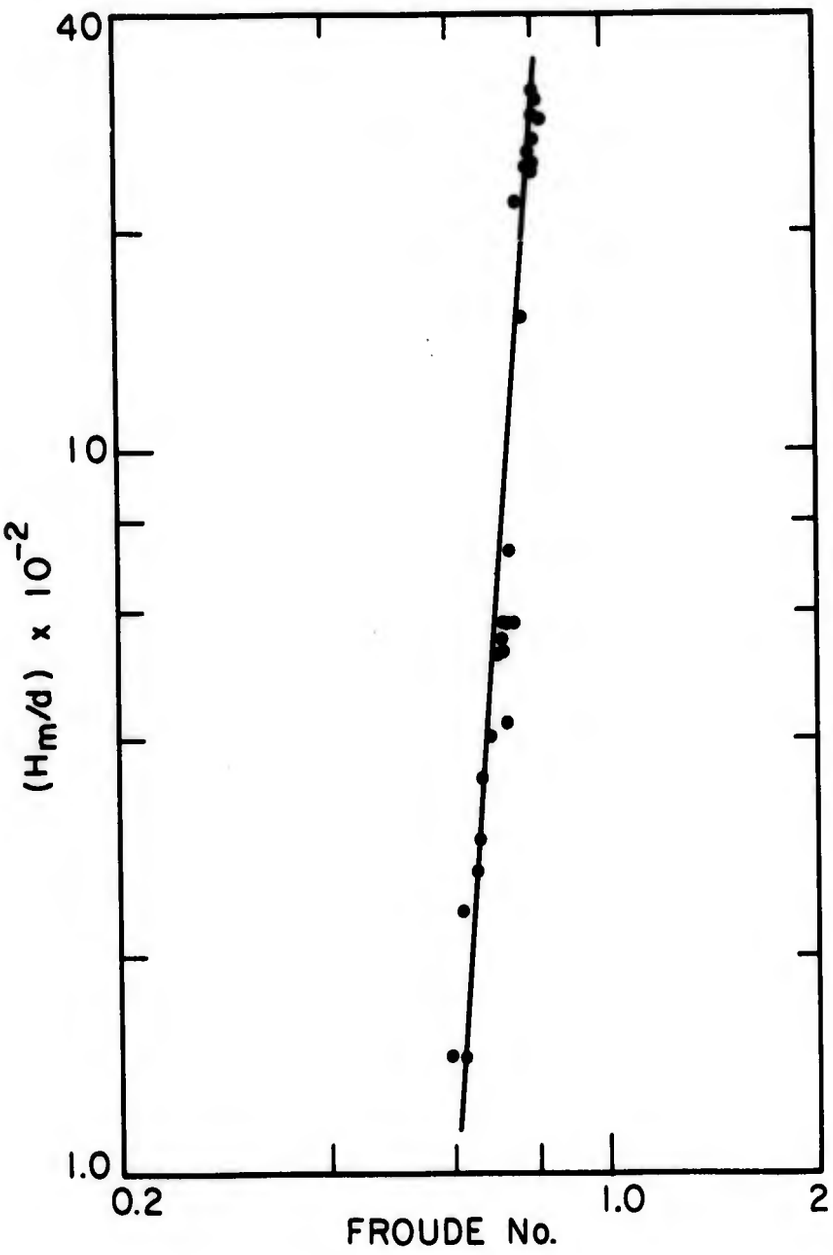

FIG. 41 H_m/d AS A FUNCTION OF FROUDE NUMBER FOR MARINER MODEL IN SHALLOW WATER (AT y/L = 0.50)
$(d = 4\frac{1}{8}")$

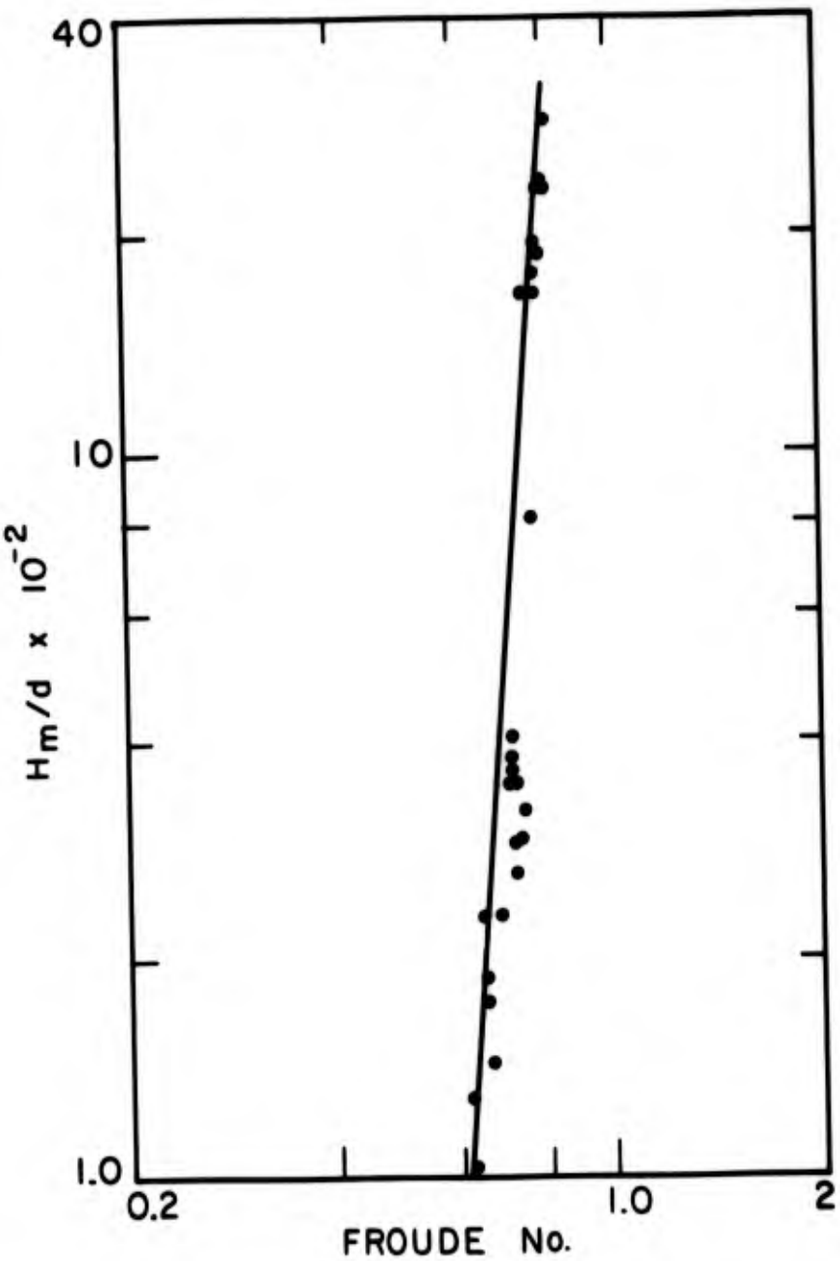

FIG. 42 H_m/d AS A FUNCTION OF FROUDE NUMBER FOR MARINER MODEL IN SHALLOW WATER (AT $y/L = 1.50$) ($d = 4\frac{1}{8}$")

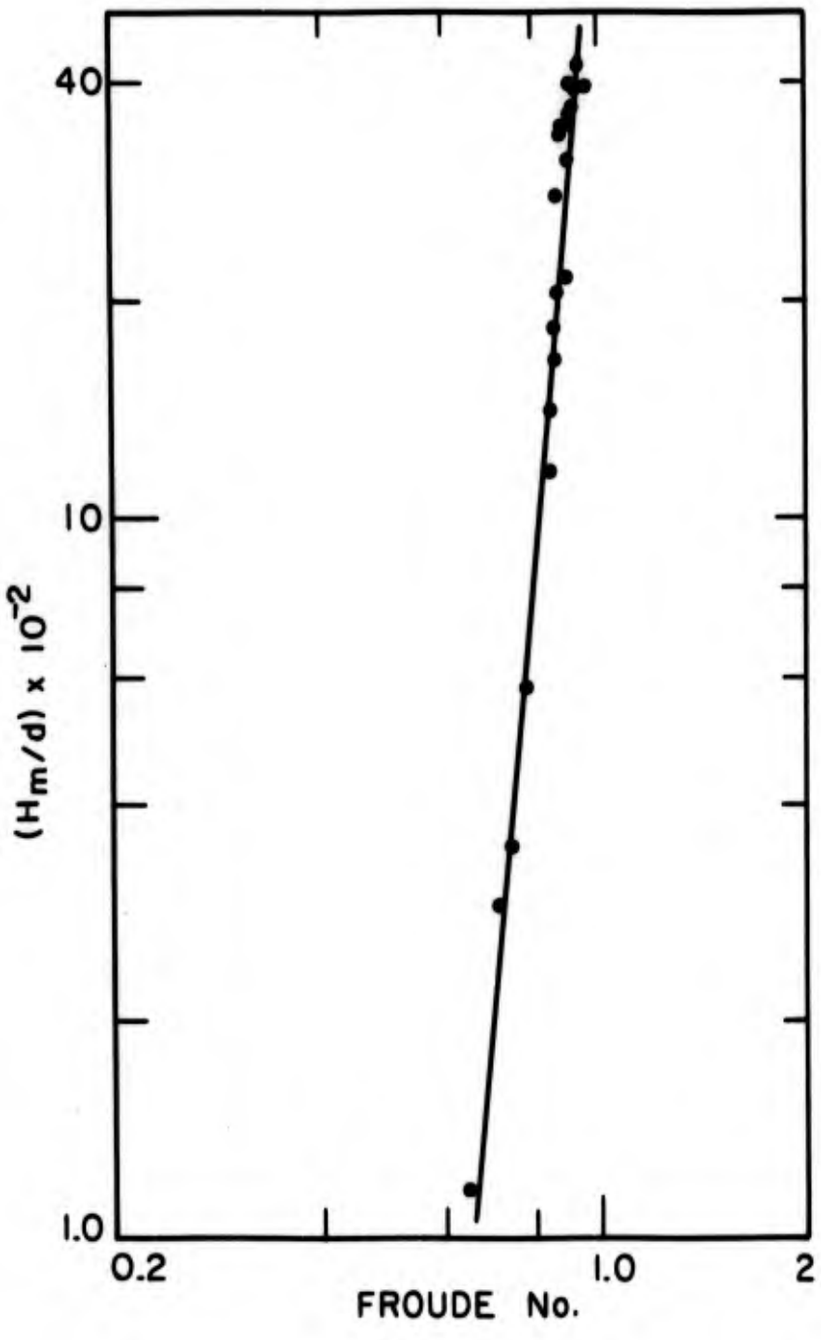

FIG. 43 H_m/d AS A FUNCTION OF FROUDE NUMBER FOR CRUISER MODEL IN SHALLOW WATER (AT y/L = 0.725)

NOTE. Data plotted refer to wave records at y/L = 0.725. Half-period remains practically constant for other three distances at y/L = 2.18, 3.62 & 5.01 with a little scatter.

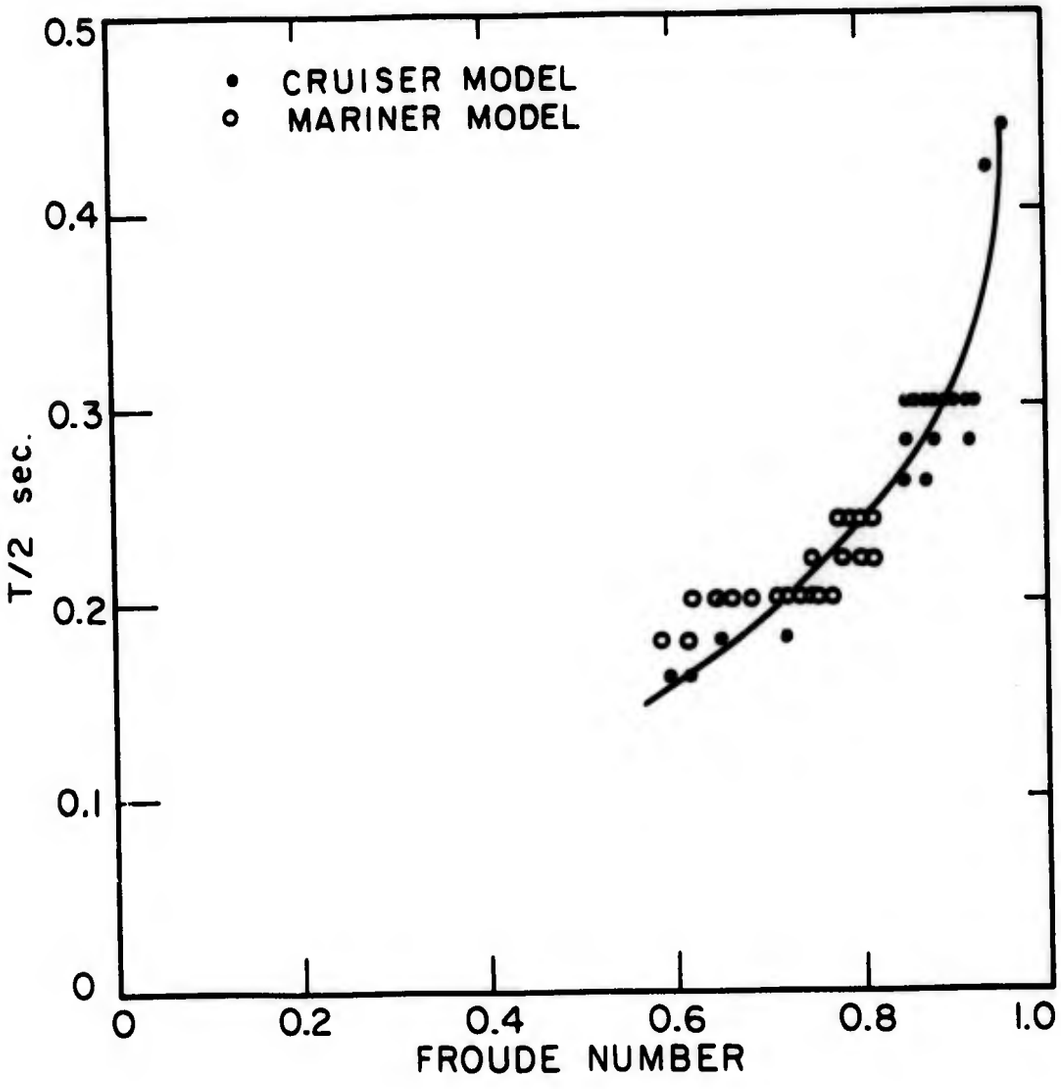

FIG. 44 HALF-PERIOD OF HIGHEST WAVE AS A FUNCTION OF FROUDE NUMBER IN SHALLOW WATER ($d = 4\frac{1}{8}"$)

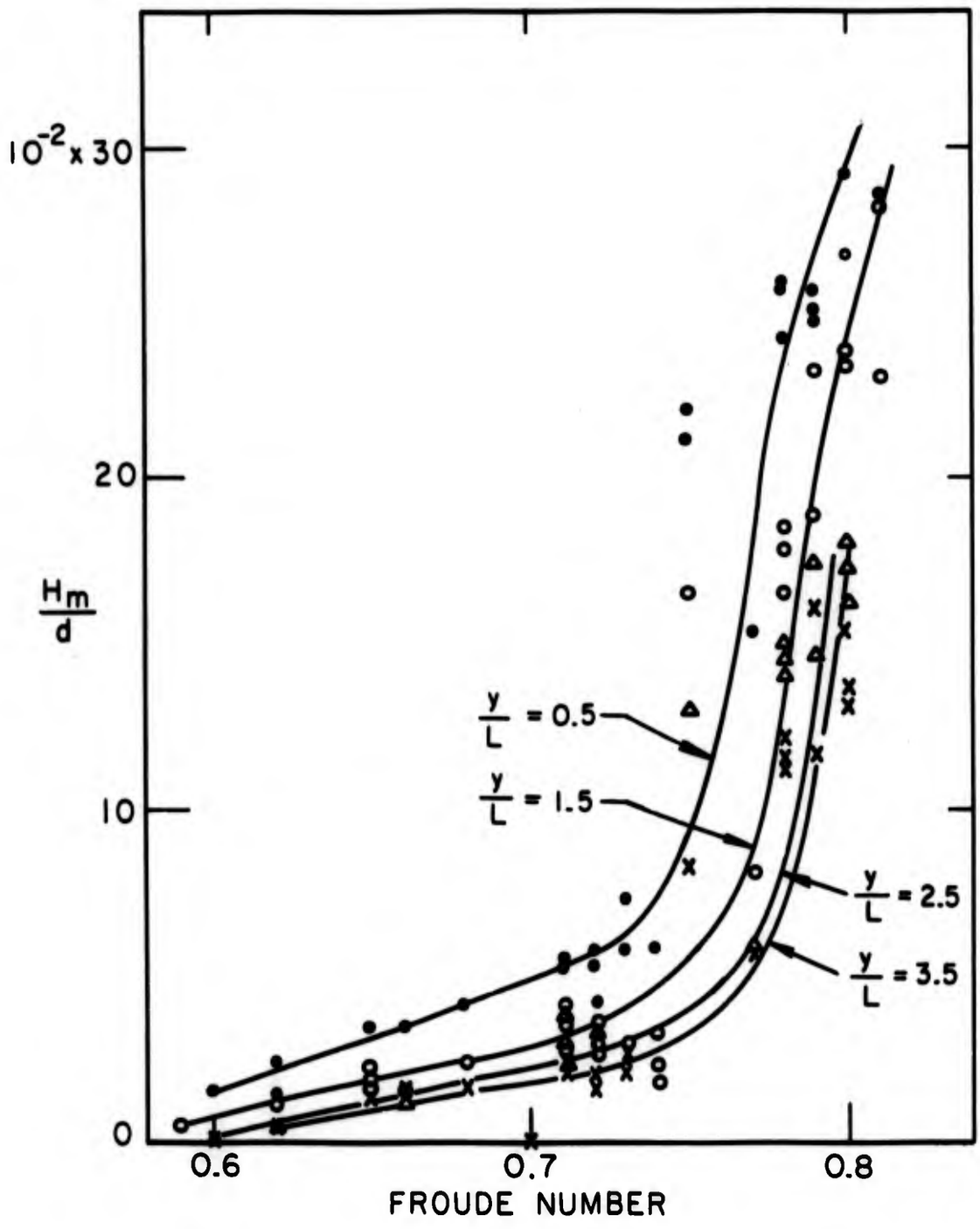

FIG. 45 DIMENSIONLESS MAXIMUM WAVE HEIGHT AS A FUNCTION OF FROUDE NUMBER AT DIFFERENT DISTANCES FROM SAILING LINE FOR MARINER MODEL IN SHALLOW WATER. ($d = 4\frac{1}{8}''$)

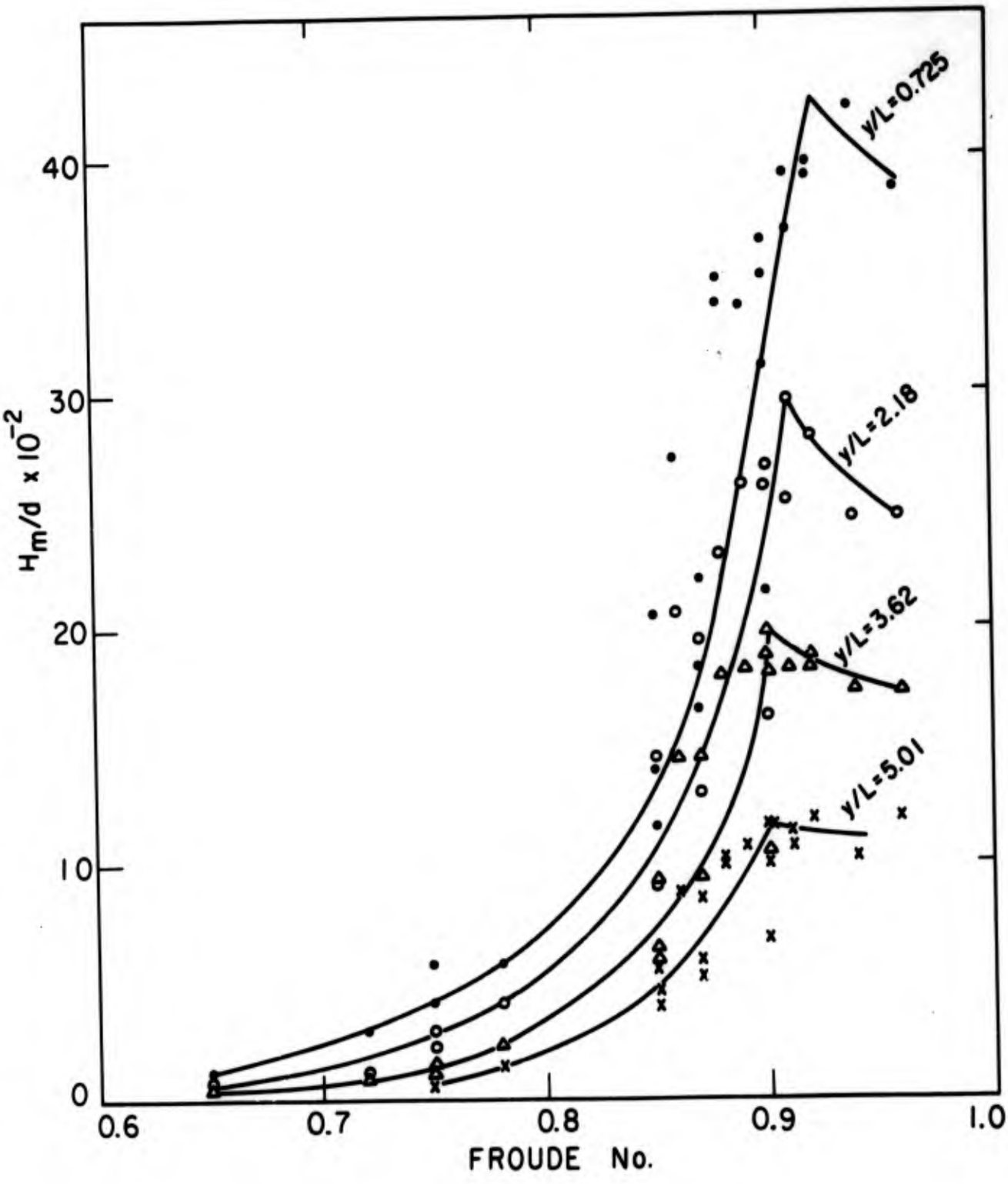

FIG. 46 DIMENSIONLESS MAXIMUM WAVE HEIGHT AS A FUNCTION OF FROUDE NUMBER AT DIFFERENT DISTANCES FROM SAILING LINE FOR CRUISER MODEL IN SHALLOW WATER ($d = 4\frac{1}{8}$")

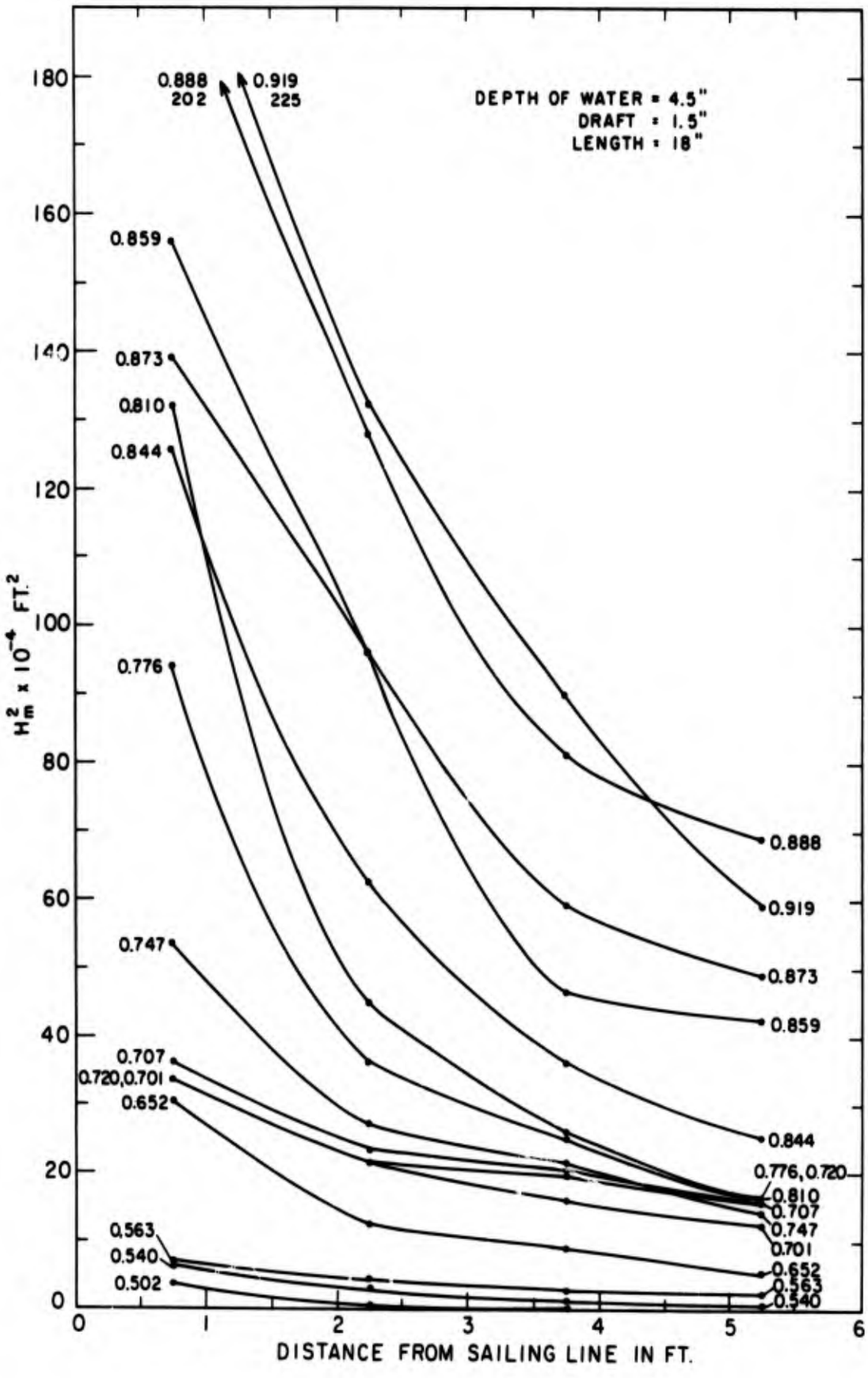

FIG 47 H_m^2 AS A FUNCTION OF DISTANCE FROM SAILING LINE WITH FROUDE NUMBER AS PARAMETER. MODEL A (SORENSEN)

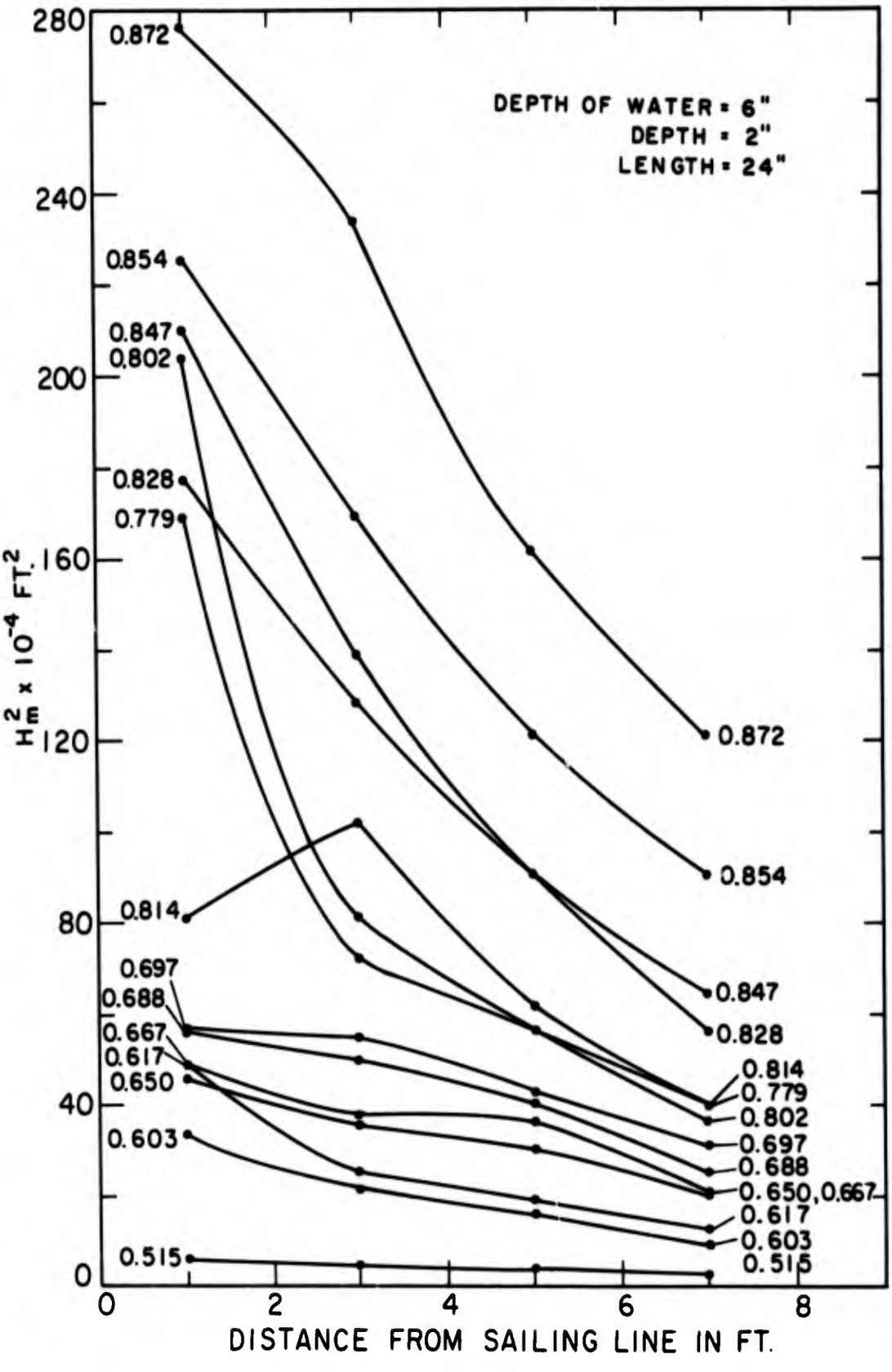

FIG 48 H_m^2 AS A FUNCTION OF DISTANCE FROM SAILING LINE WITH FROUDE NUMBER AS PARAMETER. MODEL B (SORENSEN)

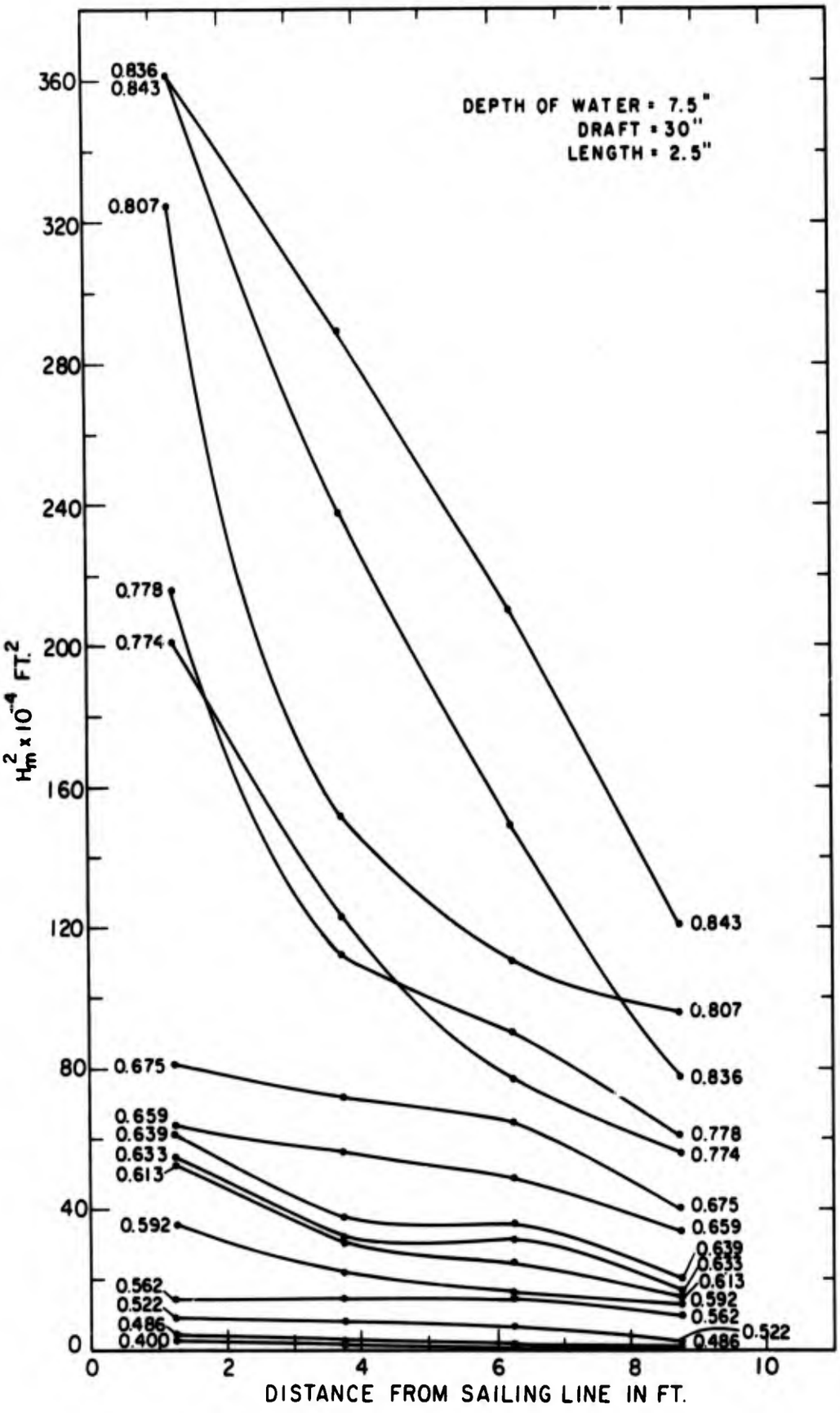

FIG 49 H_m^2 AS A FUNCTION OF DISTANCE FROM SAILING LINE WITH FROUDE NUMBER AS PARAMETER. MODEL C (SORENSEN)

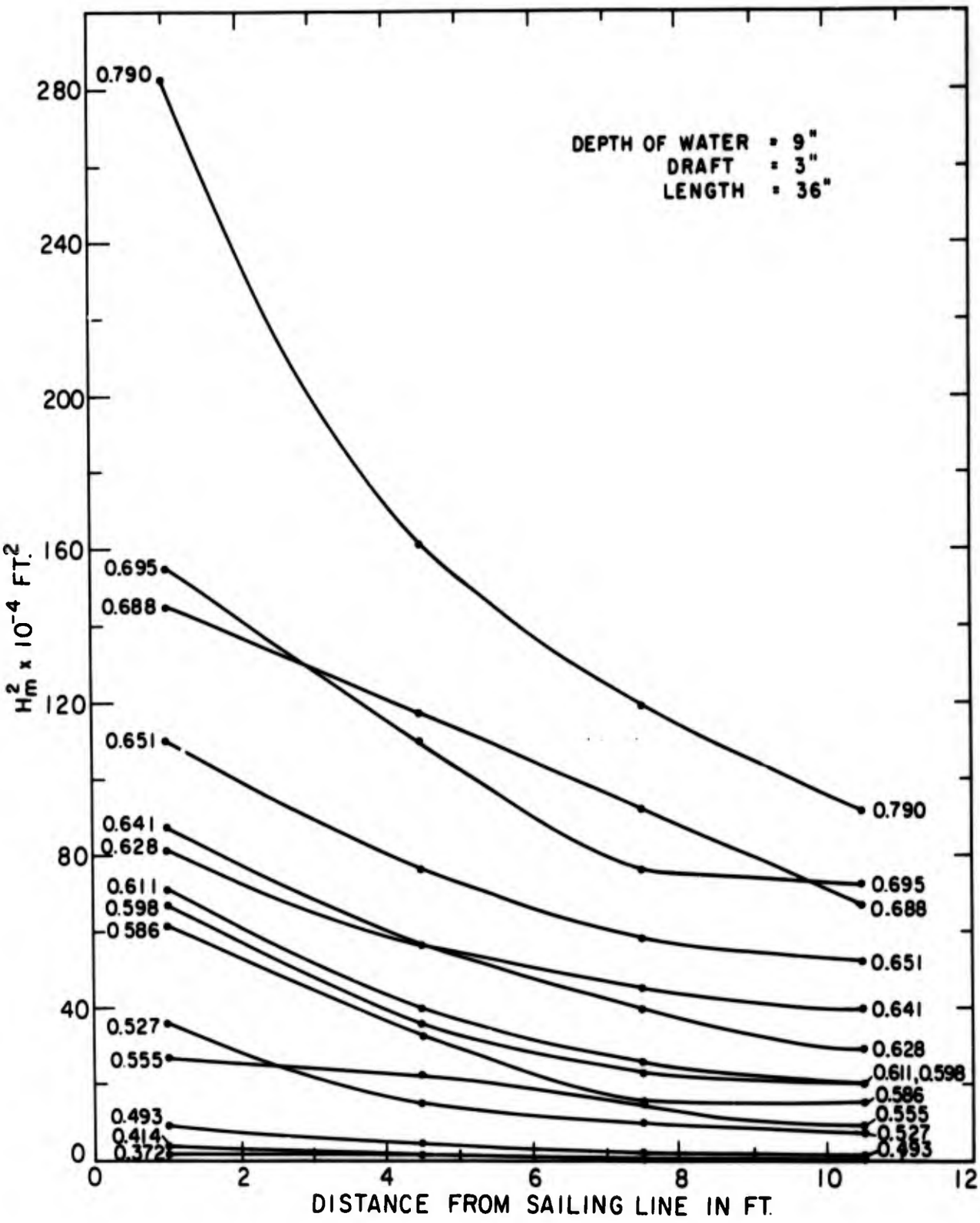

FIG 50 H_m^2 AS A FUNCTION OF DISTANCE FROM SAILING LINE WITH FROUDE NUMBER AS PARAMETER. MODEL D (SORENSEN)

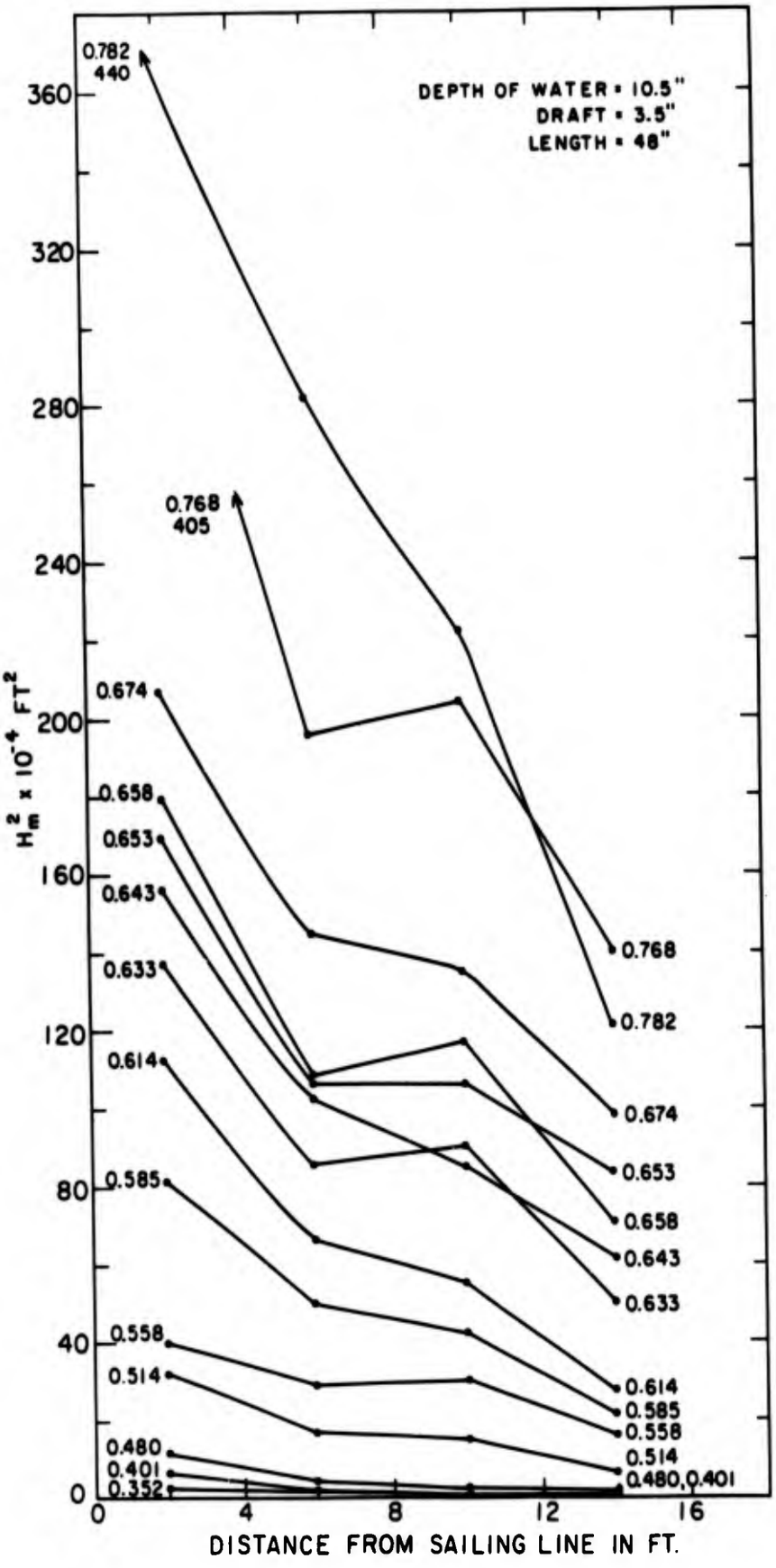

FIG 51 H_m^2 AS A FUNCTION OF DISTANCE FROM SAILING LINE WITH FROUDE NUMBER AS PARAMETER. MODEL E (SORENSEN)

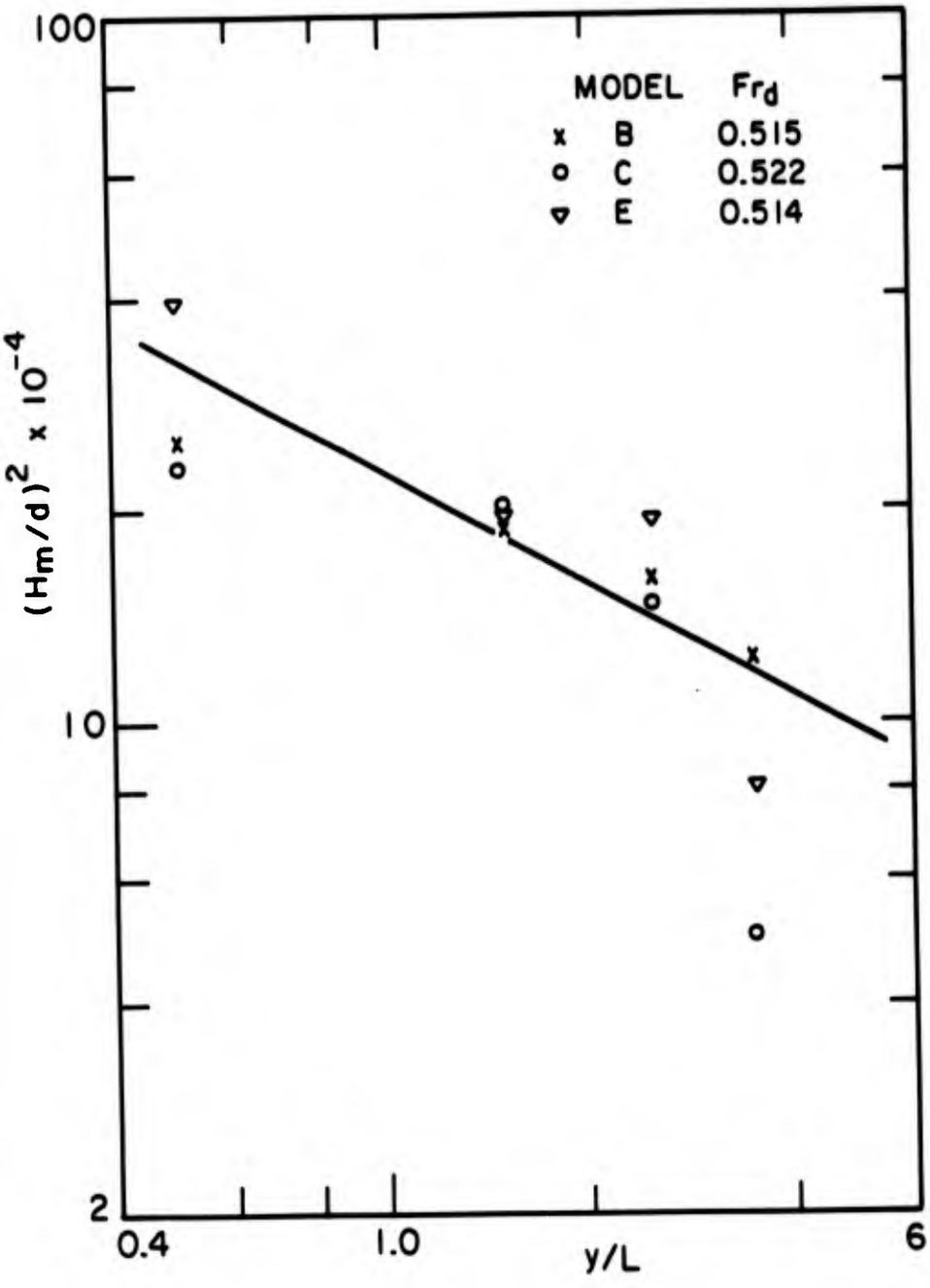

FIG. 52 $(H_m/d)^2$ AS A FUNCTION OF y/L FOR MODELS B, C & E (FROM FIG. 24 A SORENSEN)

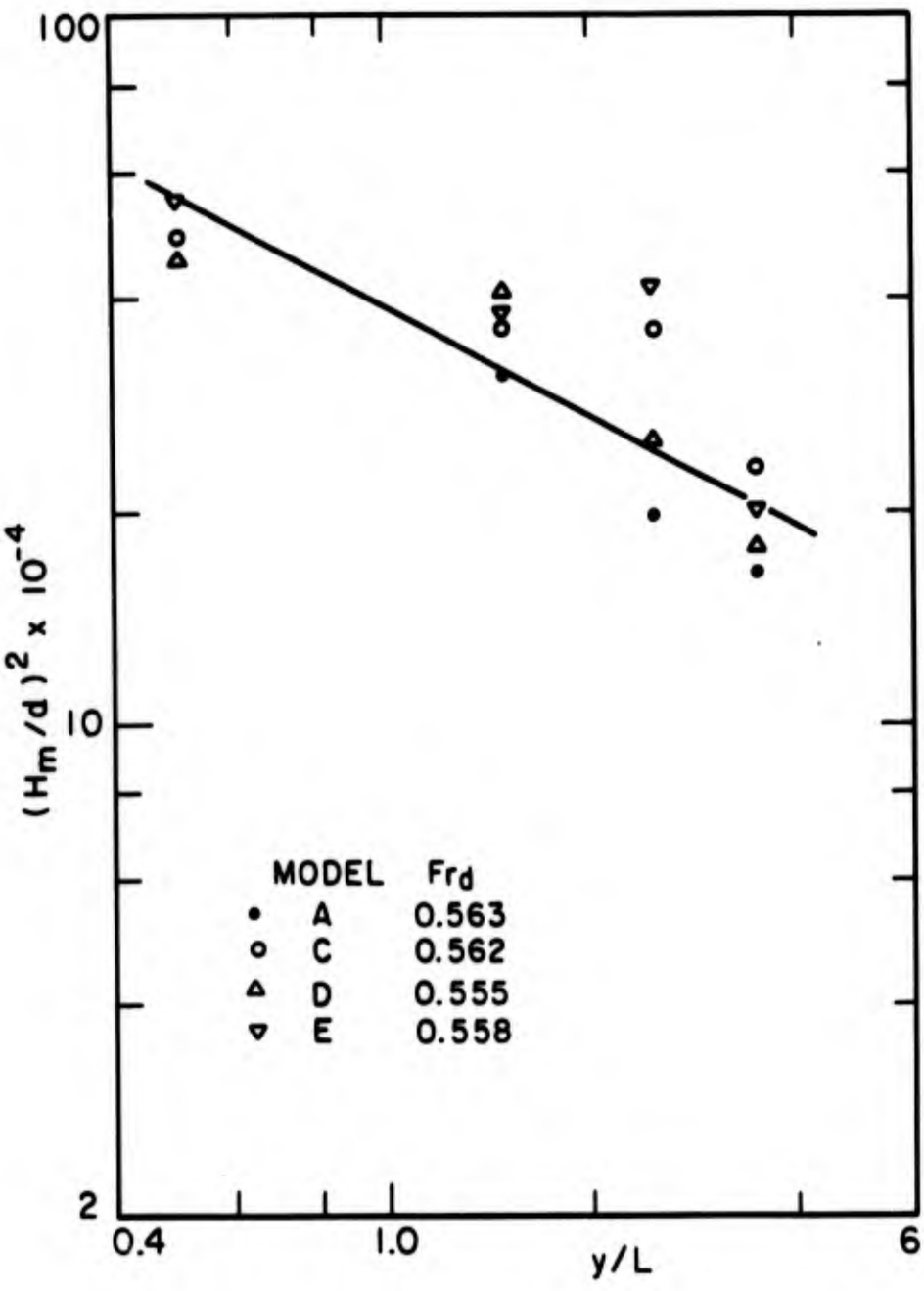

FIG. 53 $(H_m/d)^2$ AS A FUNCTION OF y/L FOR MODELS A, C, D & E (FROM FIG. 24B SORENSEN)

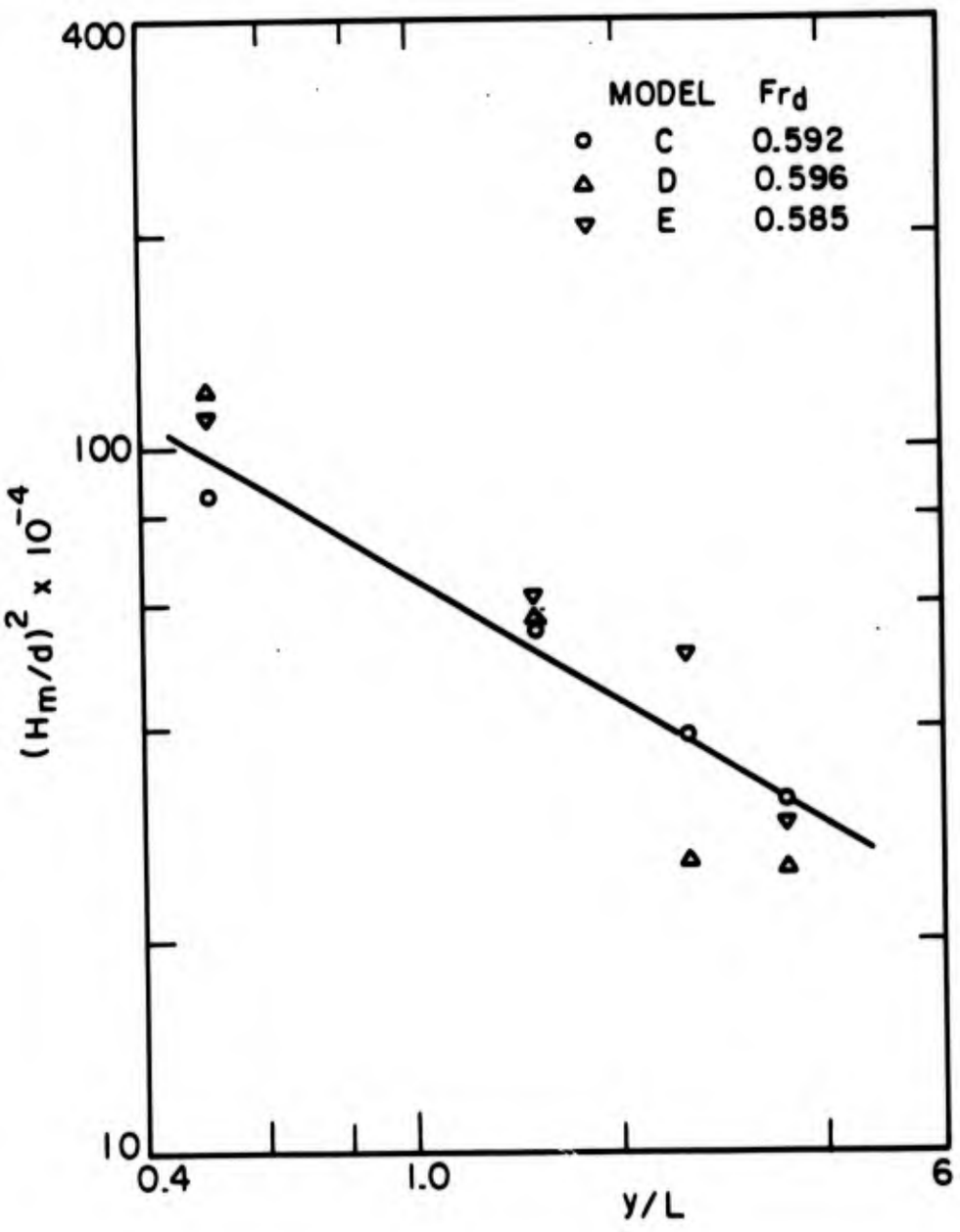

FIG. 54 $(H_m/d)^2$ AS A FUNCTION OF y/L FOR MODELS C, D & E (FROM FIG. 25A SORENSEN)

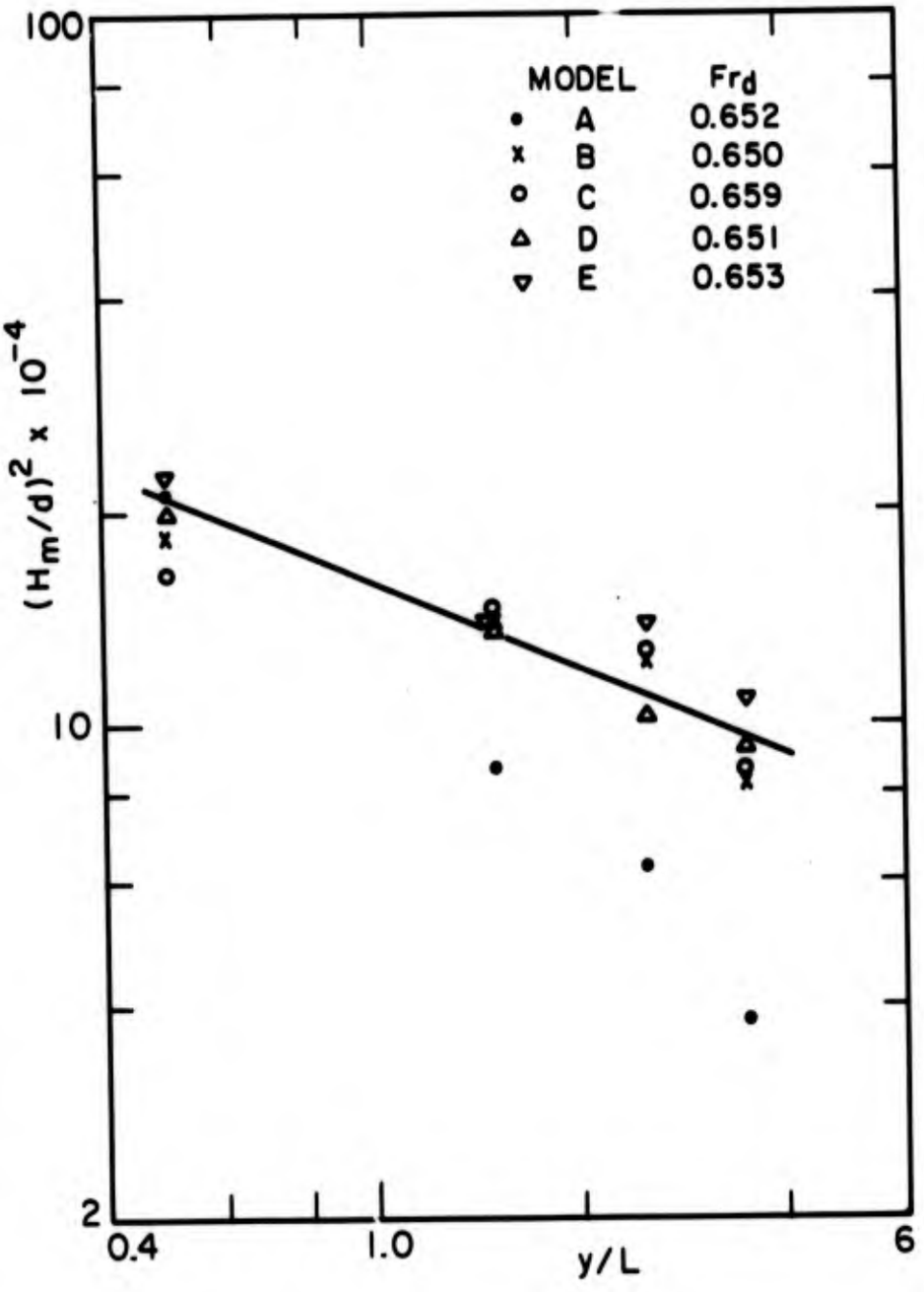

FIG. 55 $(H_m/d)^2$ AS A FUNCTION OF y/L FOR MODELS A, B, C, D & E (SORENSEN)

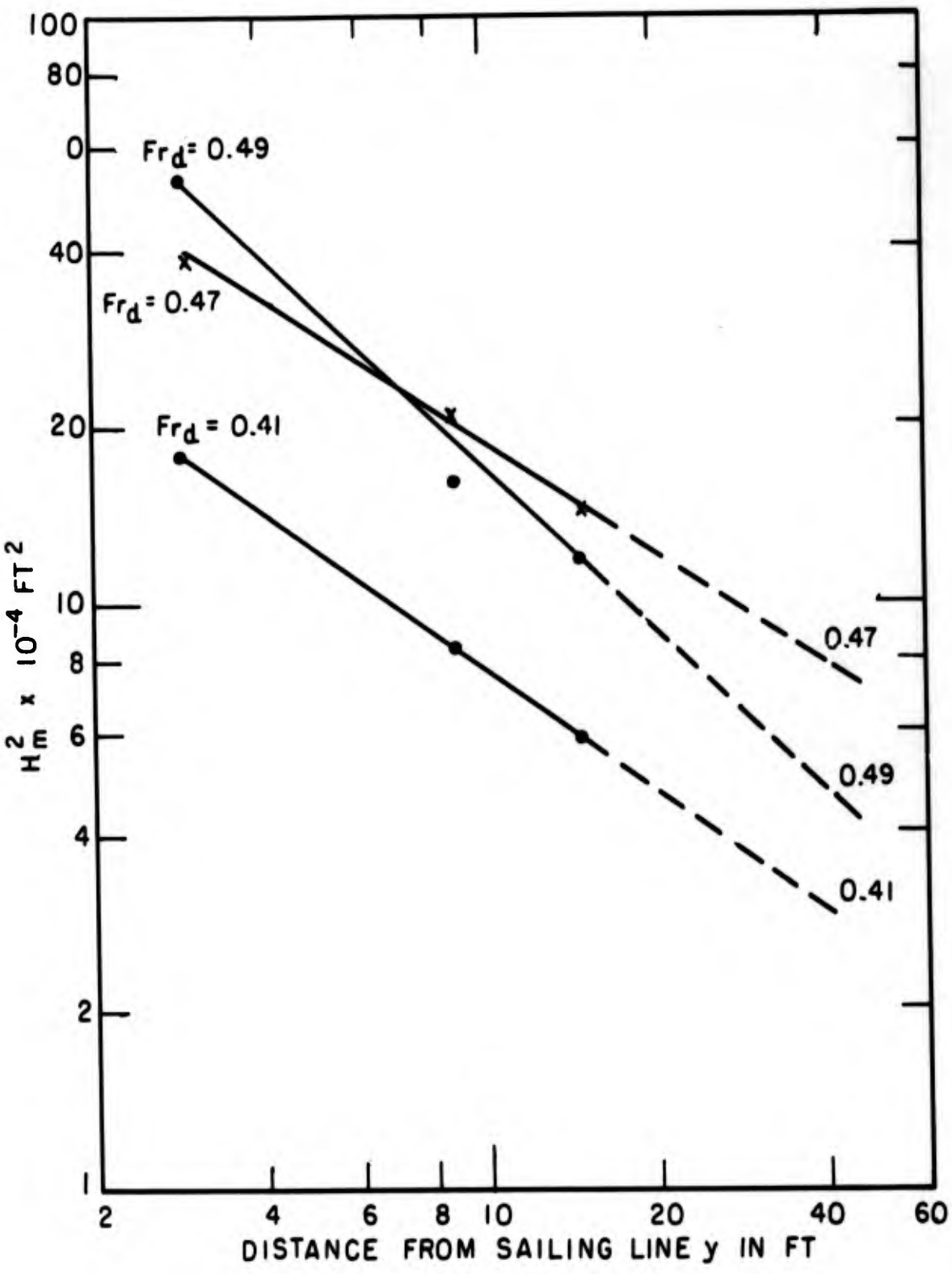

FIG. 56 MAXIMUM WAVE HEIGHT AS A FUNCTION OF DISTANCE FROM SAILING LINE FOR CRUISER MODEL IN DEEP WATER (d = 25")

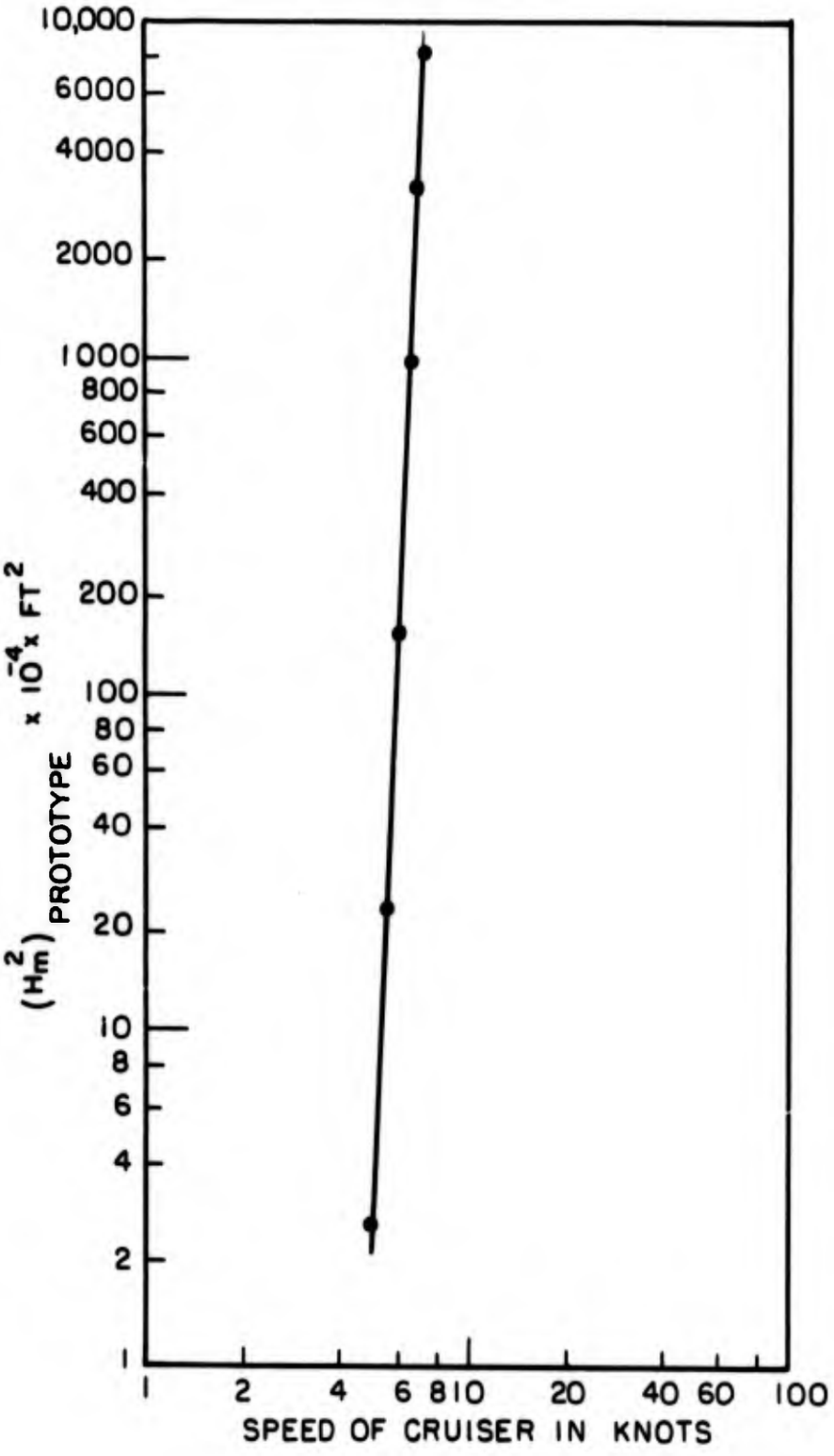

FIG. 57 H_m^2 IN FT^2 AT A DISTANCE OF 250 FT FROM SAILING LINE AS A FUNCTION OF SPEED OF CRUISER IN KNOT IN SHALLOW WATER (d = 5.5 FT)

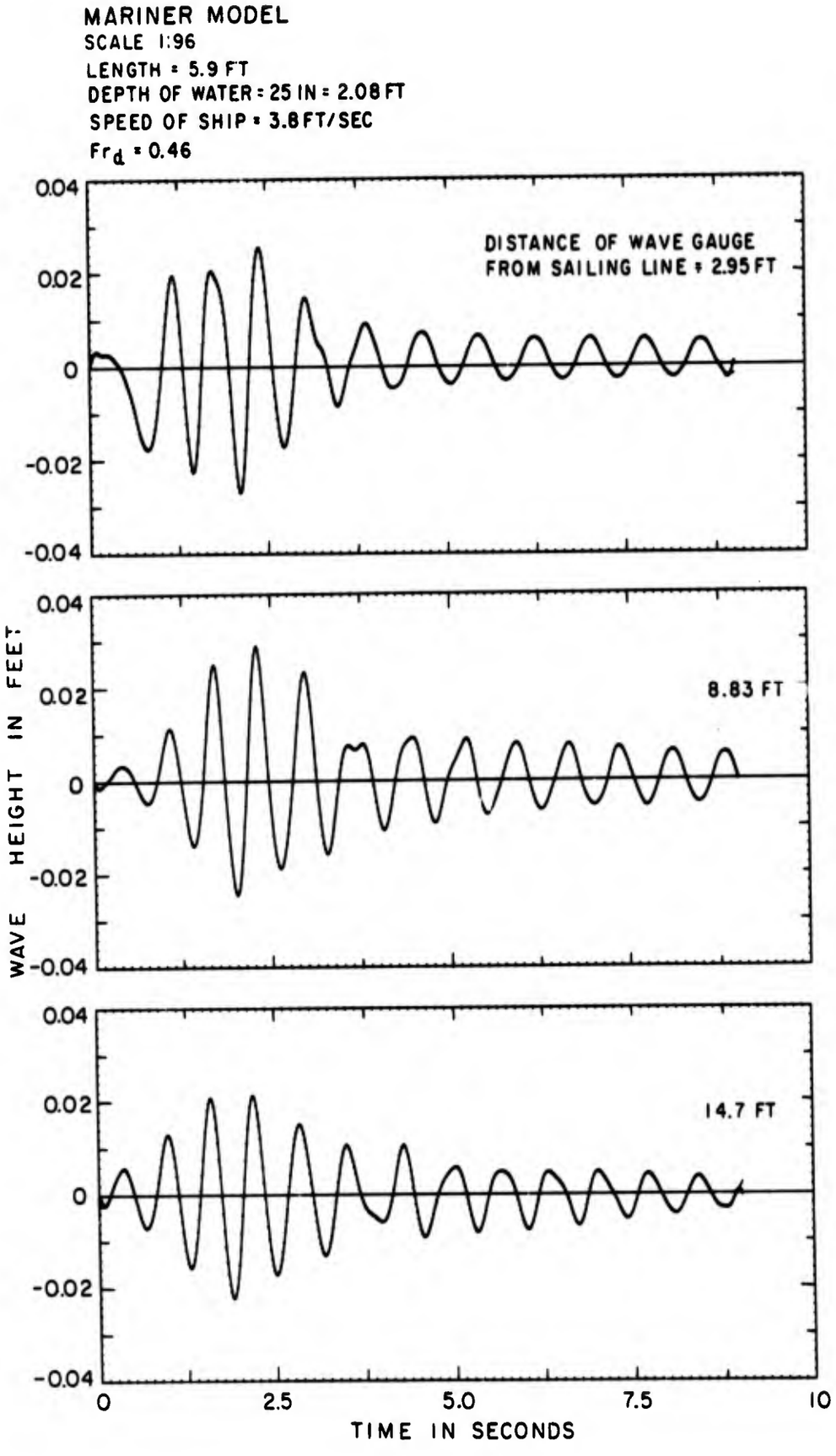

FIG. 58 LONGITUDINAL WAVE PROFILES FOR MARINER MODEL IN DEEP WATER (d = 25 IN)

CRUISER MODEL
SCALE 1:16
LENGTH = 4.06 FT
SPEED OF SHIP = 3.95 FT/SEC
DEPTH OF WATER = 25 IN = 2.08 FT
Fr_d = 0.48

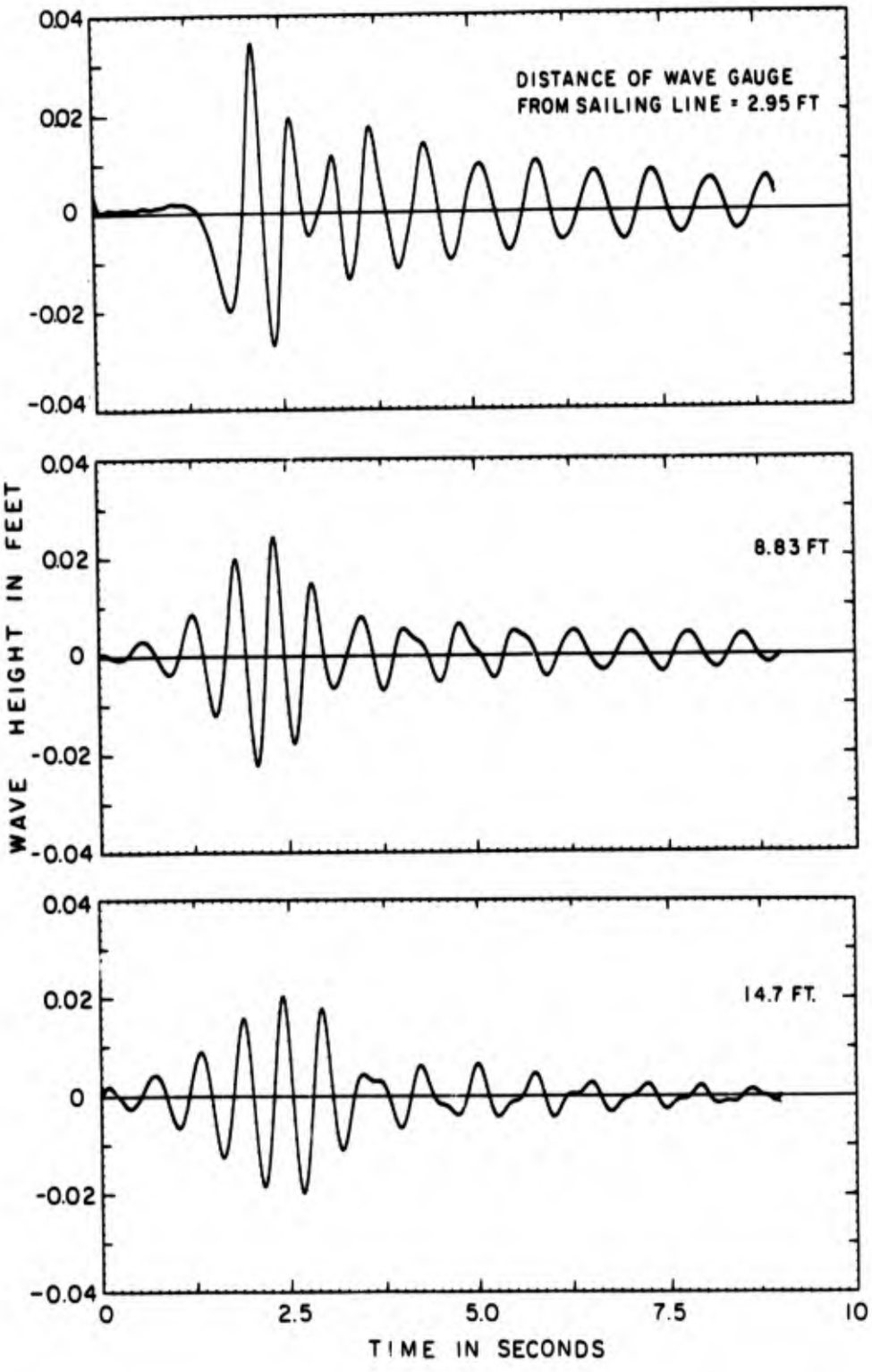

FIG.59 LONGITUDINAL WAVE PROFILES FOR CRUISER MODEL IN DEEP WATER (d = 25 IN)

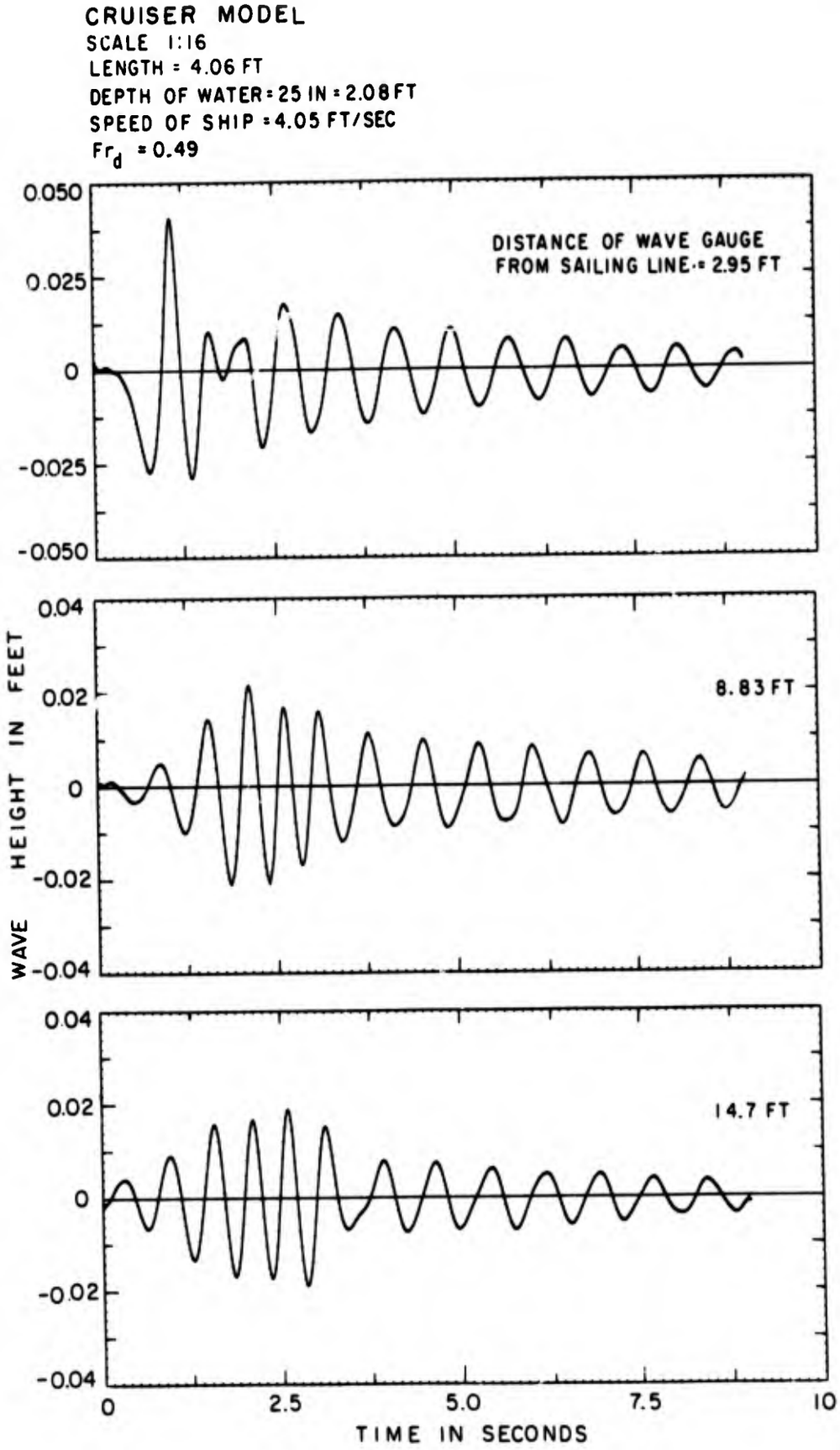

FIG 60 LONGITUDINAL WAVE PROFILES FOR CRUISER MODEL IN DEEP WATER (d = 25 IN)

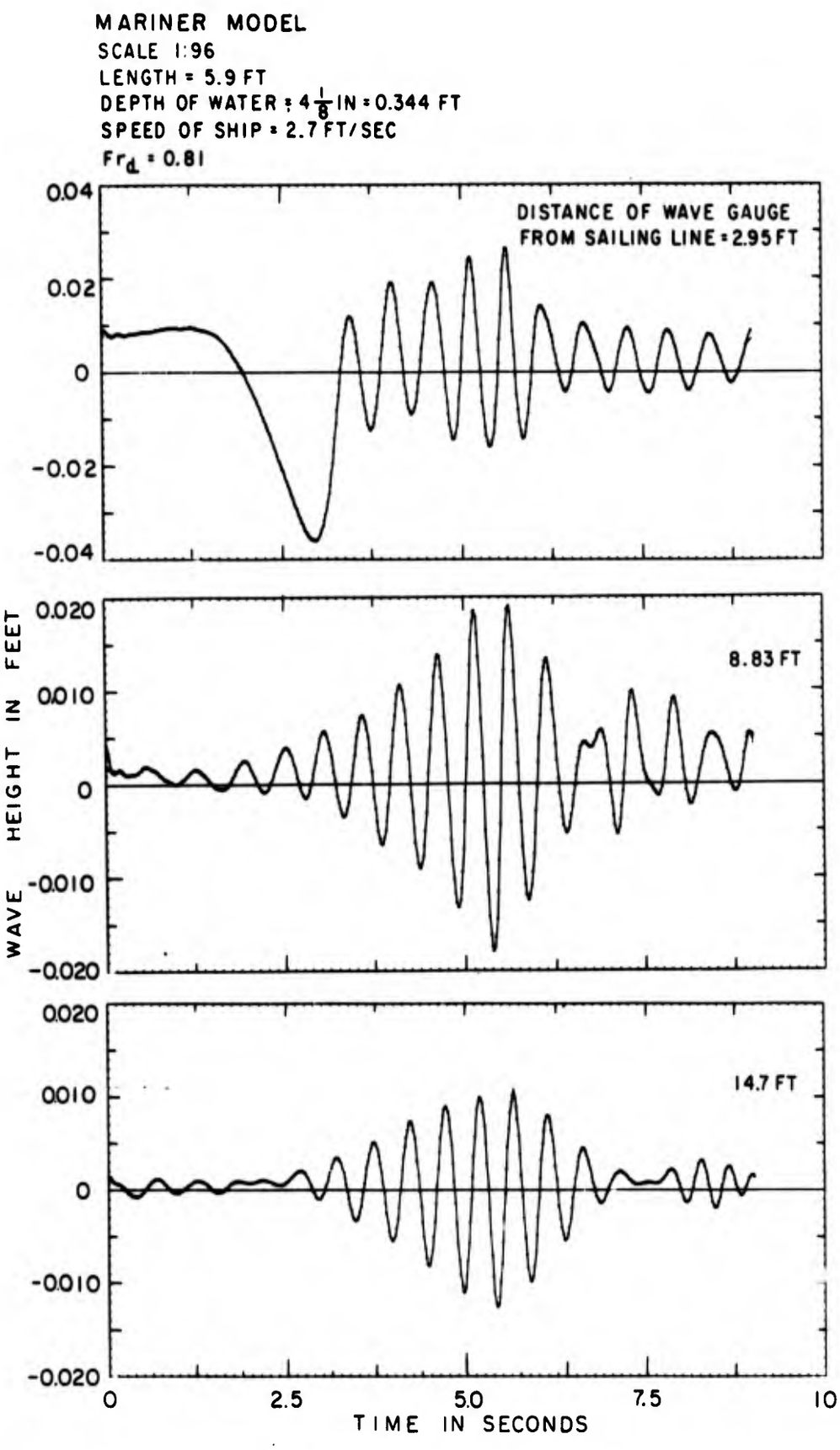

FIG. 61 LONGITUDINAL WAVE PROFILES FOR MARINER MODEL IN SHALLOW WATER (d = 4.125 IN)

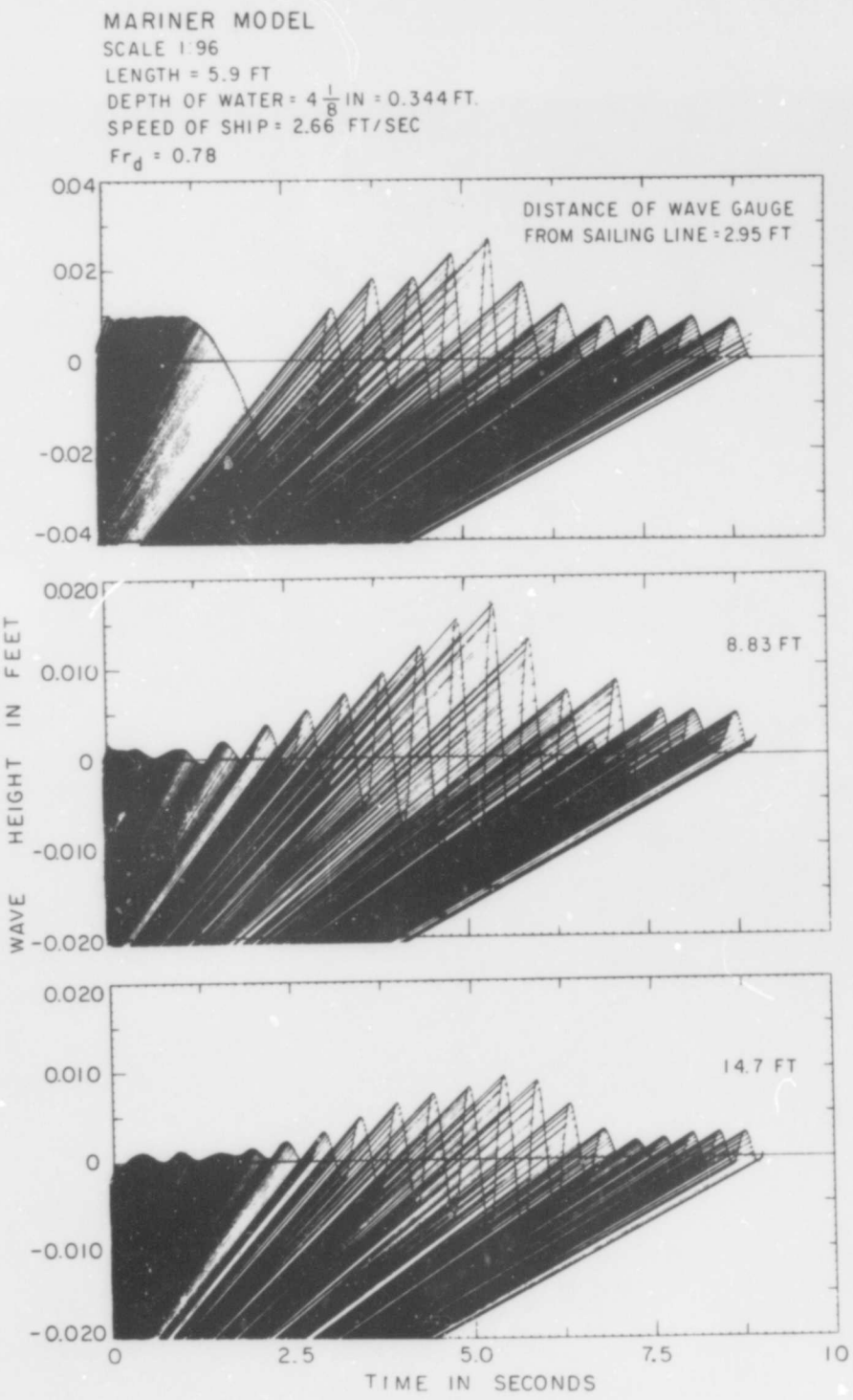

FIG. 62 LONGITUDINAL WAVE PROFILES FOR MARINER MODEL IN SHALLOW WATER (d = 4.125 IN)

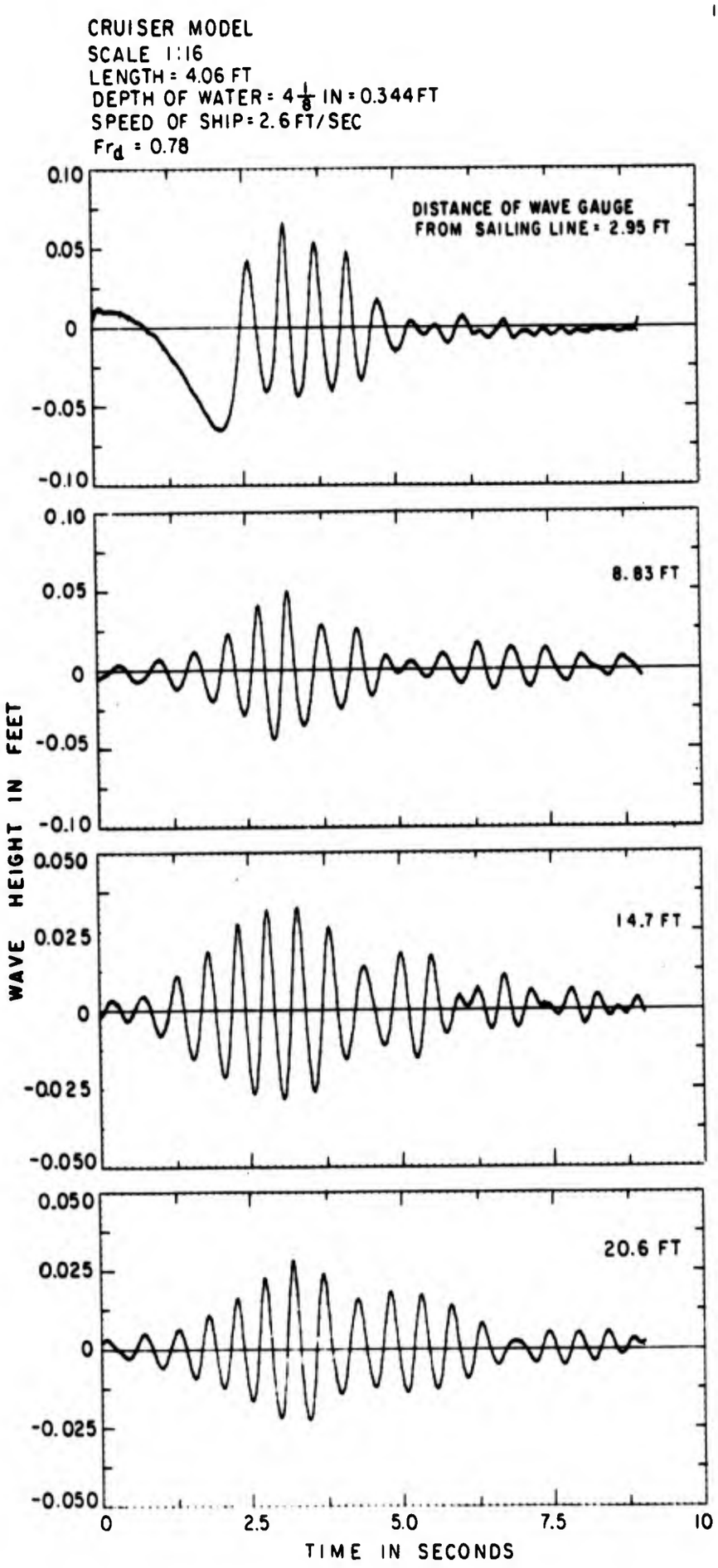

FIG.63 LONGITUDINAL WAVE PROFILES FOR CRUISER MODEL IN SHALLOW WATER (d = 4.125 IN)

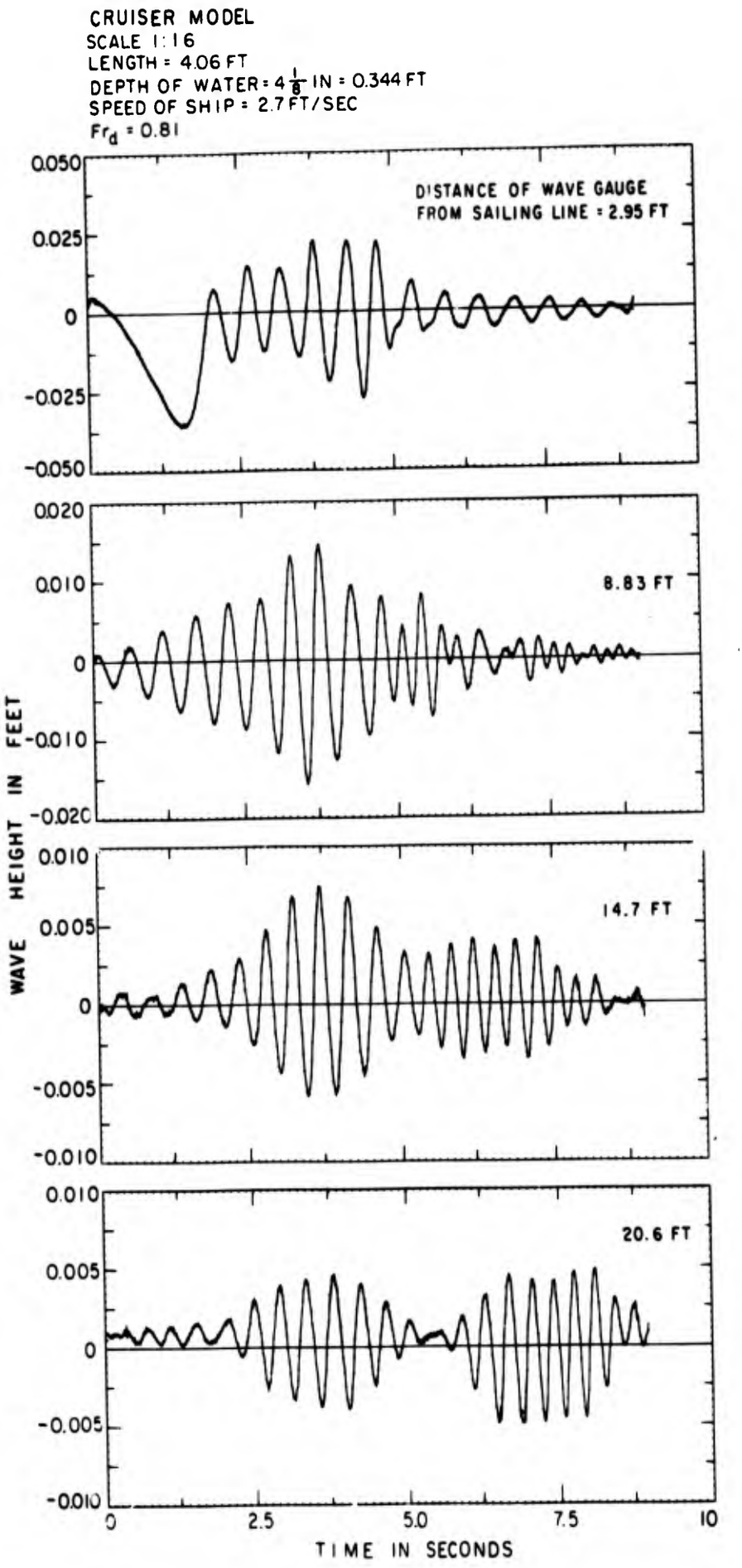

FIG 64 LONGITUDINAL WAVE PROFILES FOR CRUISER MODEL IN SHALLOW WATER (d = 4.125 IN)

UNCLASSIFIED
Security Classification

DOCUMENT CONTROL DATA - R & D

(Security classification of title, body of abstract and indexing annotation must be entered when the overall report is classified)

1. ORIGINATING ACTIVITY (Corporate author)
Hydraulic Engineering Laboratory
University of California, Berkeley

2a. REPORT SECURITY CLASSIFICATION
UNCLASSIFIED

2b. GROUP

3. REPORT TITLE
RELATIVE EFFECT OF WAVES GENERATED BY LARGE SHIPS AND SMALL BOATS IN RESTRICTED WATERWAYS

4. DESCRIPTIVE NOTES (Type of report and inclusive dates)

5. AUTHOR(S) (First name, middle initial, last name)
M. M. Das

6. REPORT DATE	7a. TOTAL NO. OF PAGES	7b. NO. OF REFS
November 1969	112	64

8a. CONTRACT OR GRANT NO.	9a. ORIGINATOR'S REPORT NUMBER(S)
Contract DACW 72-68-C-0034 b. PROJECT NO. with the Coastal Engineering Research Center c. d.	HEL-12-9 9b. OTHER REPORT NO(S) (Any other numbers that may be assigned this report)

10. DISTRIBUTION STATEMENT
This document has been approved for public release and sale; its distribution is unlimited.

11. SUPPLEMENTARY NOTES	12. SPONSORING MILITARY ACTIVITY

13. ABSTRACT

The peak wave energy in a system of waves resulting from the passage of a ship is important in engineering problems such as bank erosion, the motion of moored vessels, and forces on fixed and floating docks. With respect to bank erosion, the question often asked is whether the single passage of a large ship is more damaging than numerous passages of small pleasure craft. This study was conducted to determine the relative importance of the peak energy resulting from the passage of a cargo ship and a pleasure cruiser. The characteristics of the waves generated by these vessels moving at various speeds in deep and shallow water were determined from model studies. A numerical example is given in which prototype values of peak wave energy were predicted from the model data, and then ratios of the peak energies computed. The importance of ship speed is evident in these comparisons.

DD FORM 1 NOV 68 1473 REPLACES DD FORM 1473, 1 JAN 64, WHICH IS OBSOLETE FOR ARMY USE.

UNCLASSIFIED
Security Classification